UNIVERSITÀ DEGLI STUDI DI PADOVA

Dipartimento di Ingegneria dell'Informazione

Corso di Laurea Magistrale in Ingegneria delle Telecomunicazioni

---

TESI DI LAUREA MAGISTRALE

Raman Based Reach Extender for Application in XG-PON System

Relatore: Prof. Andrea Galtarossa

Correlatori: Prof. Paul Townsend
Dott. Giuseppe Talli
Dott. Cleitus Antony

Laureando: Marco Dalla Santa

Matricola 1056943

Anno Accademico 2013-2014

Abstract

Long reach passive optical networks (PONs) are receiving increasing attention as the ultimate solution for the new generation access networks, able to provide high bandwidth internet access. In order to satisfy the increasing broadband access demand in a cost-effective way PON technology needs to keep improving the available capabilities especially for what regards the length reach and the number of users sharing the network.

In this work a solution to extend the reach of 10-Gigabit-capable passive optical network (XG-PON) based on Raman amplification of the upstream transmission is presented, where for the first time quantum dot (QD) lasers are employed as Raman pumps at these wavelength. This reach extender is working in backward propagation configuration maintaining the totally passive nature of the distribution network. The key points investigated in the project are the power budget increase gained with the reach extender, the efficiency of the same which is posing some uncertainty because of working below the single mode fibre (SMF) cut off wavelength and the suitability of the scheme in a burst mode time division multiple access (TDMA) transmission.

The project successfully demonstrated the transmission over a 50 km SMF link supporting 64 split, suggesting Raman amplification as a practicable solution to increase the span of fibre to the home (FTTH) networks. This opens to the possibility of reducing the number of electronic switching nodes in the network with great reduction in investment and operational cost.

Contents

List of Figures

List of Tables

List of Abbreviations

AE	active ethernet
AFG	arbitrary function generator
APD	avalanche photodiode
ASE	amplified spontaneous emission
BER	bit error rate
BPF	band pass filter
CDR	clock data recovery
CWDM	coarse wavelength division multiplexing
DCA	digital communications analyser
DCF	dispersion compensating fibre
DFB	distributed feedback
DML	directly modulated laser
DR	dynamic range
DRB	double Rayleigh backscattering
DSL	digital subscriber line
DUT	device under test
ED	error detector
EDFA	erbium doped fibre amplifier
ER	extinction ratio
FBG	fibre Bragg grating
FEC	forward error correction
FTTH	fibre to the home
GPIB	general purpose interface bus
G-PON	Gigabit-capable passive optical network
GUI	graphical user interface
LI	light current
MQW	multiple quantum well
MZM	Mach-Zehnder modulator
NEP	noise equivalent power
NF	noise figure
NZDF	non zero dispersion fibre
ODN	optical distribution network
OLT	optical line terminal
ONU	optical network unit
OSA	optical spectrum analyser

OSNR	optical signal to noise ratio
OTL	optical trunk line
PBC	polarisation beam combiner
PER	polarisation extinction ratio
PG	pattern generator
PIN	positive-intrinsic-negative
PM	power meter
PMF	polarisation maintaining fibre
PON	passive optical network
pp	peak to peak
PRBS	pseudo random binary sequence
QD	quantum dot
QW	quantum well
RF	radio frequency
RIN	relative intensity noise
SBS	stimulated Brillouin scattering
SMF	single mode fibre
SMSR	side mode suppression ratio
SNR	signal to noise ratio
SOA	semiconductor optical amplifier
SRS	stimulated Raman scattering
TDM	time division multiplexing
TDMA	time division multiple access
TIA	transimpedance amplifier
TLD	tunable laser diode
TOSA	transmitter optical subassembly
VOA	variable optical attenuator
WDM	wavelength division multiplexing
xDFA	rare-earth doped fibre amplifier
XG-PON	10-Gigabit-capable passive optical network

Chapter 1

Introduction

In the last 20 years an exceptional growth in bandwidth demand to access the internet is constantly registered and this trend is expected to continue, if not increase, over the next years. This growth is due to the deeper penetration of the internet access across the globe, driven by services with increasing popularity like cloud storage and computing, video streaming, internet television and newly the rapid diffusion of mobile devices. In Fig. 1.1 this trend is visible through the last years, with the video services playing the major role [1].

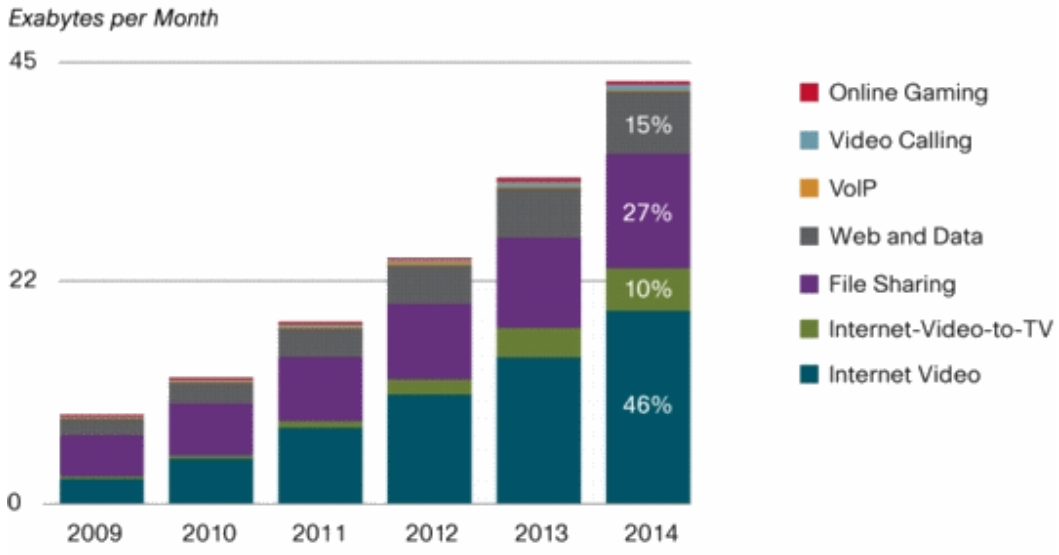

Fig. 1.1: Worldwide IP data traffic evolution [1]

The most diffused physical layer communication technologies are summarised in Fig. 1.2 where they are compared in term of data rate and transmission distance [2]. It is evident how the only viable way when moving to high bit-rate and long distances are optical communication solutions. Optical fibre is indeed the leading technology for long haul data link, being the only transmission medium capable to guarantee massive bandwidth over hundreds or thousands of kilometres. However to respond to the increasing traffic demand and guarantee a broadband experience to the users even the last mile networks are registering a strong interest and development towards optical fibre physical medium over the last years.

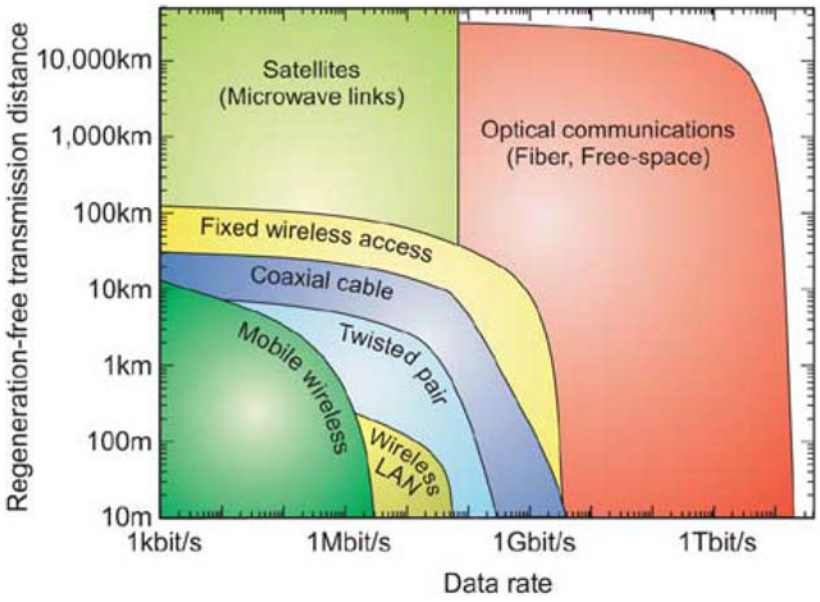

Fig. 1.2: Transmission technologies distance versus data rate in regeneration-free transmission [2]

1.1 Fibre to the home technology

Nowadays the internet communication network architecture can be divided in three main parts (Fig. 1.3): the more central one is the core network which is made of long haul links like submarine intercontinental and international connections and links between major exchanges. Then the metro network accomplishes the connections from the main exchange points linked to the core network to the local aggregation points. The access network is lastly responsible to bring the internet from the local switches to the customers house. Core and metro networks can afford high cost investments thanks to the widely shared architecture which permits to write off the expenses; moreover they must provide an extremely wideband service being the internet backbone. On the other side access network are usually limited by the available investments and the providers look for the best compromise between performances and costs. Therefore while in core and metro networks the well-established technology is the optical fibre, access networks are only recently moving towards this direction, thanks to the development of more affordable optical components and solutions enabling sharing of resources. Three major technologies are competing in this field: wireless, copper and optical fibre. Worldwide last span networks are still mostly based on copper transmission medium, either co-axial or twisted pair; the possibility of using the already installed telephonic copper networks and the digital subscriber line (DSL) technology were the key point enabling a low cost and broadband internet access to the final users. A common alternative is the wireless access which is using technologies like WiFi (802.11), WiMAX (802.16), 3G and 4G mobile broadband and is diffused especially

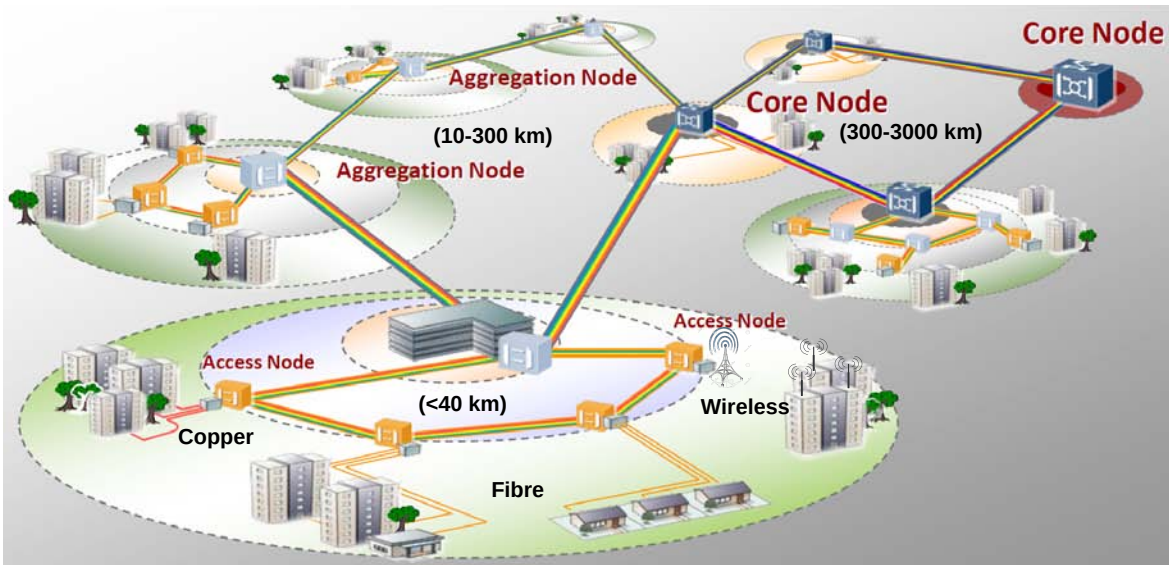

Fig. 1.3: Global network hierarchy; core, metro and access network

in rural environment. Because of the low outside plant costs and the shared point-to-multiple point architecture they come at relatively low costs, however it cannot guarantee high bandwidth services. In addition both these two solutions can support only short distances in order to not compromise the effective bandwidth. These limitations, the demand of always higher bandwidth services and the progress in optical components manufacture with relative lowering of the costs are the reasons of the recent development of fibre to the home (FTTH) [8]. Fig. 1.4 [3] clearly shows the trend in access network technology in Japan: DSL is being rapidly replaced by FTTH services, at the center of new investments.

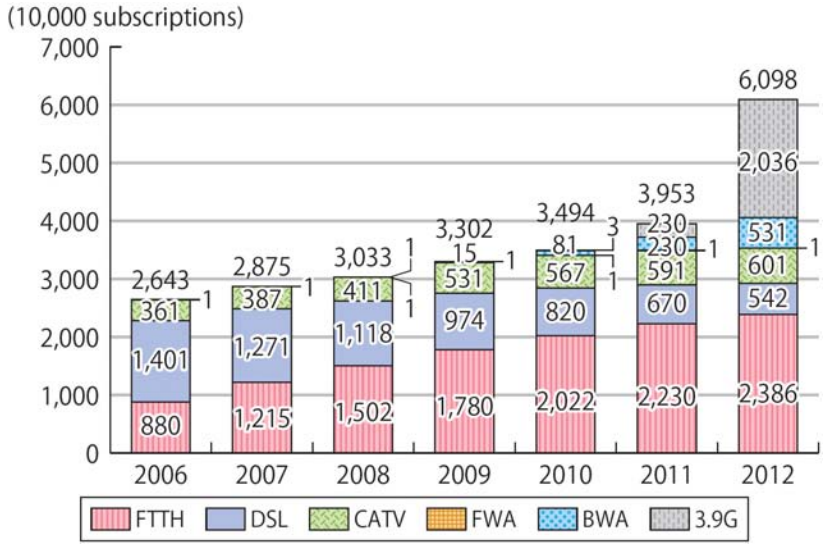

Fig. 1.4: Number of broadband subscribers in recent years in Japan [3]

In 1.5 [4] we can see the worldwide growth rate of different access technology from the last quarter of 2012 and the first quarter 2013, where fibre based networks are scoring

the higher increase percentage.

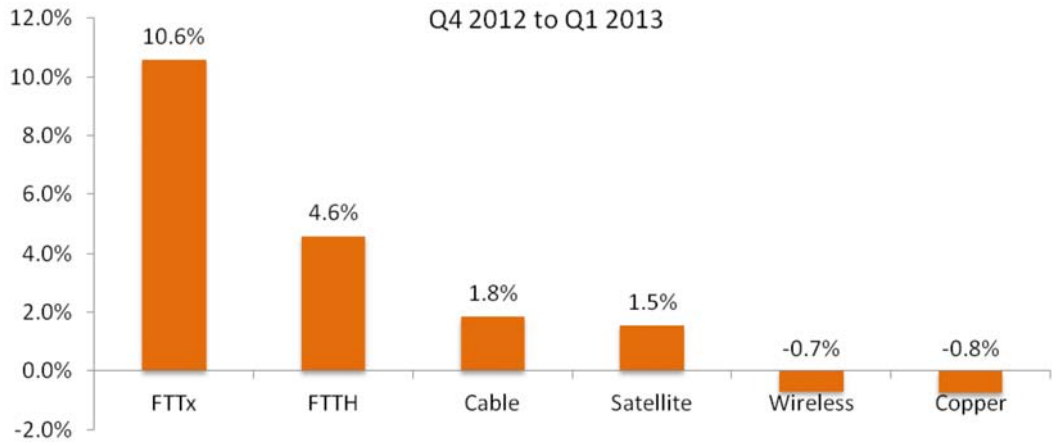

Fig. 1.5: Worldwide growth rates in access network technologies [4]

1.2 Motivation and objectives of this work

The most promising enabling solution for FTTH is represented by passive optical networks (PONs) which have experienced a rapid development in research and a rapid succession in the definition of new generation standards. PONs, which will be better treated in Chapter 2, have a point-to-multipoint structure based on passive splitters along the link without active components; it hence involves a shared network architecture between multiple users and can support time division multiplexing (TDM) and/or wavelength division multiplexing (WDM) protocols. These aspects make PONs highly cost-effective for affordable FTTH solutions. New generation networks are looking for solutions which can increase the span length and number of customers for a singe network, thus to increase the penetration capabilities and reduce the costs. To overcome the first generation standard length of 20 km to 60 km or more the most crucial point is the upstream transmission which needs amplification of the optical signal. The challenging point about that are the intrinsic attenuation loss and the burst mode nature of the upstream flow, which consists of TDM packets with different optical power, each one corresponding to one customer. Amplification is not always necessary in the downstream because it is typically placed in the lower attenuation window of the optical spectrum, and when needed it can be achieved in a more straightforward way seeing that the problem of burst mode operation is not present. Amplification should be made in a way that is not compromising the cost effectiveness of the network, and if possible its passive nature. Amplification by Raman scattering has been proposed with a renewed interest as an alternative over rare-earth doped fibre amplifiers (xDFAs) and semiconductor optical amplifiers (SOAs) thanks to some intrinsic advantages and evolution in the enabling technology [6]. Moreover the possibility of backward Ra-

man configuration can lead to an amplification scheme which is not compromising the passive nature of the distribution network. Some previous works have already been carried out showing the feasibility of Raman amplified link in PON architecture. In this work we will evaluate for the first time, at the best of our knowledge, an amplification scheme for the recent 10-Gigabit-capable passive optical network (XG-PON) standard employing distributed Raman amplification with quantum dot (QD) lasers used as light pump. This work is developed under the European project Quaternian which aims to apply QD technology to the last span of optical communication systems. Semiconductor QDs lasers offer performance advantages such as low noise, temperature insensitivity and reduced non-linearities and recently high power devices at the necessary wavelength and contained size and price have been developed. The Quaternian project goal is to exploit the QD device advances to reduce the cost of transponders, to extend the reach of PONs and to support higher data throughputs to mobile internet devices [9].

1.3 Outline of the thesis

We will focus this work on exploiting the capabilities of a reach extender for XG-PON providing distributed Raman optical amplification to the upstream transmission. For the first time QD lasers were used as Raman pumps at this wavelength. The main investigated topics were the quantification of the gained power budget and the suitability of the reach extender in burst mode operation.

The general context and the motivation for this research have been introduced in chapter 1.
In Chapter 2 a summary of the current state of communication technology is presented, focusing on optical access networks and PON recent evolution and the challenging aspects to deal with for increasing the performances.
In Chapter 3 a brief overview of the physical principles of Raman scattering and amplifiers technology is presented; afterwards the attention will be moved on a full characterisation of the QD pump laser diodes, the Raman pump module structure and its capabilities in term of power budget increase.
In Chapter 4 we will explain the process and the key points of designing the experimental setups for evaluation of the Raman reach extender at first in continuous mode and then in an effective burst mode emulation test bench.
In Chapter 5 the results of the setups characterisation and performances of Raman distributed amplifier are reported for both the evaluation schemes.

Chapter 2

Optical Access Networks

Access networks are a strong competitor in the technology supporting broadband services, with the main technologies currently employed represented by copper (either twisted pair or coaxial), wireless and optical fibre. The competition is mostly driven by the research of the best compromise between a cost affordable solution and its effective bandwidth.
In the last years FTTH is being considered as the most promising technology to deliver a broadband internet access to customers. Because of the optical fibre superior performances achievable with respect to other solutions it is experiencing a fast development in the new generation access networks, where the limitation is mostly due to the cost effectiveness.

2.1 Evolution of access network technologies

Different technologies have been developed to support FTTH networks, considering different out plant architecture in the physical link topology; Fig. 2.1 shows the major competing technologies. The point to point solution is using a dedicated fibre for every user from the nearest local exchange point, making it an attractive solution for the performance aspect but with the side effect of higher deployment costs. The other solutions are taking advantage from a shared fibre architecture between multiple users to reduce costs, distinguishing two ways in which the signals are broken out. In one case, called active ethernet (AE), the signals are split or merged using an active electronic switching device in the outside plant network. In the second scheme, named PON, simpler passive optical splitters are employed instead of the active switches leading to many advantages such as lower capital expenditures and operational costs, better reliability and easiness in upgrades of data rate and signal format. Thanks to these advantages PON is by far the most widely deployed in optical access technology.

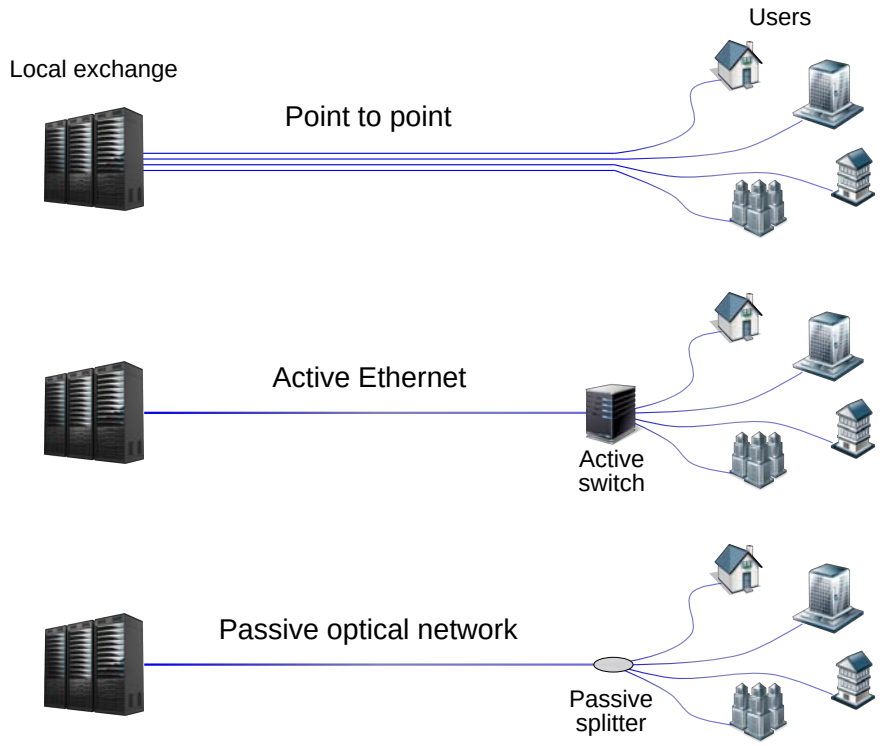

Fig. 2.1: FTTH technologies

2.2 Passive optical networks evolution

A PON architecture can vary from the use of a single high ratio passive splitter to multiple lower ratio splitter distributed along the network, based on the environment conditions and users distribution. Complex structures like the one in Fig. 2.2 are thus possible, where different types of users are sharing the same network with different bandwidth and reliability demands, economic resources, environmental conditions. Different protocols have been thus developed for PONs considering many solutions which better fit for various cases such as TDM, WDM, dynamic bandwidth allocation.

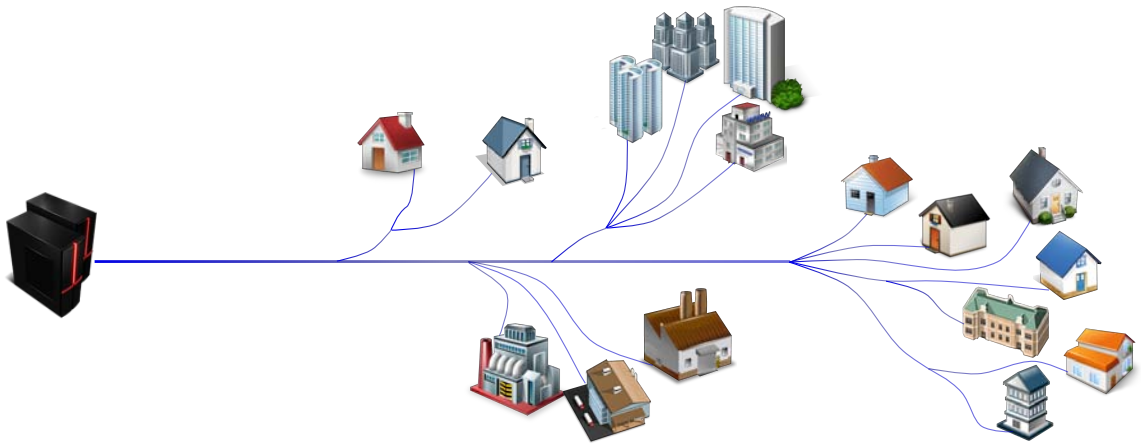

Fig. 2.2: Example of PON system

Fig. 2.3 shows the evolution of PON standards in the recent years, with the correspondent capacity increase.

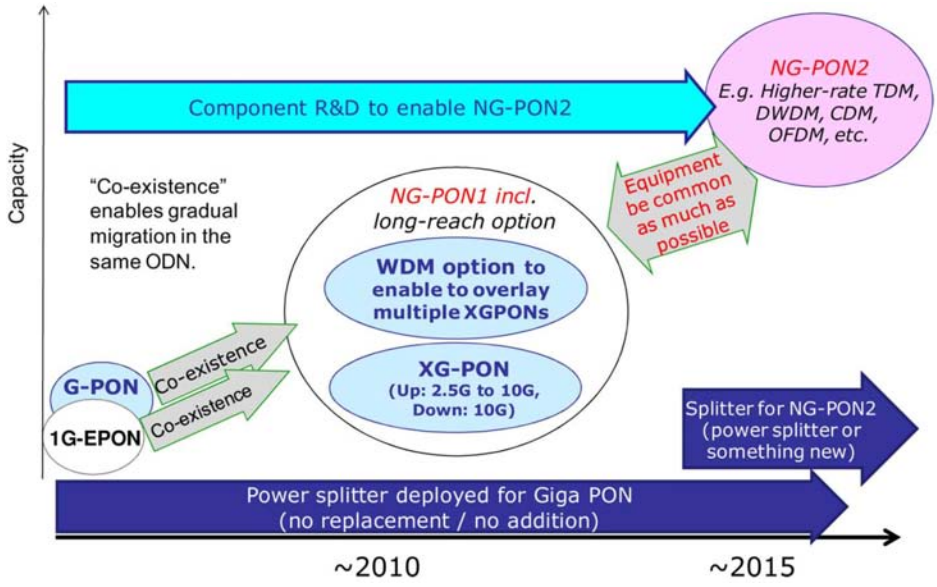

Fig. 2.3: PON standard evolution [5]

In this work we will analyse a XG-PON system which is the evolution of the previous Gigabit-capable passive optical network (G-PON) protocol, aiming to reach a link length of 60 km with transmission speed of 10 Gb/s in downstream and 2.5 Gb/s in upstream. An important aspect to take in account in the migration from one system to the other is the coexistence of the two. Typically the physical structure of such a network is distinguished in an optical line terminal (OLT) which is the local exchange point connected to the metro network, a first fibre segment shared among all the users called optical trunk line (OTL), the last mile of the network after the passive splitter named optical distribution network (ODN) and the final users referred to as optical network units (ONUs) (2.4). This standard is based on a purely time division multiple access (TDMA) transmission protocol with WDM used for coexistence of upstream

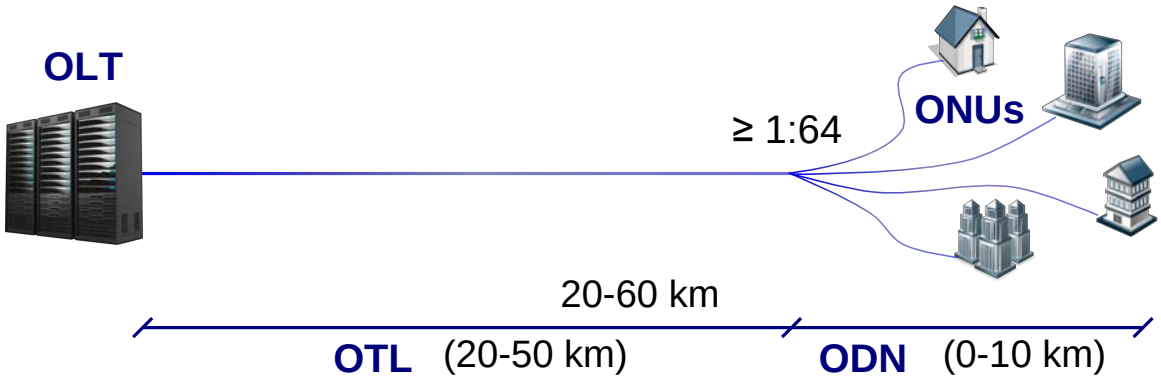

Fig. 2.4: PON basic structural elements

and downstream flows on the same physical support. All the ONUs must be kept synchronised in order to operate a TDMA transmission in which a specific time slot is reserved for every user. The downstream transmission is of type broadcast because of the passive component employed in the network cannot perform routing operations, which means that every ONU is receiving the entire downstream flow and extracting only the portion addressed to it. The upstream transmission is of burst mode type in which only one ONU at a time is transmitting, in its assigned temporal window. Because of the different attenuation losses associated to every ONU physical link the packets reaching the OLT receiver have different optical powers.

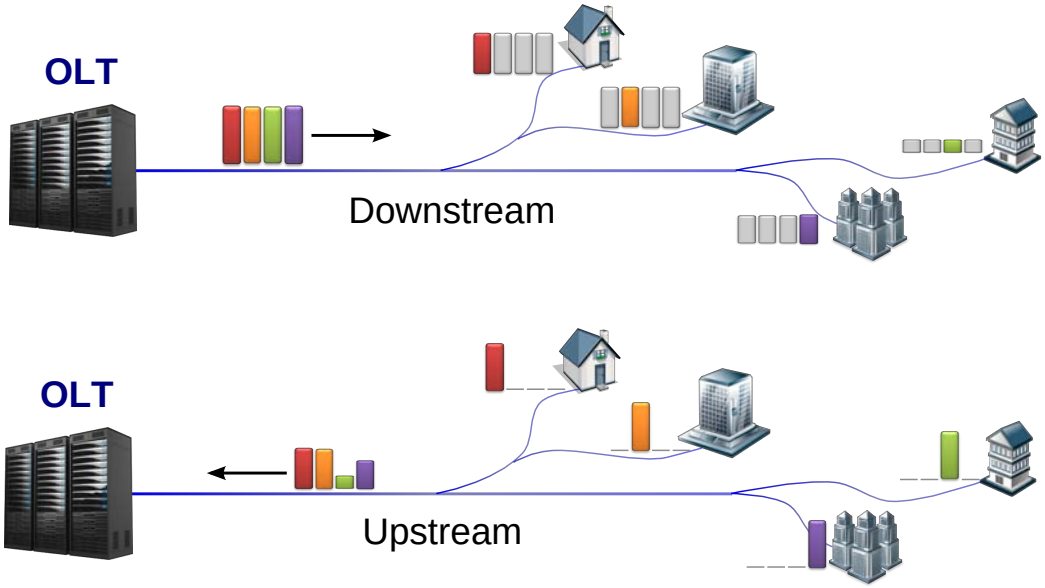

Fig. 2.5: XG-PON downstream and upstream TDMA transmission scheme

Two separate transmission bands for upstream and downstream are located as shown in Fig. 2.6 compared with the G-PON ones, where the black line is the attenuation profile of a single mode fibre (SMF). As clearly visible the bands are located in two different transmission windows, well separated to reduce crosstalk effects. The downstream band is placed in the lowest intrinsic attenuation region of silica fibres, while the upstream coincide with higher attenuation but is near to the zero dispersion wavelength of standard SMF. The choice of the upstream window in O-band is also coming from historical reasons: given that semiconductor devices were available at those wavelengths with a more mature and cheap technology it was more convenient for the ONU transmitters which are in high number and not shared among users.

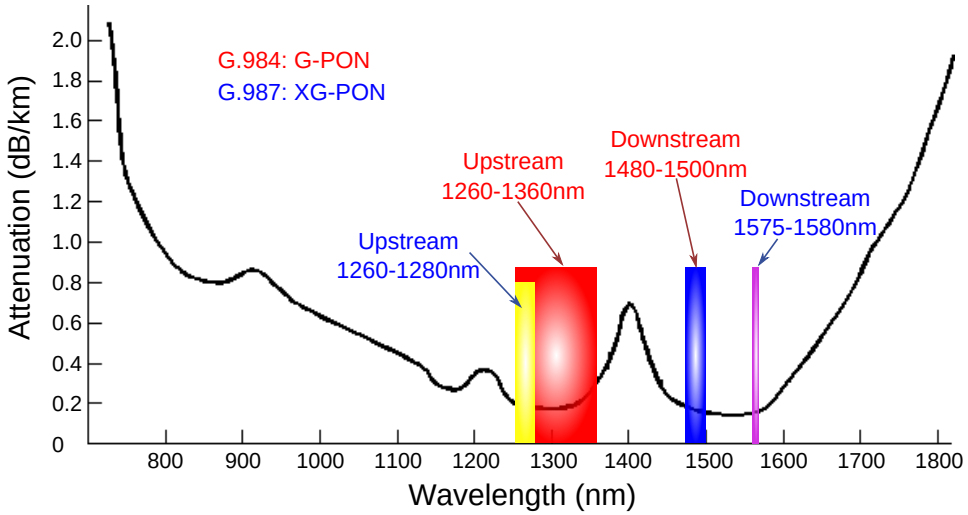

Fig. 2.6: XG-PON wavelength allocation

2.3 Reach extension challenges

In order to improve the geographic coverage capabilities of PONs and their cost-effectiveness large efforts are made to increase both the length of the transmission links and the split ratio. The goal is to move from the G-PON typical length of 20 km near to the maximum logical length of the XG-PON protocol equal to 60 km, with a 64 split ratio. The most challenging aspect is the upstream transmission which needs amplification as the network reach increases. This is necessary because of being placed in the O-band of the spectrum it suffers from relatively high attenuation, and it is also coming from transceiver equipped with low cost directly modulated laser (DML) diodes. On the other side the downstream is less limited by attenuation and can use a higher quality externally modulated laser which provides higher optical power, extinction ratio (ER), better linewidth to prevent dispersion. In fact its cost is shared among the users and it is thus worthwhile to invest in the transmitter quality to avoid outside plant optical amplification. Moreover the upstream amplification needs more attention because of burst mode nature of the traffic which is requiring a proper calibration of the amplifier to avoid heavy saturation or optical signal to noise ratio (OSNR) degradation effects. Two of the proposed schemes are in Fig. 2.7. The first solution is to place a reach extender in the outside plant of the network where an optical amplifier is boosting the transmission before the OTL fibre. In works like [10] a reach extender containing two SOAs, one for the upstream and one for the downstream, is demonstrated to successfully increase the reach of a G-PON system up to 60 km total length and 1:128 splits. SOAs are preferred over erbium doped fibre amplifiers (EDFAs) for this purpose because of they are available at every wavelength of interest and they do not suffer of prolonged gain transients due to the carrier lifetime like xDFAs. However this solution requires an out of plant active extender compromising

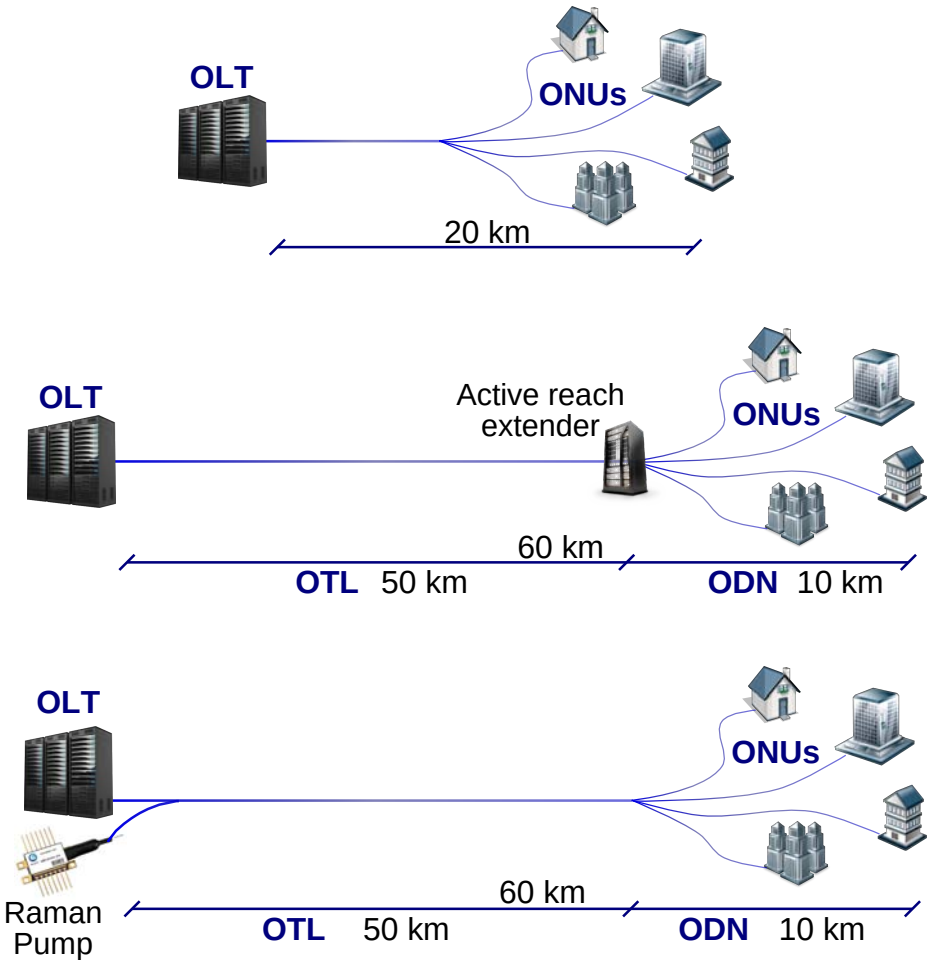

Fig. 2.7: PON reach extension schemes

the passive nature of the network, increasing the maintenance costs and reducing its reliability.

The second scheme depicted is based on Raman amplification in backward propagation configuration, in this way the Raman pumps of the reach extender can be placed in the OLT cabinet without modifying the outside network plant with the addition of active components. This approach have been successfully demonstrated in works like [11], [12], [13] for the G-PON upstream band, but to the best of our knowledge no works have addressed the XG-PON one.

Amplification through Raman scattering is offering some intrinsic advantages over other amplifiers like the possibility of design arbitrary gain profiles and distributed scheme which improves the noise figure (NF). However one of the factors causing Raman amplification to be in the center of a renewed interest in the last years is the progress in semiconductor technology which has provided always higher power fibre coupled lasers as Fig. 2.8 shows. This compact and cheap laser diode helps to make the installation of Raman amplifiers a more affordable and interesting solution for the investors.

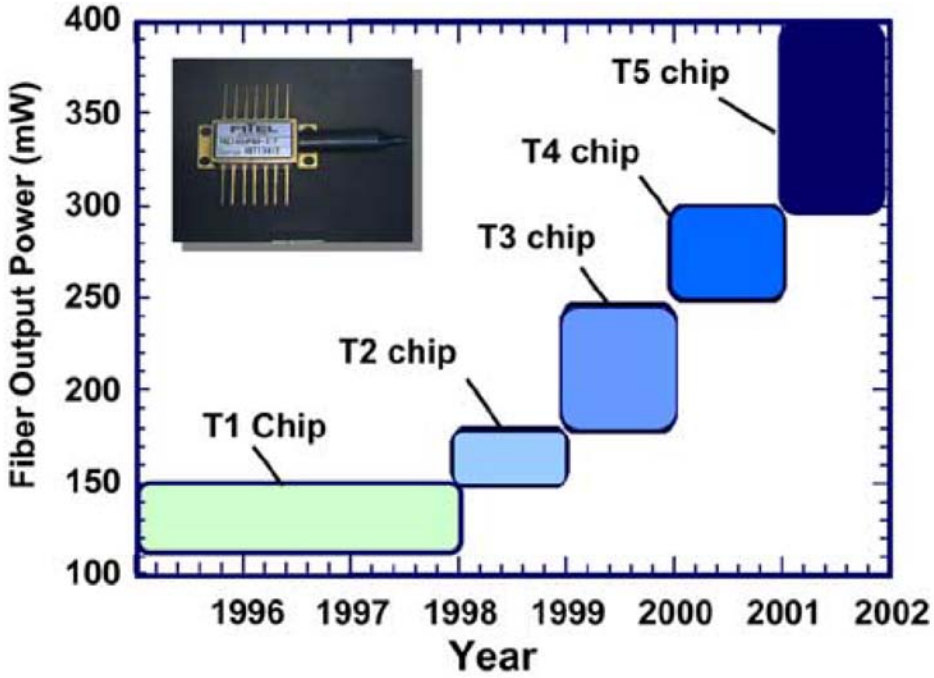

Fig. 2.8: Trend of nominal output pump power available in the market [6]

2.4 Conclusions

A brief overview of the internet network architecture and especially of PON systems for FTTH application in access network was presented in this chapter. Particular attention was posed on the capability extension of PON protocol discussing the challenging point, some works existing in literature and the most promising solutions. In the next chapter we will start to go deeper in the mechanisms of Raman amplification to understand the key point of this solution and how it is advantageous for FTTH development.

Chapter 3

Raman Amplification

3.1 Introduction

In this chapter we will initially introduce the main theoretical aspects of spontaneous Raman scattering and optical amplification by stimulated Raman scattering (SRS). A brief overview of optical fibre Raman amplifiers design with many possible solutions and the relative advantages or disadvantages will follow. We will then present the characterisation results of the QD lasers employed in this work, the structure of the Raman pump module built with them and its performances in term of induced Raman gain in a scenario of interest for the XG-PON upstream amplification.

3.2 Raman scattering

Raman effect is an inelastic scattering occurring when an optical field is incident on a molecule in which an absorbed photon is re-emitted at a different frequency, and hence energy. The bound electrons of the medium oscillates at the optical frequency, producing optical radiation at the same frequency, while the molecular structure is oscillating at frequencies of various molecular vibrations. The sum and difference frequency terms between the optical and vibrational frequencies cause the Raman scattered photons in the re-radiated electromagnetic field; the energy gap between the absorbed and the scattered particle is equal to the energy difference between the interested molecule vibrational modes. In a quantum mechanic description the photon is inelastically scattered by a quasiparticle, representing an excited state of the molecule modes of vibration, called phonon. Photon energy can be lost, with a correspondent shift to lower frequencies and heating of the molecular lattice (Stokes process), or gained, with consequent shift of the light to higher frequencies and lattice cooling (anti-Stokes process) [14]. The frequency shift is equal to the oscillation frequency of the created or annihilated phonon, and the resulting spectrum is determined by the material properties. Raman scattering is a spontaneous process that takes place randomly and can occur in all materials.

Raman scattering can also be stimulated by artificially providing a high number of available Stokes photons in the medium, for example injecting them along with the original radiation (the anti-Stokes process is not mentioned from here on because it is

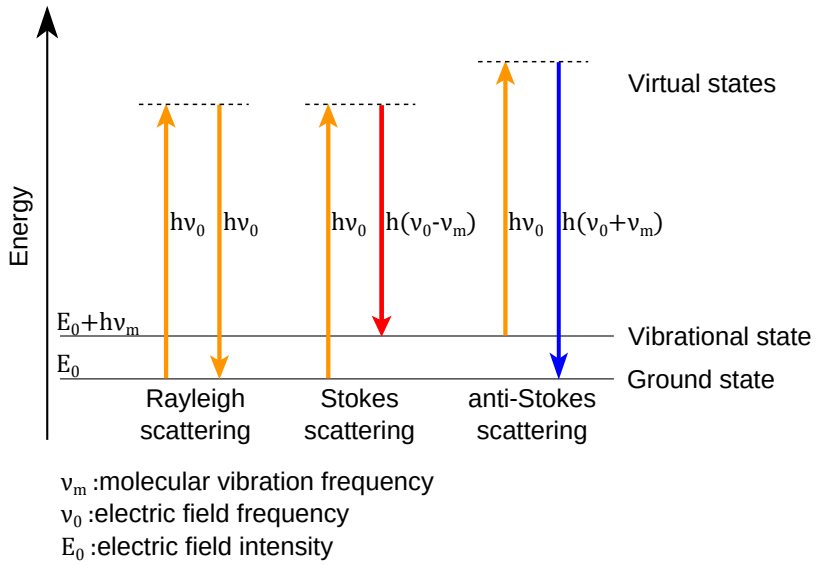

Fig. 3.1: Raman Stokes and anti-Stokes scattering, compared with an elastic (Rayleigh) scattering

typically orders of magnitude weaker than the Stokes one [14]). In that scenario the rate conversion of "pump" photons (higher frequency) into "signal" photons is strongly increased over the spontaneous case, giving rise to SRS and thus amplification of the signal radiation. When the two optical radiations, pump and signal, are propagating along the longitudinal (z) axis of a fibre their power (respectively P_p and P_s) evolution can be expressed as [7]

$$\frac{dP_s}{dz} = g_R P_p P_s - \alpha_s P_s \tag{3.1}$$

and

$$\pm\frac{dP_p}{dz} = -\frac{\omega_p}{\omega_s} g_R P_p P_s - \alpha_p P_p \tag{3.2}$$

where $g_R[W^{-1}m^{-1}]$ is the normalised Raman gain coefficient of the fibre, $\alpha_{p/s}$ are the attenuation coefficients of pump and signal beams and $\omega_{p/s}$ their respective frequencies. The $\pm$ signs represent the case of co and counter propagating pump wave respectively. In Eq.3.1 the signal is experiencing loss due to the intrinsic attenuation but is also taking advantage of the gain coming from SRS. On the other side the pump 3.2, in top of the attenuation loss, is showing depletion due to the energy transfer caused by SRS [14]. Ignoring this term, which can be considered negligible with respect to intrinsic pump loss for the backward pumping case, Eq. 3.2 can be solved (for the counter propagating case) as

$$P_p(z) = P_0 e^{-\alpha_p(L-z)} \tag{3.3}$$

with P_0 being the input pump power and L the fibre length. From this result we can

also derive

$$P_s(L) = P_s(0)e^{(g_R P_0 L_{eff} - \alpha_s L)} = G_N(L)P_s(0) \tag{3.4}$$

where we have defined

$$L_{eff} = \frac{1 - e^{-\alpha_p L}}{\alpha_p} \tag{3.5}$$

and G_N is representing the net gain. Equation 3.4 is a first-order approximation of the signal power evolution along the optical fibre experiencing Raman gain.

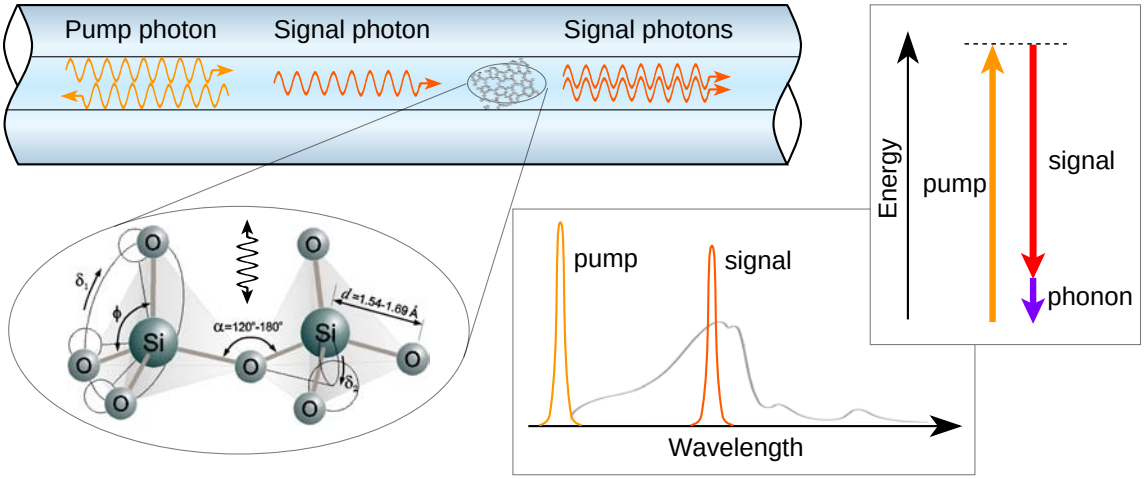

Fig. 3.2: Example of Raman pump and signal radiations

The typical Raman spectrum in silica is mostly determined by the bending motion of the Si-O-Si bond and because of the continuum of molecular vibrational frequencies attributable to the amorphous nature of the glass the peaks appear broad if compared to crystalline materials, as shown in Fig. 3.3 [15]. Also the spectrum of Si-O-Ge and Ge-O-Ge are shown, which are the other molecular bonds present in germanium doped fibres.

As visible the three materials have spectrum which differ for magnitude of the effect, peak shift and broadness of the same; these contributes are combined in a germanium doped fibre in various ways depending on the specific fabrication features. Fig. 3.4 shows the Raman gain coefficient for different types of germanosilicate fibres: looking at the dispersion compensating fibre (DCF) profile it is evident the influence of germanium concentration which is higher in this type of fibre and lead to a higher gain coefficient; indeed the effective area dependence is clear when comparing the spectrum of fibres with different core diameter. One important aspect is that the magnitude of the Raman gain coefficient does not depend on the relative direction of propagation of the pump and signal radiations.

The non zero dispersion fibre (NZDF) spectrum, which is similar to the one of the SMF employed in this work, shows a broadband characteristic coming from the amorphous

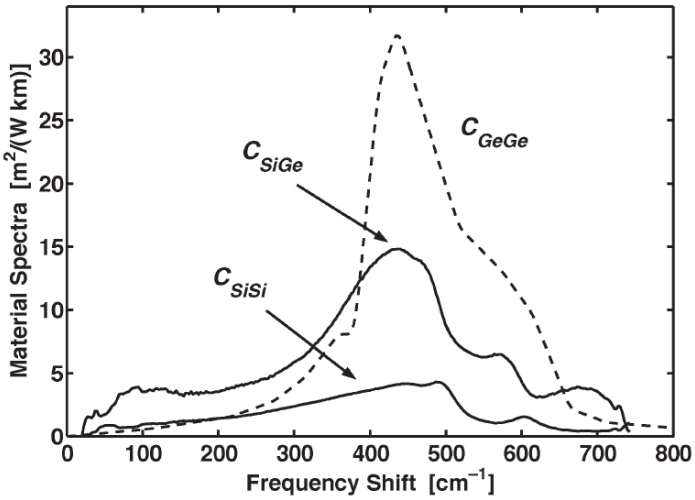

Fig. 3.3: Raman spectrum of Si/Ge-O-Si/Ge materials [7]

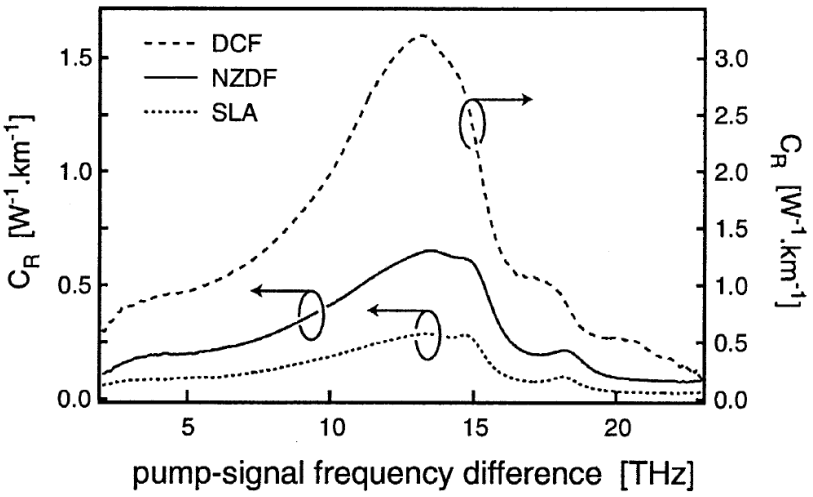

Fig. 3.4: Raman spectrum for three germanosilicate fibres [7]

nature of silica glass, with the main peak mostly due to the germanium core and a secondary peak attributable to the silica. The maximum of the gain coefficient appears at a Stokes frequency shift of approximately 13.2 THz from the pump signal.

Another remarkable aspect of Raman scattering is the response time: it is related to the nuclear rotations and vibrations, thus longer than the electronic response time; however being evaluated to be less than 100 fs it appears essentially instantaneous for applications such as telecommunication systems [15]. The Raman response functions for silica oxide and germanium oxide are shown in Fig. 3.5, showing response times way faster than the typical time intervals occurring in Gb/s fibre communication systems.

One ulterior important aspect of Raman gain to be remembered in the realization of amplifiers is the polarisation dependence of the same. We have seen that the effective area plays an important role on the gain coefficient value because of the pump and signal need to be spatially overlapped. As result the peak coupling strength between

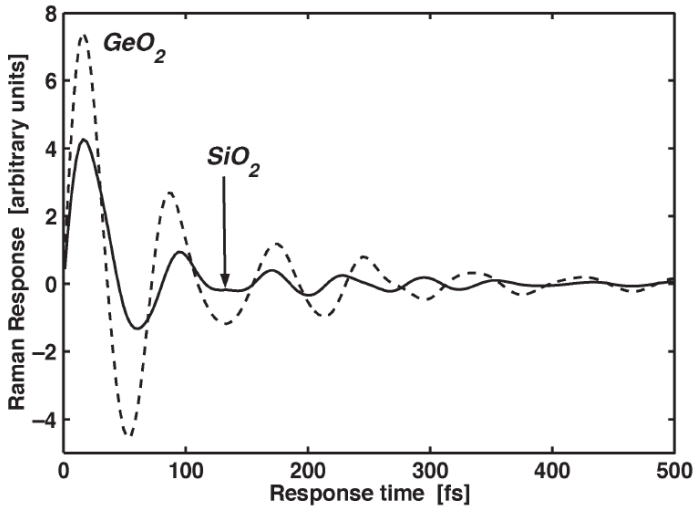

Fig. 3.5: Raman response function for two mediums [7]

a pump and signal shows roughly one order of magnitude difference among the copolarised and orthogonal polarised cases (Fig. 3.6). It is hence essential to control this aspect in an amplifier to guarantee the desired flatness in the gain profile.

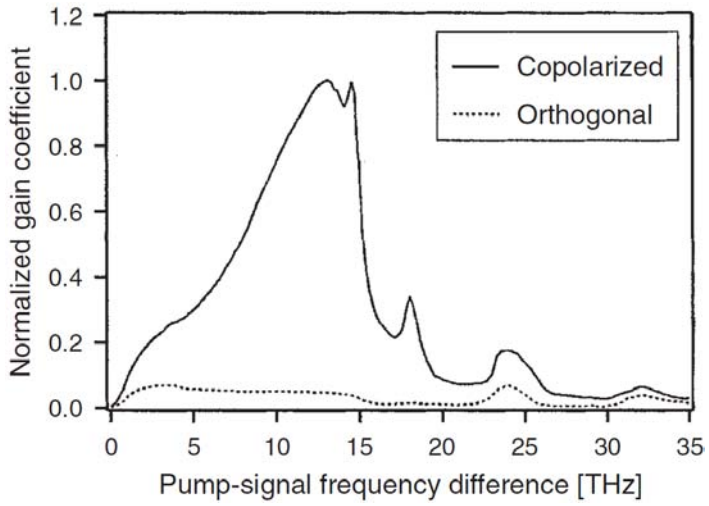

Fig. 3.6: Raman gain spectrum for copolarised and orthogonal polarised pump and signal [7]

Having mentioned the spatial overlapping of the two signals, one other aspect that may introduce loss in efficiency is the propagation of higher order modes than the fundamental one. When working at high frequencies, around the cutoff of the fibre, the pump may become multimode while the signal still propagates in single mode; the energy coupled in secondary modes is less efficiently converted in signal photons causing a decrease in the gain coefficient [15]. Fig. 3.7 shows the gain coefficient (for 13 THz pump-signal shift and copolarised beams) between different propagation modes of pump and signal, obtained in this case varying the core radius.
The graph is clearly showing that the coupling efficiency between different propagation

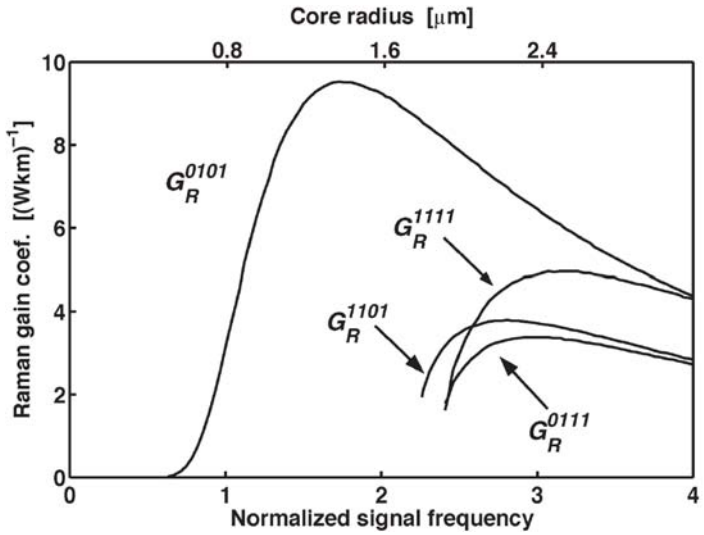

Fig. 3.7: Raman gain coefficient in function of core radius; the labels indicates the pump mode (first 2 digits e.g. 01) and signal mode (last 2 digits e.g. 11) [7]

modes is noticeable reduced with respect to the case of same mode; thus, especially in the condition of the pump propagating in multiple modes and the signal in single mode, a lower gain is expected for equal pump power injected.

3.3 Raman amplifiers

Different schemes have been proposed to provide efficient Raman amplification in optical fibres. A general schematic is reported in Fig. 3.8 where both a copropagating and a counterpropagating pump are depicted.

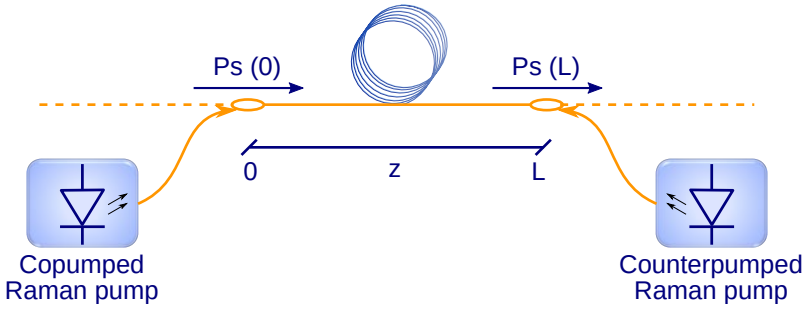

Fig. 3.8: Basic scheme of Raman fibre amplifier with both co and counter propagating pumps

Starting from this configuration we can define two types of amplifiers distinguishing whether the fibre which provides gain is a dedicated one or is the same used for the transmission. In the first case we are talking about discrete amplifiers where few kilometres of special fibre, e.g. a DCF which we have seen having a higher gain coefficient, is used as active medium and spatially confined in a discrete module. Indeed in the second case we have a distributed amplifier, whose optical medium used for amplifi-

cation is the same in which the transmission is taking place, thus typically a SMF of tens of kilometres. Because of the small cross-section of Raman scattering, distributed amplification usually ensure better performances, while the discrete one pose problems in increasing efficiency and other trades off. However even the latter maintains interest because of arbitrary location of gain spectrum which cannot be achieved with xDFAs and better linearity.

A second distinction, which regards both the typologies just introduced, is made looking at the reciprocal direction of pump and signal. Three configurations are possible: copropagating when the pump and signal are propagating along the same direction, counterpropagating for the opposite and a hybrid architecture in which both pumps are employed. Copropagating scheme offers in general a better NF because of the signal along the fibre is maintained at a higher power level preventing the OSNR to degrade; however it may introduce problems related to non linearities arising from the high power pump and signal beam at the input of the fibre. It is also suffering from higher relative intensity noise (RIN) transfer because of the two radiations are propagating in the same direction and the polarisation dependence of the gain is more pronounced. On the other side the counterpropagating system provides a higher NF because of the lower power level reached by the signal along the link, but has more tolerance to RIN transfer (typically three order of magnitude difference in the acceptable pump fluctuation frequency) and polarisation dependence coming from the average effect of two optical beams propagating in opposite directions. When considering network topologies like PONs counter propagating amplifiers may also offer the advantage to place the pump lasers at the receiver side of the network where an active node is already existing, without the necessity to place new cabinets along the transmission link. Fig. 3.9 shows the power of the signal along the fibre for different percentages of co and counter propagation pump power.

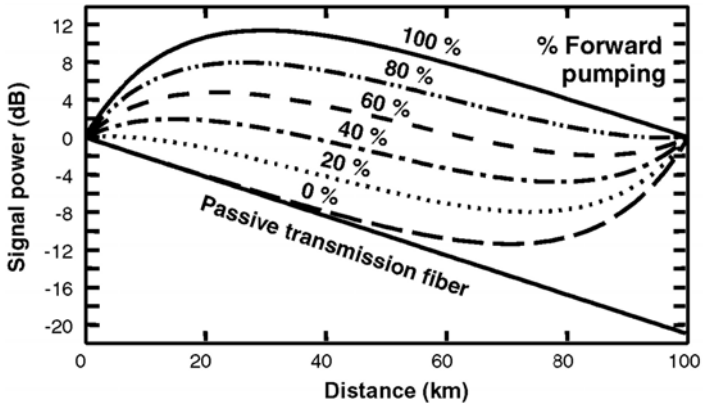

Fig. 3.9: Signal power evolution along the fibre for various pumps configuration [7]

The main cause of OSNR degradation in all cases is the amplified spontaneous emission (ASE) noise which is an unavoidable characteristic coming from the amplification of

spontaneous Raman scattering.

A remarkable feature of all Raman amplifiers is the possibility to design an arbitrary shaped gain profile by carefully planning the pump profile. Multiple pump lasers at different wavelength can be employed to engineer the resultant gain spectrum. That means that the only limit to the take in account, beyond the attenuation coefficient of the fibre, is the availability of high power lasers at the desired wavelength and does not depend on the material energy levels as in the case of xDFA amplifiers which rely on rare earth emission linewidth (Fig. 3.10)

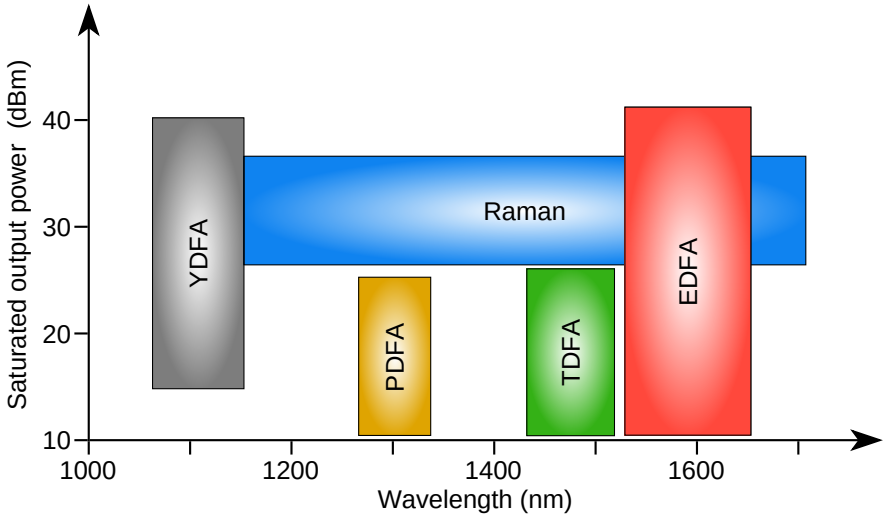

Fig. 3.10: Wavelength bands of amplification covered by xDFA amplifiers and Raman

When designing these broadband amplifiers the strong Raman interaction between pumps must be considered because the shorter pumps amplify not only the signal but also the longer wavelength pumps, so the powers have to be distributed carefully. Ultra broadband gain amplifiers have been demonstrated with this approach (Fig. 3.11), bandwidth greater than 200 nm have been reached [16], unimaginable to obtain with EDFAs.

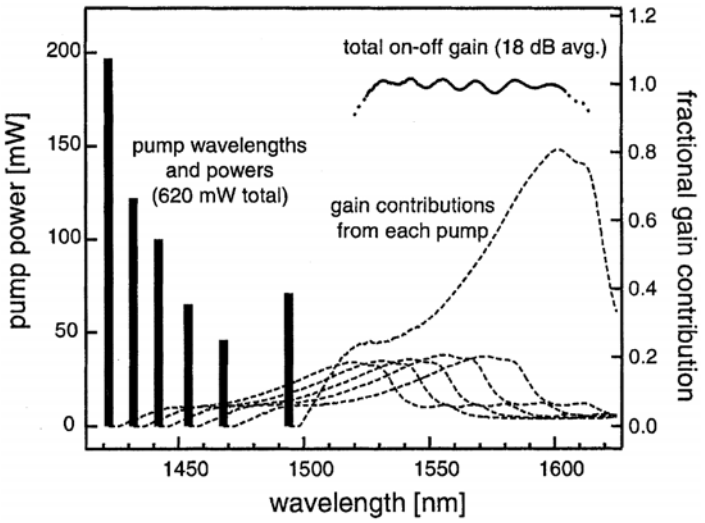

Fig. 3.11: Example of broadband amplifier obtained with multiple Raman pumps

3.4 Characterisation of quantum dot laser diodes

From the previous sections we have seen how Raman amplification needs high power laser diodes to supply an appropriate pump signal. In this work new QD lasers are used for that purpose seen that they can provide very high fibre coupled optical power and that new diodes are available at emission wavelengths suitable for amplification of the XG-PON upstream band (1260-1280 nm).

3.4.1 Pump specifications

The analysed pump lasers are newly research devices designed for application in Raman amplifiers due to appreciable characteristics such as low noise, temperature insensitivity, reduced non-linearities, high efficiency [17] [18] [19] [20]. The compound semiconductor material system is based on InAs/GaAs, with indium arsenide QDs in gallium arsenide with aluminium gallium arsenide barriers, all on gallium arsenide substrates. The lasing wavelength window for this system is between 1064 nm and 1320 nm, controlled by QD size, distribution, and indium concentration. Thus, these QD lasers fill the wavelength gap between quantum well (QW) lasers based on either GaAs (< 1100 nm) or InP (> 1300 nm). Furthermore, despite the relatively low concentration of the discrete gain medium, compared for example to continuous QW layers, QD enable high power devices with high wall plug efficiency [21].
The particular diodes used in this work have a central emitting wavelength of 1210 nm at which they provide a nominal output optical power of 350 mW. The relevant specifics from the datasheet of the two devices are reported in the Tab. 3.1 and 3.2
The devices come in a standard 14 pin butterfly package with diode temperature controller and optical output coupled in a pigtail fibre; the latter is a polarisation

Parameter	Value	Unit
Minimum operating output power	350	mW
Wavelength shift with fibre Bragg grating (FBG) temperature	7	pm/°C
Operating temperature range	15 - 40	°C
Max forward current	2000	mA

Tab. 3.1: Laser diodes specifications

Device name	Threshold current (mA)	Mean wavelength (nm)	3 dB Spectral width (nm)	Slope efficiency (W/A)	Polarisation extinction ratio (dB)
A3	115	1210.6	0.81	0.44	20
A7	119	1210.7	0.76	0.4	19

Tab. 3.2: Laser diodes tested parameters

maintaining fibre (PMF) PM980, which preserving the polarisation state in output from the laser, will provide a higher power coupling efficiency in the setup configuration we will introduce later. The emission wavelength is also stabilised with an external FBG in the fibre pigtail placed at 80 cm from the chip. The low wavelength shift of the FBG with the temperature assures stability wavelength operation in a wide range of temperatures of the output fibre, thus a strictly temperature controlled operation environment is not needed.

3.4.2 Optical spectrum features

The power spectral density distribution of the two lasers was analysed using an optical spectrum analyser (OSA). The measurements were acquired for the recommended operation bias current of 900 mA and to quantify the effect of the chip temperature on the optical spectrum the analysis were repeated for many temperature values in the recommended operation range. In the graphs of Fig. 3.12, 3.13, 3.14, 3.15 the spectral power density of the diodes are shown for a 20 nm and 120 nm span, in which the respective OSA resolutions of 0.05 nm and 0.5 nm were used, measured for different operation temperature.

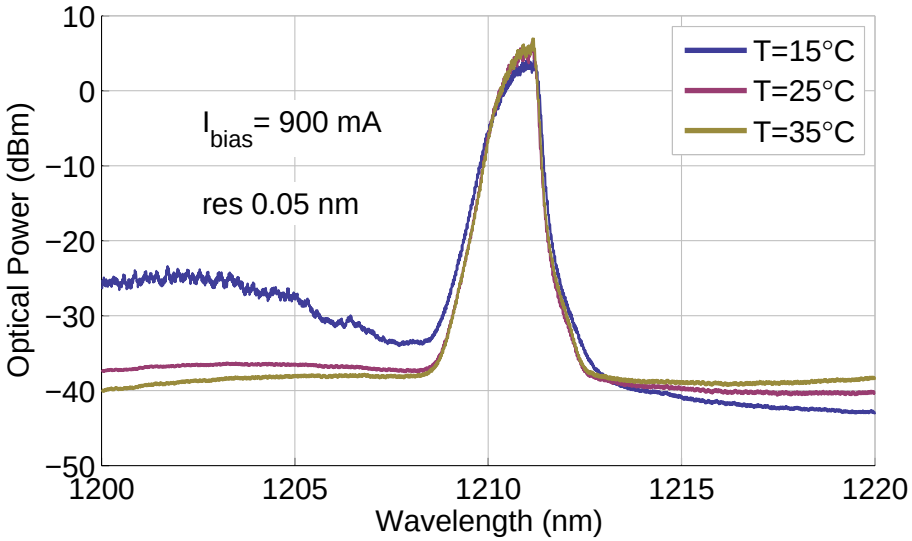

Fig. 3.12: Spectrum of A3 laser diode over a 20 nm span

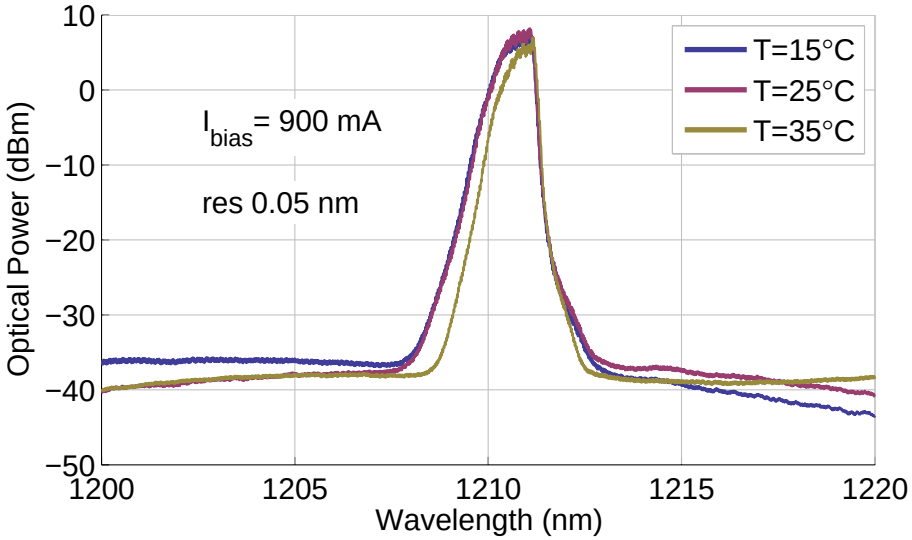

Fig. 3.13: Spectrum of A7 laser diode over a 20 nm span

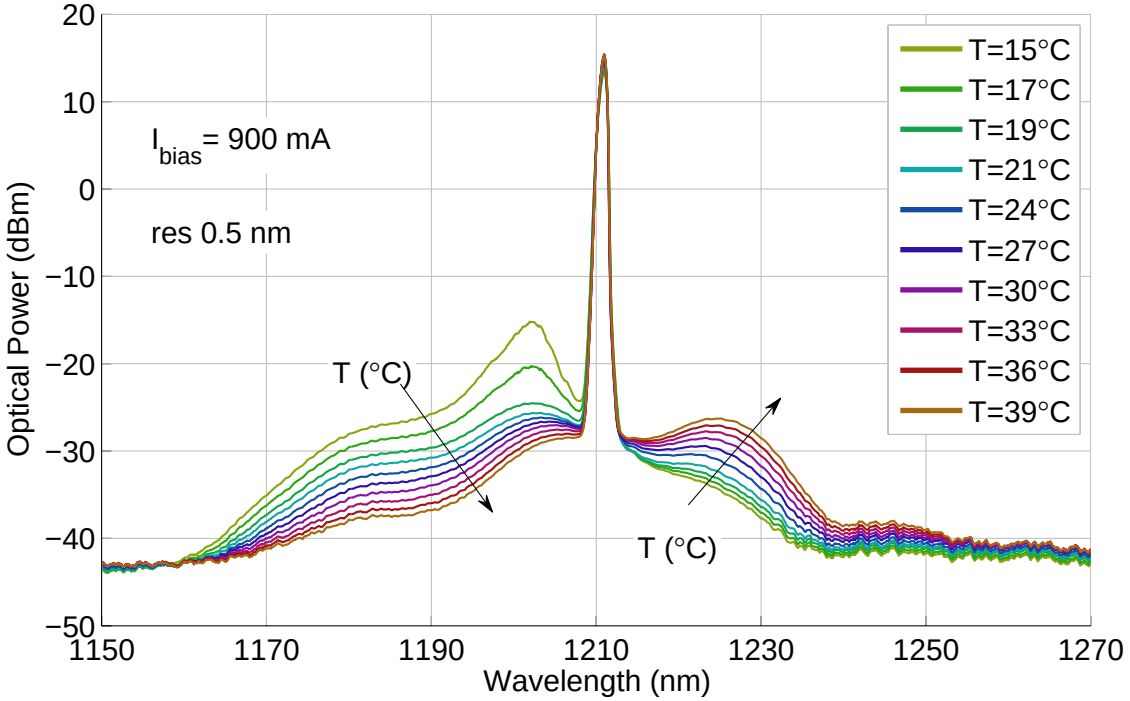

Fig. 3.14: Spectrum of A3 laser diode over a 120 nm span

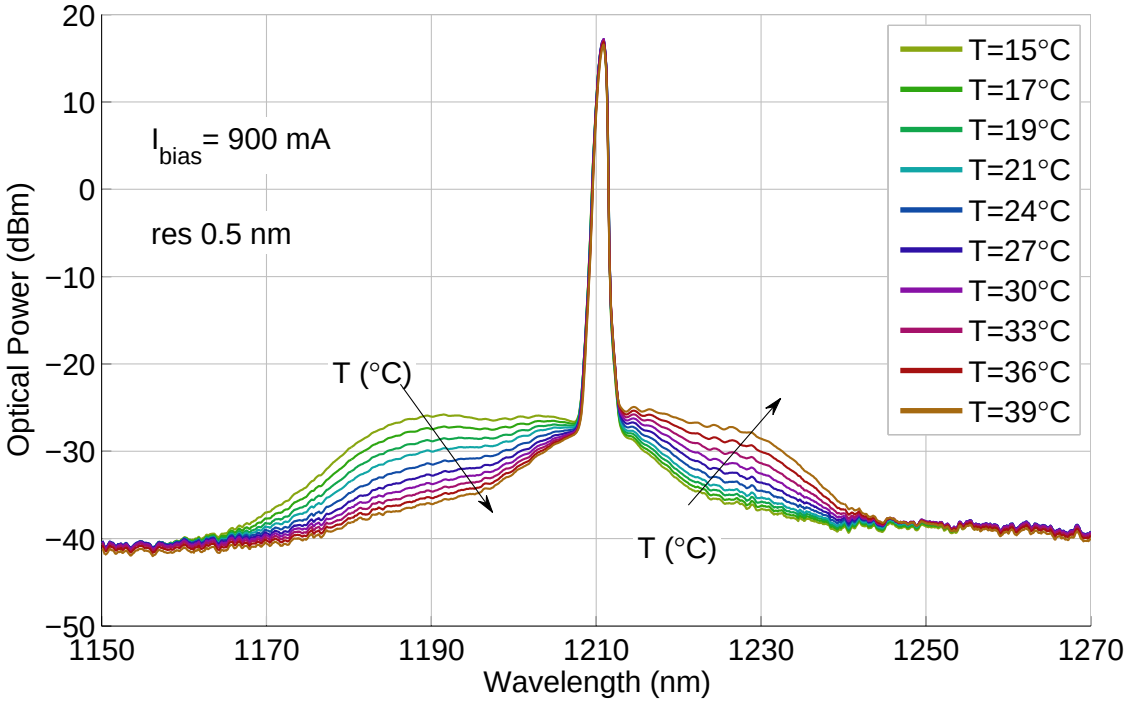

Fig. 3.15: Spectrum of A7 laser diode over a 120 nm span

As clearly appears from the figures the diodes are showing variation in the out of band spectrum for different temperatures but not appreciable shifts for what regards the emission wavelength, confirming the temperature insensitivity of the QD lasers. The devices show a slight narrowing of the bandwidth as the temperature increases, with different magnitude of the effect between the two, and not significant variations in the peak power. When they are operating at safe temperature values the out of band noise is contained and the side mode suppression ratio (SMSR) is well beyond 35 dB. That means that there is no need for a high precision, and thus expensive, temperature control of the pump to avoid degradation of performances related to its optical frequency.
The broadband of the lasers is a desired effect designed to avoid high reflection loss from stimulated Brillouin scattering (SBS) when injecting a high power beam into the fibre, thus to prevent important pump depletion to occur in the first span of the fibre. Designing a pump with linewidth way larger than the SBS bandwidth, which can vary from 20 to 100 MHz in silica SMFs, will cause the Brillouin gain to be reduced to a negligible magnitude [22].

3.4.3 Light-current curves

After the spectral features investigation a light current (LI) characterisation of the two lasers has been carried out. This curve shows the trend of the optical power emitted by a laser as a function of its forward current and was obtained monitoring the output power when varying the injected bias current from 0 mA up to the maximum value of 1700 mA, while maintaining the chip at a constant controlled temperature. The LI measures have been repeated for different temperature values of the chip to quantify how threshold current and output power are affected. The results are reported in Fig. 3.16, 3.17.

The two lasers show a slight different max power, as expected from the datasheets, but the general behaviour as a function of the temperature shows low sensitivity for a wide range operation conditions, especially if compared with usual distributed feedback (DFB) devices. The lasers do not show a strong temperature dependence, but while the threshold current in both devices is monotonically increasing with that, the output optical power shows small amplitude changes and does not follow a well defined trend, showing different variations between the two lasers. However considered in a dB scale these variations are contained and attributable to differences coming from the fabrication process; it also has to be remembered that certain variations in performances are acceptable given that these are new research devices and the use of QD technology is relatively recent.

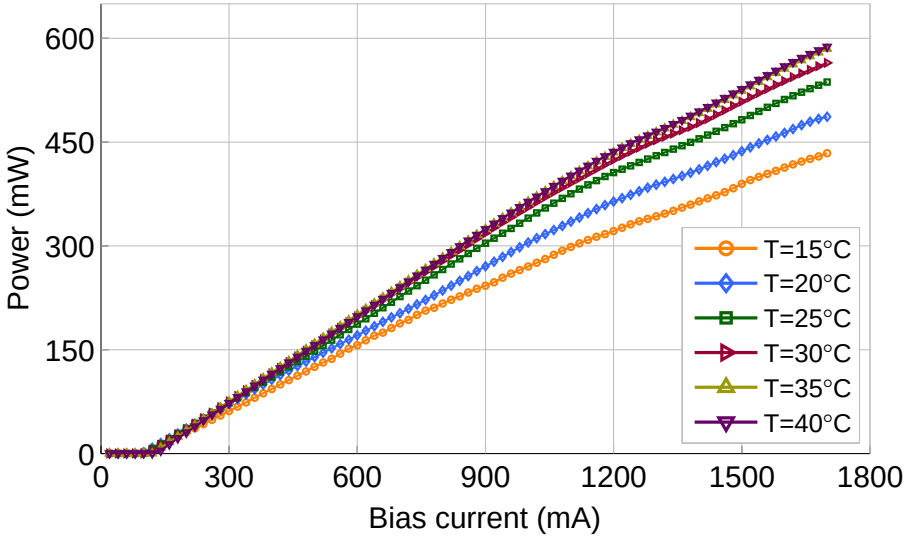

Fig. 3.16: LI curve of A3 Laser diode

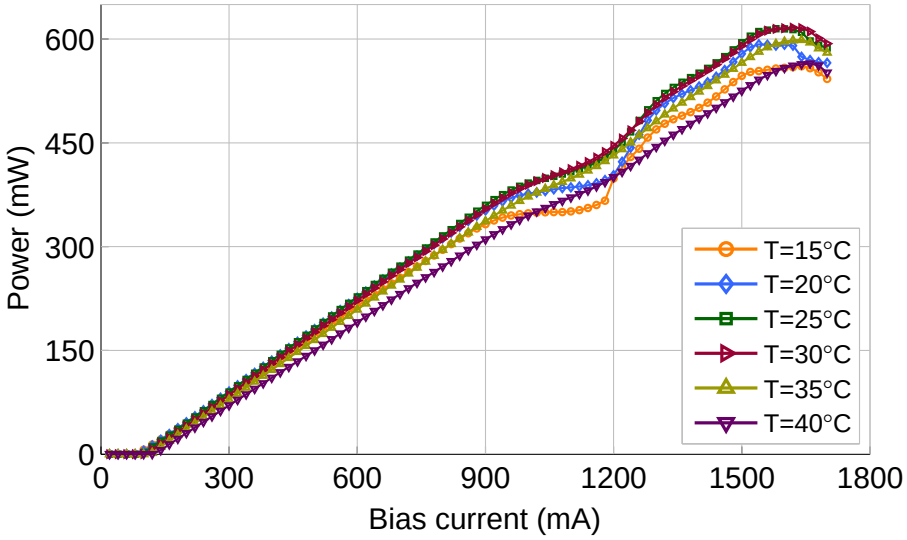

Fig. 3.17: LI curve of A7 Laser diode

3.5 Raman pump module

The Raman reach extender module was built using the two lasers characterised in the previous section. As seen in the introductory part the Raman effect is dependent on the polarisation state of the pump beam and the probe signal, even if we do not expect this to be important in a backward propagation architecture. Hence the pump module includes the two devices combined with a polarisation beam combiner (PBC) as shown in Fig. 3.19. Employing this particular component the pump output signal gets distributed on both the polarisation axes reducing polarisation dependence of Raman gain. The second reason for using this component is that this design is advantageous to maximise the power coupling efficiency; given that the lasers are equipped with PMF

pigtail and have a specified polarisation extinction ratio (PER) in excess of 15 dB, negligible losses of power in the orthogonal polarisation state filtered by the PBC are assured. In this way a higher pump power can be reached and the lasers can be driven at lower bias currents, away from the maximum limit and thus ensuring better slope efficiency, lifetime and reliability.

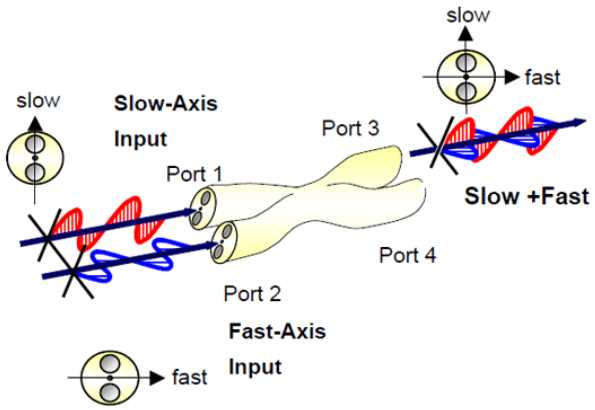

Fig. 3.18: Polarisation beam combiner diagram

The reach extender scheme also needs a coarse wavelength division multiplexing (CWDM) to inject the pump beam into the OTL fibre while preserving the upstream optical signal for the OLT side receiver; the CWDM component used offers the feature to combine two optical band in a common port output and filter its incoming signal splitting it in two bands of interest; in this way the XG-PON upstream band (1260-1280 nm) is separated from the pump backscattered signal (1210 nm) which seen the high pump power can be remarkable when compared to the upstream flow.

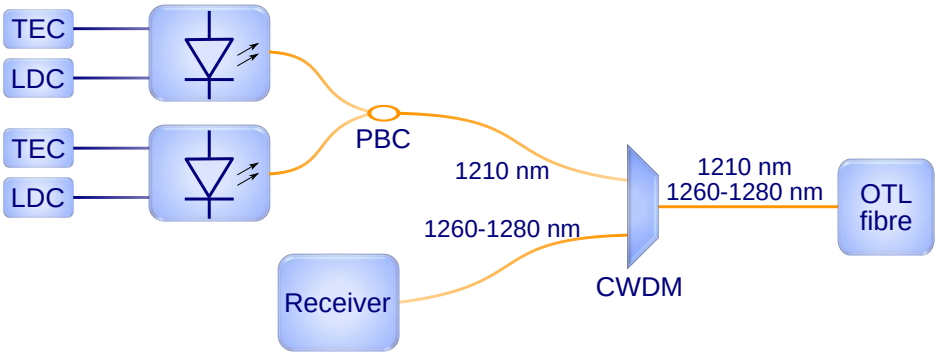

PBC: polarisation beam combiner
TEC: temperature controller
LDC: laser diode controller
CWDM: coarse wavelength division multiplexer
OTL: optical trunk line

Fig. 3.19: Setup diagram of the Raman pump module

Once the Raman pump module was setted up another LI characterisation was carried out, this time monitoring the pump optical power after the CWDM component; in

this way the insertion losses and eventual other non linear effects arising from the PBC and CWDM filter were taken in account and thus the effective power that will be injected into the OTL fibre was measured.
The measurement process for the LI curves and the parameters examined range of interest was the same described in the previous section; obtained results are reported in Fig. 3.20, 3.21

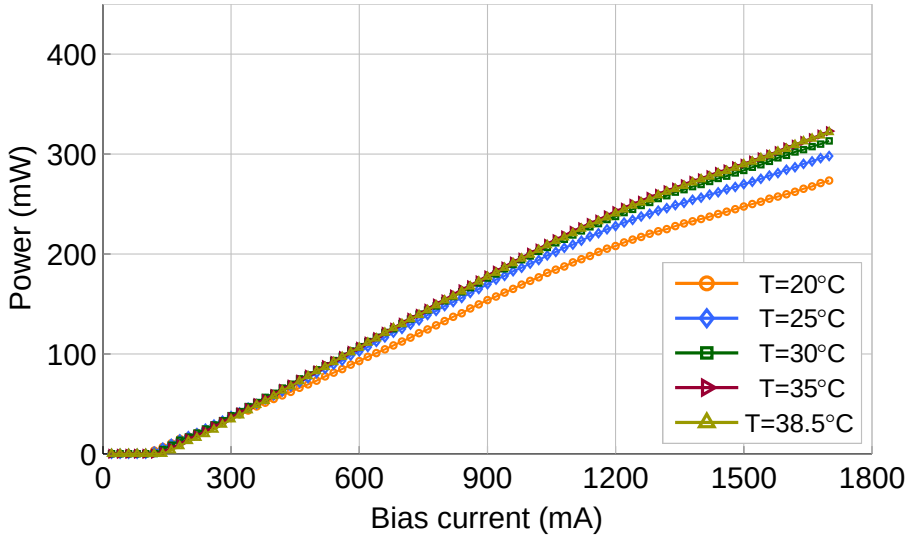

Fig. 3.20: LI curve of A3 device measured at pump module output

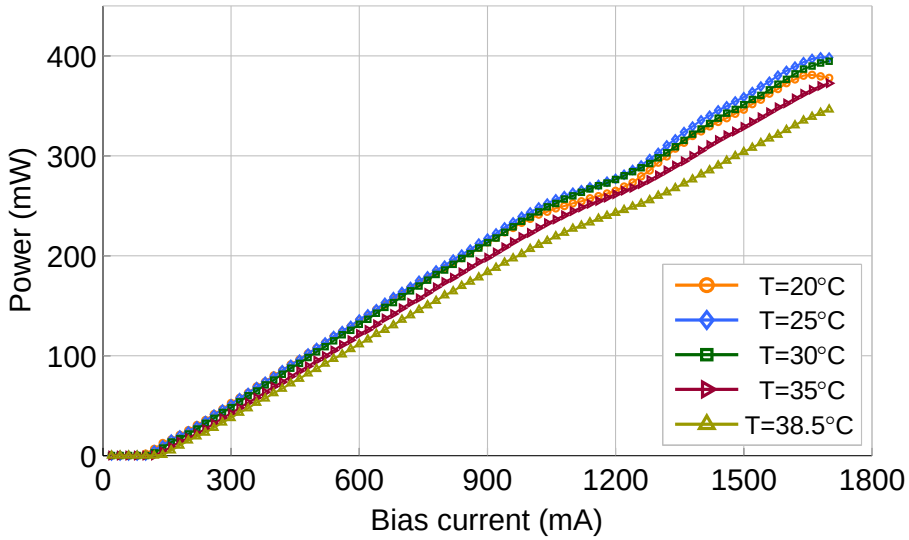

Fig. 3.21: LI curve of A7 device measured at pump module output

As it can be seen from the figures, once taken in account of a certain power offset due to the insertion losses of the passive components, a similar trend to the LI curves of the single lasers is confirmed. Noticeable discrepancies are visible only in a chip (A7) for bias current near to the maximum advised operation values; that may suggest a

slight degradation of the PER for high bias currents or some non linearities in the response of the PBC and CWDM for high input optical power.
To further evaluate the chip temperature influence on the emitted optical power, the latter has been also monitored for some fixed bias current values by sweeping the temperature between the advised operating values at 1 °C steps, obtaining the trends reported in Fig. 3.22, 3.23

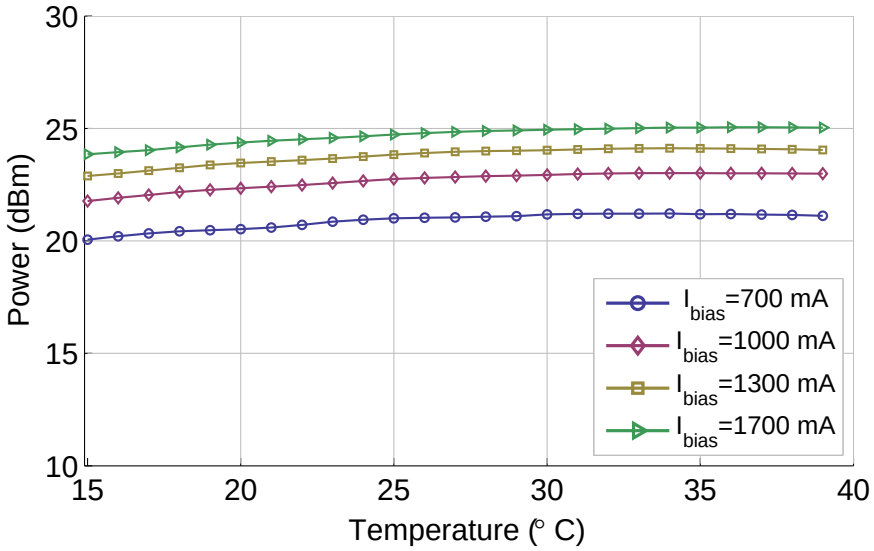

Fig. 3.22: Light power versus temperature of A3 device measured at pump module output

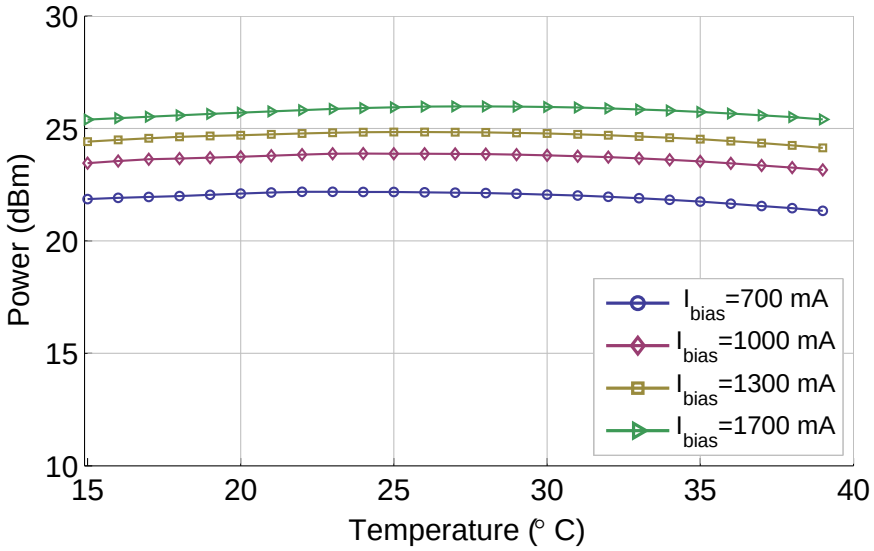

Fig. 3.23: Light power versus temperature of A7 device measured at pump module output

The graph shows a slightly different trend between the two lasers, but the entity of the dependent variation is relatively small showing a better temperature stability with

respect to other commercial lasers based on heterostructure or QW technology. That also suggests that an accurate selection of the operating temperature for every laser is not necessary to reach the highest optical power.
The pump module was capable to generate a maximum output power available in input of the OTL fibre of 28.8 dBm, obtained driving both lasers at 1700 mA bias current. Other operating pump power values has been measured driving the two lasers with different bias currents corresponding to the same output power, thus to guarantee a symmetric polarisation state in output of the Raman reach extender.

3.6 Raman reach extender gain

In this section the performances of the pump module of which above are evaluated in term of the gain that is induced via Raman amplification on a probe signal at various wavelength. From the theory we expect the Raman gain to have a peak in correspondence of the Stokes shift frequency of 13.2 THz [14] from the pump signal, which in O-band means about 70 nm shift towards a higher wavelength, but to fully examine the gain spectrum profile a wide range of probe wavelengths has been investigated, comprehending the entire XG-PON upstream band (1260-1280 nm). The setup depicted in Fig. 3.24 has been used to measure the induced Raman gain in a 50 km long SMF.

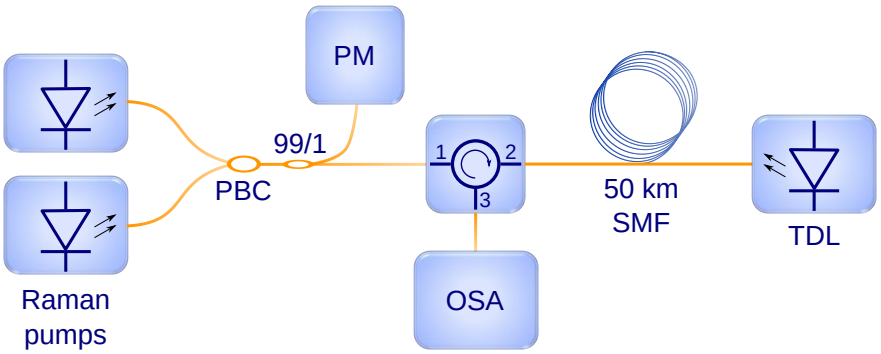

Fig. 3.24: Experimental for evaluation of distributed Raman gain through 50 km fibre

In this setup the Raman pump is injected in the fibre at 1210 nm and counter propagates with respect to the probe signal. The latter is generated by a tunable laser diode (TLD) emitting in a range of wavelength from 1250 nm to 1320 nm and sent into the other extremity of the fibre. At the reach extender side a circulator injects the pump

beam into the fibre and drives the incoming signal to an OSA, also preventing it to enter the reach extender module. The OSA measures with the needed accuracy the power spectral density of the incoming signal, and that is necessary to discriminate the signal power at the specific wavelength being analysed from other sources. In fact because of the wide spectrum of Raman gain and the considerably high power of the pump the consequent ASE and pump backscattering arising would make unreliable a measurement obtained from a power meter which integrates the power all over the optical spectrum.

The gain of a distributed Raman amplifier, given the different nature with respect to a discrete amplifier, is defined as ON/OFF gain which is the difference in the probe signal power observed with the Raman pumps turn on and off. Thus, in the experimental setup, the power of the signal generated from the TLD has been measured at first with the pump off, when it is experiencing only the losses due to the fibre attenuation. Hereafter its power has been monitored with the OSA, for increasing pump powers. This process was carried out for the wavelength range 1250-1320 nm in 2 nm step resolution.

The results obtained are shown in Fig. 3.25 where multiple lines of gain as a function of wavelength are plotted corresponding to increasing pump powers, and Fig. 3.26 where the gain magnitude is shown in function of the pump power for some significant wavelengths.

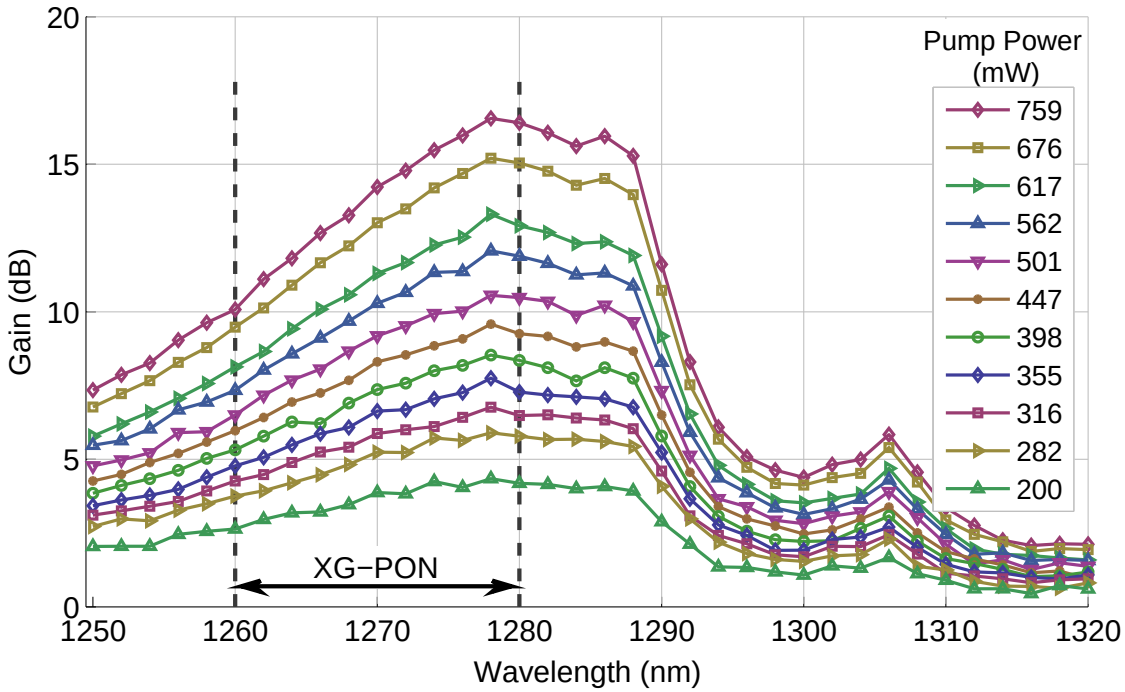

Fig. 3.25: Raman gain for different pump powers in function of wavelength

As can be seen from the resulting data the Raman gain shows a peak of 16.5 dB, when the maximun pump power of 28.8 dB is used, for the probe signal at $\lambda = 1278$ nm,

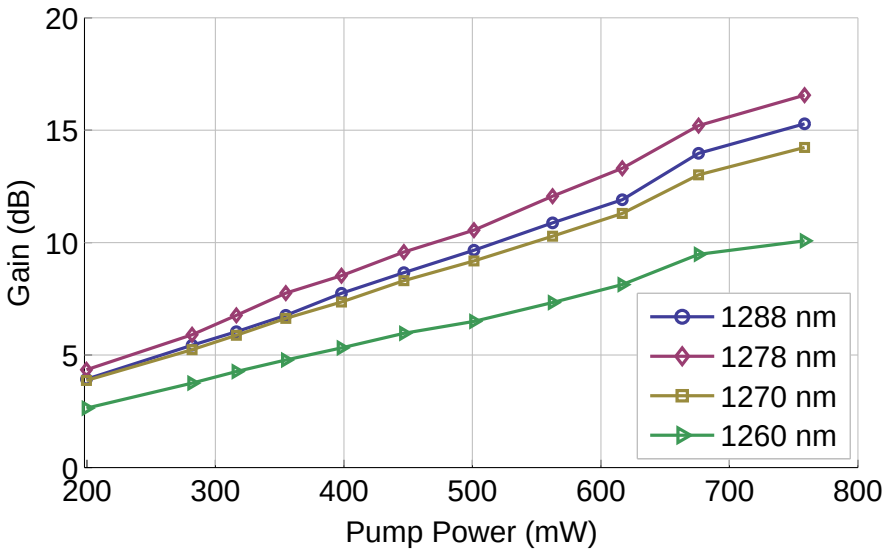

Fig. 3.26: Raman gain for various wavelengths in function of pump power

which corresponds to a shift of about 70 nm from the pump beam, as expected. The spectrum profile reflects the usual Raman spectrum observed in silica SMF fibres, showing a 20 nm wide band region in which the gain is contained in a 2.5 dB flatness range. From Fig. 3.26 the gain also appears to increase with linear proportion to the pump power expressed in mW, trend which remains similar for all the wavelengths analysed, where only the magnitude of the gain differs.

This result is not the best scenario for the XG-PON upstream band, allocated by the standard in the interval 1260-1280 nm, given that the gain at 1260 nm drops at 10 dB. Anyway we can infer a remarkable aspect in the gain spectrum profile: because of its broadband and flatness properties, by moving the pump signal 10 nm lower we would expect the high gain region to correspond to the desired interval. QD lasers with similar characteristics are available at the wavelength 1200 nm and the results suggest that they can be a viable solution for distributed amplification in the entire XG-PON upstream band, without need of more expensive multiple pump Raman amplifiers.

To confirm the expected advantage of the backward pumping configuration in regards to the influence of the polarisation of pump and probe signal on the gain, a similar measurement was repeated with only one of the lasers active at a time and then with both, supplying in every case the same amount of total optical power.

Fig. 3.27 shows that the three measured traces are practically overlapping, meaning no dependence on the pump polarisation state of the Raman on/off gain. The probe signal polarisation was not controlled and free to evolve in the fibre propagation, as the ONU traffic would be like.

Another analysis was carried out on the data to reveal whether the Raman amplification was varying its efficiency in the different conditions: the Raman gain coefficient $g_r \left[\frac{1}{Wkm}\right]$ was calculated for the various pump powers, from the effective length ex-

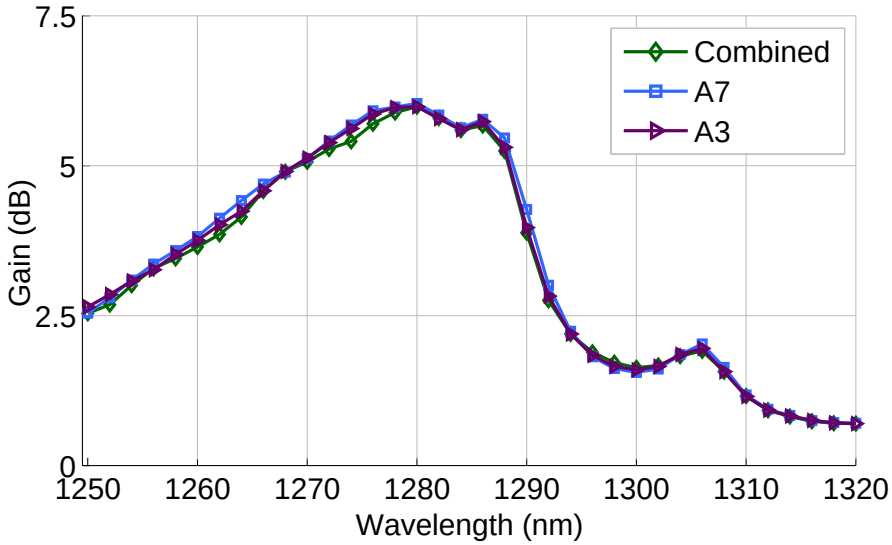

Fig. 3.27: Raman gain spectrum for different pump devices activated

pression in 3.5 and the measured gain expressed as [7]

$$G_{ON/OFF} = \frac{P_s(L) \text{ with pump on}}{P_s(L) \text{ with pump off}} = e^{g_r P_0 L_{eff}} \tag{3.6}$$

The results are shown in Fig. 3.28 and are visibly corresponding for every injected power, suggesting no important penalties coming from non linearities at higher power. We have seen that the pumps have been designed with a broad line to avoid SBS and the counterpropagating configuration does not cause the signal to reach high power level and thus encounter issues related to double Rayleigh backscattering (DRB). Comparing the obtained results with others present in literature [11] [12] [13] we can see how the gain measured in this experiment is in line with previous works in the gain magnitude corresponding to a certain pump power. Considering that those works were conducted at higher wavelengths it suggests that even if the pump signal at 1210 nm is well below the single mode cut off wavelength of the SMF (1260 nm) there is no important efficiency loss due to multimode propagation of the pump and reduced mode coupling with the fundamental one of the signal.

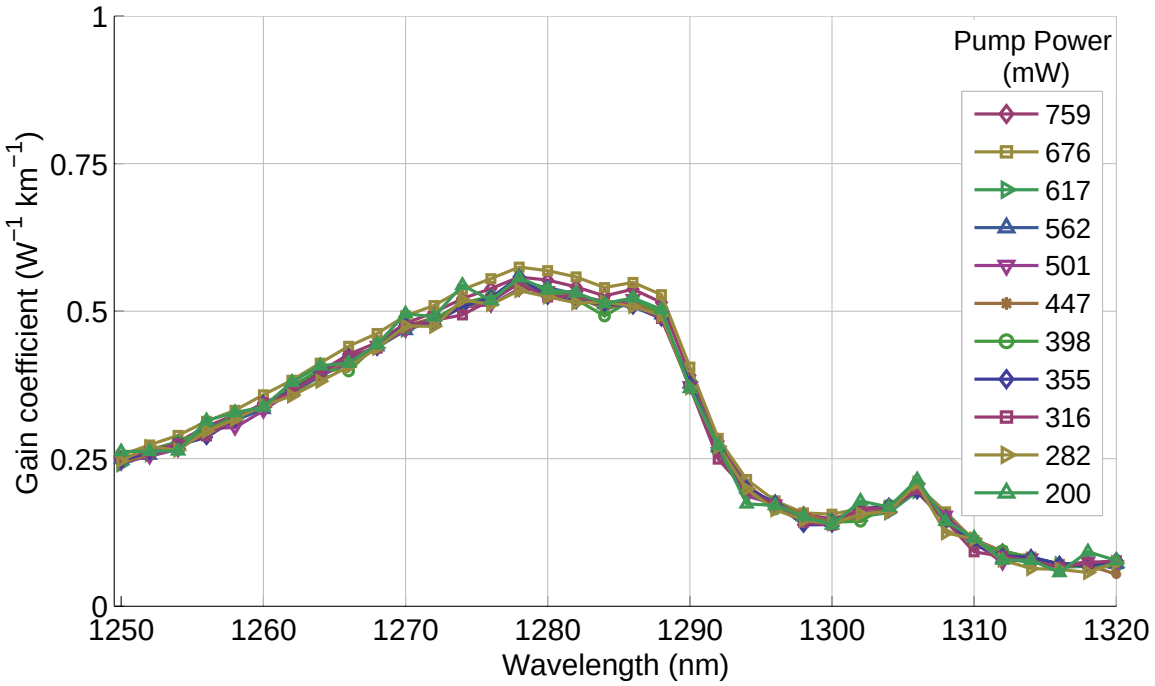

Fig. 3.28: Raman gain coefficient for different pump powers as function of wavelength

3.7 Conclusions

In this chapter a brief introduction on Raman scattering and amplifiers technology was proposed. Afterwards the available QD pump lasers were characterised in their main aspects of interest for use in reach extender module, showing promising features in both optical power and wavelength spectrum, along with appreciable temperature insensitivity. The induced Raman gain on a probe signal in 50 km of SMF was quantified and found to be between 10 and 16 dB in the band of interest. The gain efficiency was compared for increasing pump power and with previous works suggesting no major impairments arising in the system. From these initial results it would be possible to predict that the Raman gain values obtained for every wavelength and pump power will correspond to an equivalent increase in the link power budget. However seen the complexity of the network architecture and the challenging points regarding the burst upstream transmission in XG-PON this can be considered only a starting point in the analysis, important to outline the entity of the reach extension performances that can be expected.

Chapter 4

Measurement System Design

4.1 Introduction

In this chapter we will explain the methodology adopted to evaluate the performance of the Raman reach extender, in an emulated XG-PON upstream application. In the previous chapter, some preliminary results were obtained with important consequences on the aim of this work, relative to the achievable Raman distributed gain. Along with that also the needing of a properly structured setup for the evaluation of the Raman amplifier under study emerged, in fact a deeper analysis is necessary to evaluate possible impairments arising in a real transmission link.
In section 4.2 a first experimental setup that was built to examine the upstream transmission in continuous mode from an ONU which emulates tunable losses in the ODN and transmission over a 50 km SMF is presented. Afterwards in section 4.3 we will show the implementation of a setup which provides effective emulation of a simultaneous transmission from different ONUs experiencing independent ODN losses and injecting TDM burst traffic in the common OTL.

4.2 Continuous mode experimental setup

This first setup allows the characterisation of Raman amplification impact on an upstream signal that experiences different losses corresponding to different ODN configurations, such as variable length of the fibre and different number of splits before reaching the OTL. The system is depicted in Fig. 4.2

In the experimental setup the optical signal coming from the client transmitter at ONU side is generated by an uncooled DML emitting at the central wavelength of 1270 nm. This DML is a multiple quantum well (MQW) buried heterostructure distributed feedback (DFB) laser, packaged in a transmitter optical subassembly (TOSA). These laser diodes are commercially available devices which come at contained price and thus suitable for employment in low cost ONU side transmitters, guaranteeing uncooled wide-temperature TDM and CWDM applications, operating up to 85 °C temperature and 10.7 Gb/s modulation speed. The data mod-

Fig. 4.1: DML

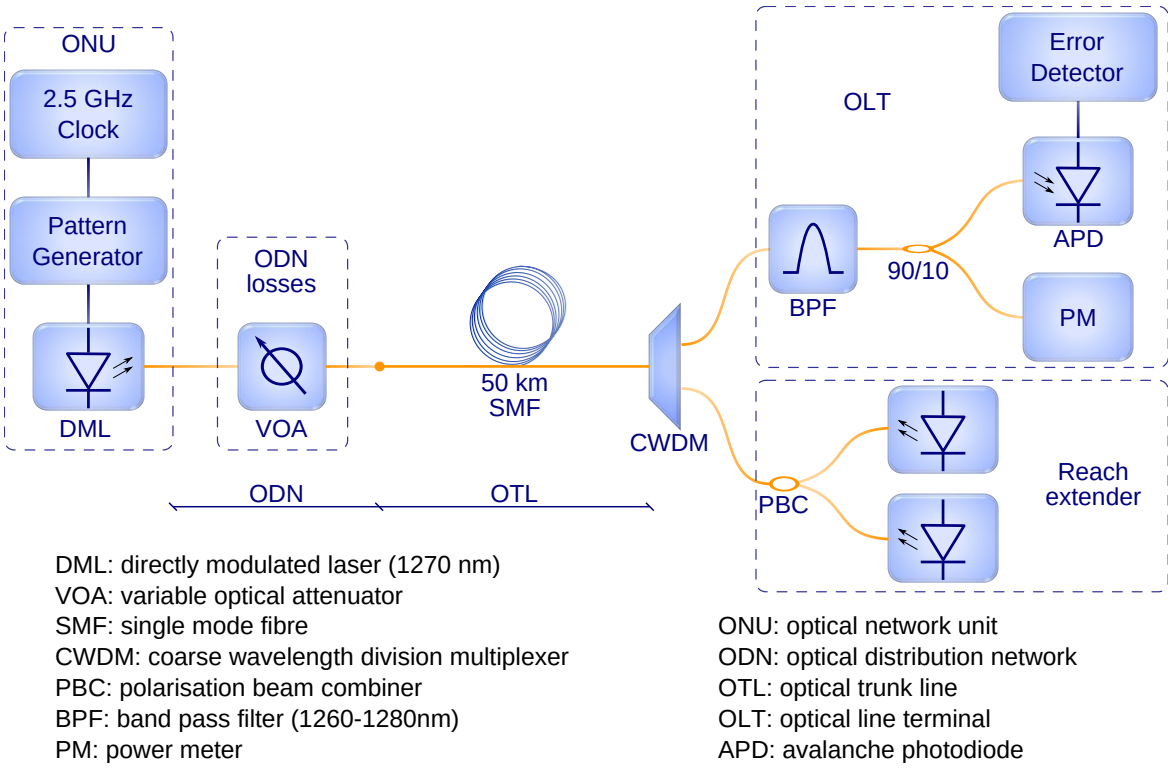

Fig. 4.2: Test bench for continuous mode operation

ulation is provided by a commercial driver controlled by a pattern generator (PG) operating at 2.5 Gb/s and transmitting a pseudo random binary sequence (PRBS), in this case PRBS7.

Different ODN losses are emulated adding a controlled attenuation with a variable optical attenuator (VOA) after the DML, that translates in adjusting the optical power launched in to the OTL fibre. The different input powers can be attributed to different ODN cases that are being compared, including dissimilarities in the transceiver lasers, different path lengths of the ODN fibre and different number of optical splitters that are passed before reaching the OTL. On the other extremity of the link the Raman pumps are used in the counter-propagating configuration discussed before and the pump signal is injected into the OTL fibre using the CWDM component of the pump module described in 3.5. The port of the CWDM component which allows the incoming upstream traffic is connected to a passband filter with 20 nm wide passband centred at 1270 nm, selecting the XG-PON standard upstream band. The output signal is then divided with a 90/10 coupler whose 10% port is connected to a power meter (PM) and 90% port to an electro optical receiver. The latter is a commercially available transceiver equipped with an avalanche photodiode (APD) with measured sensitivity of -33 dBm for a bit error rate (BER) value of 10^{-9} at 2.5 Gb/s, which hence allows the reception of a low power optical stream. This transceiver converts the optical signal into an electric one generated by an internal circuitry with a constant voltage level, not in linear proportion with the received optical power. Because the

electrical signal has a constant and high amplitude level (hundreds of millivolts) it is not going to stress the electrical sensitivity of the following components. This signal is then sent to an error detector (ED) equipped with clock data recovery (CDR) and provided with the same logical binary test pattern of the PG. In this way the overall performance of the system is evaluated in term of BER measured at the OLT side as a function of the received optical power, monitored with the PM. Because of the broadband ASE entering the PM a calibration has to be performed for every injected pump power in order to measure the effective power of the signal distinguished from other sources. The downstream signal has not been implemented in this test bench because the wavelength location in L-band (1575-1580 nm) is well beyond the Raman gain bandwidth of the upstream band itself, thus it is not expected to introduce substantial differences in the quantities under evaluation.
With this setup a characterisation in term of BER versus received optical power of the signal can be done working in continuous mode transmission for a wide range of optical input to the OTL fibre and confirm whether the Raman induced gain is constant for a large interval of probe signal power and if the actual data transmission will suffer other penalties. Leading the setup back to a more general representation like the one in Fig. 4.3, a reference BER curve is firstly acquired without any device under test (DUT) and hence used as term of comparison for the measurements. This curve, having introduced only increasing thermal noise, reflects the sensitivity of the APD in the specific operating conditions and will be used as a reference. The impairments introduced by other network components will be evaluated as a penalty expressing the additional power needed at the receiver to guarantee the same value of BER. The constant slope of the curve in Fig. 4.4 suggests no secondary impairments appearing in the reference measure but the added thermal noise. The results obtained with this setup will be showed and discussed later in 5.2.

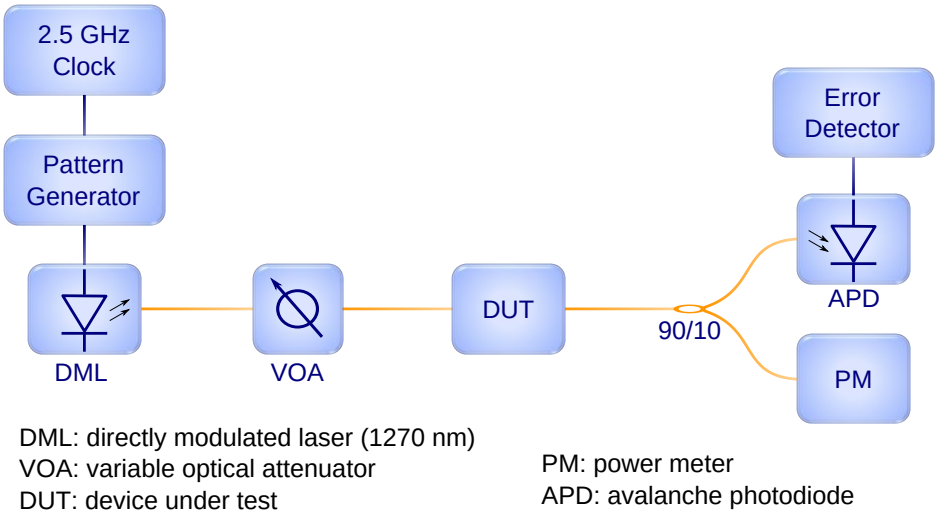

Fig. 4.3: General configuration of continuous mode test setup

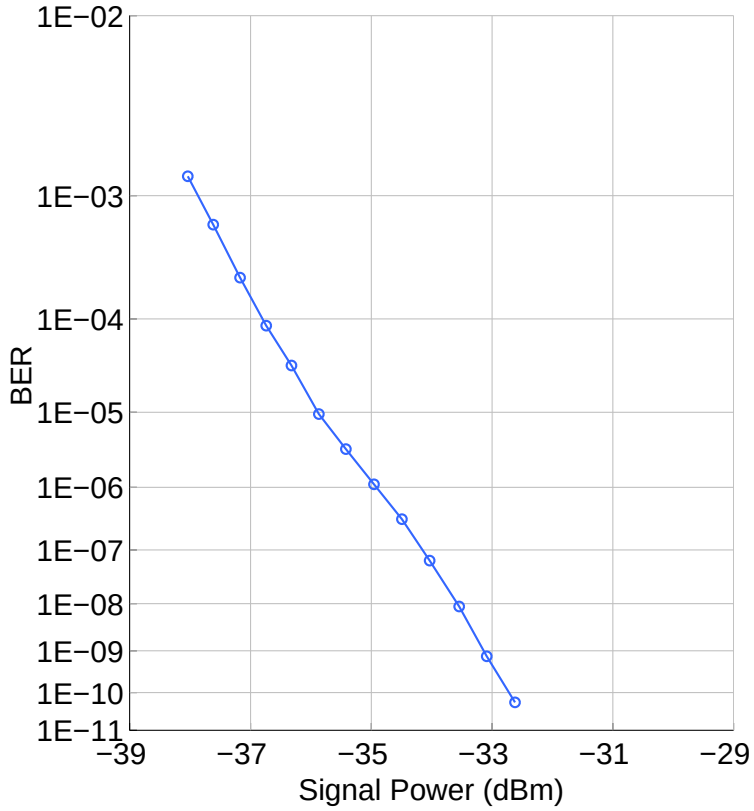

Fig. 4.4: BER reference curve for the APD without any DUT

4.3 Burst mode transmitter

In the previous section we have described a setup to measure the Raman reach extender capabilities in continuous mode transmission. However we know that the real upstream transmission in XG-PON is taking place in burst mode, hence it appears an interesting challenge to conduct a performance analysis in a more realistic scenario to evaluate other impairments arising from interferences between different ONUs. A second more comprehensive experimental setup was thus developed for the emulation of actual burst traffic entering the OTL fibre, with the ability to generate different dynamic ranges; with this one we would be able to quantify whether transients in the Raman gain between consecutive packets with different optical powers, or other aspects, are degrading the performances.

Two different configurations were developed and characterised for the generation of TDM burst traffic, the approaches are described in detail in this section where we will go through the various steps of the respective realization procedures. The first option that will be shown was making use of a SOA working in variable gain mode thus to generate packets with different powers from a single optical beam in input. Afterwards the considered alternative was built up using two independent DML transmitters emulating two ONUs with different assembled characteristics attributable to

the respective network paths and transmitter discrepancies.

4.3.1 SOA based burst transmitter

The first design for the generation of burst traffic was based on the idea of using an SOA with time varying gain, thus to amplify with different magnitude a single modulated probe signal and hence obtain temporally adjacent packets with different average power. We used an SOA optimised for amplification in the 1310 nm optical band, whose input was a 2.5 Gb/s modulated signal at constant power generated by a 1270 nm DML. Biasing the amplifier with a particular time varying function the resulting output will show different optical powers for consecutive temporal slots. The basic concept is outlined below in Fig. 4.5.

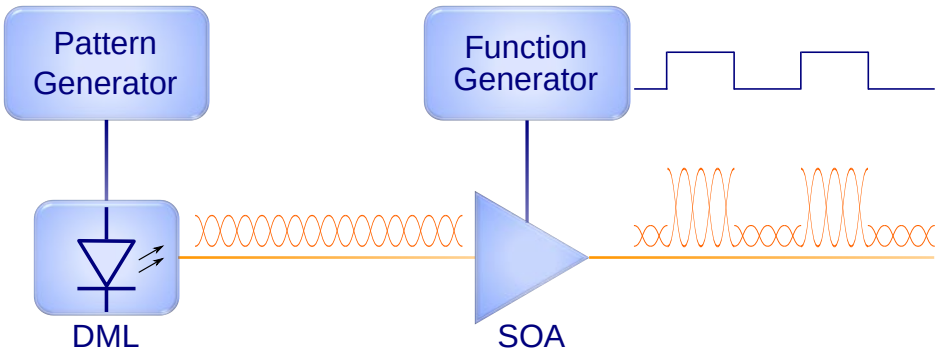

Fig. 4.5: Conceptual scheme of a SOA based burst transmitter

From the introductory chapter we have seen that because of the fast response time to gain variations, a device like a SOA is expected to be suitable for this sort of application, in fact the guard time provided by the XG-PON protocol [23] is long enough to absorb the resulting transients. However to effectively exploit the capabilities of that conceptual design many implementation aspects must be looked after, thus to achieve the possibility of conducting meaningful measurements separately for the two types of packet generated. The setup diagram which puts into practice the sketched scheme introduced earlier is depicted in Fig. 4.6.

The optical signal source was the same DML at central wavelength 1270 nm used in the continuous mode characterisation setup, working at 2.5 Gb/s modulation speed supplied by the PG. This was controlled by a clock generator which was also supplying a 10 MHz reference signal to an arbitrary function generator (AFG) to assure synchronisation between the instruments. The SOA used was an optimised device for amplification in the optical O-band driven by the mentioned AFG with a square wave with two different voltage levels. By linking these two levels to the resultant gains, different dynamic ranges could be generated. We will refer to the two type of packets as loud packet and soft packet, respectively for the higher power and the lower power one. After the SOA a band pass filter (BPF) with bandpass between 1260 and

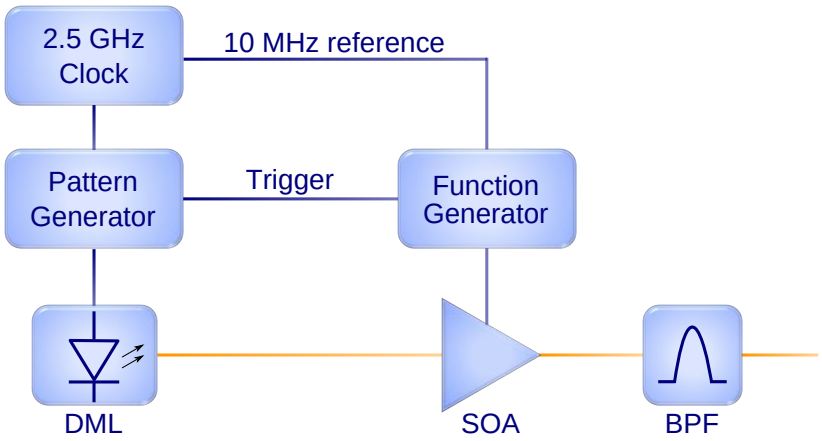

Fig. 4.6: SOA based burst transmitter setup diagram

1280 nm was placed to reduce the ASE total power, removing part of the out of band components. A narrow band filter would have produced better ASE noise suppression. However it was not available at the time of these measurements and moreover, seen that the DML is uncooled and hence subjected to slight shifting in the wavelength, it could have caused uncontrolled attenuations in the signal.
This configuration can generate a stream with two distinct power levels, however simply controlling the envelope function of the gain is not sufficient to then perform meaningful measurements. In order to preserve the knowledge of the bits that belong to one packet or to the other, there must be a timing synchronisation between the PG and the AFG. In order to distinguish and measure the BER of the two incoming streams with the ED, a unique relation between the transmitted data and the correspondent power level must be kept. To satisfy these needs an appropriate binary pattern has been loaded in the PG and a trigger signal was used to control the AFG output synchronisation. This particular binary pattern includes two similar packets corresponding to the different power levels and each of these packets is composed by four fields with the following purposes:

- Guardband: corresponding to the transition time between the transmission of two consecutive packets, it is needed to accommodate the switching transients coming from physical devices and to tolerate synchronisation misalignment between different ONUs. In this case it is a 256 bits long field padded with logical zeros during which the SOA switchs to a different gain value;

- Preamble: this field is filled with a particular pattern which is meant to allow the burst mode receiver to set the appropriate electrical gain based on the packet optical power and for the CDR to lock the clock;

- Payload: the largest part of the packet, this is the portion which actually carries information data from the users, and the one where we are mostly interested in evaluate the BER performances. The information content is here emulated with a PRBS;
- End of burst: a short closure field which adds tolerance to the burst enabling signal and to the global synchronisation of the network where an anticipated start of burst from other ONUs would result in data loss.

The whole pattern is then built accosting two of these packets where the payload is chosen to be PRBS7 for one and $\overline{\text{PRBS7}}$ for the other in order to stress in a similar way both; this choice is useful to easily distinguish them but also to avoid problems with the synchronisation at the ED that will arise if using the same PRBS with correlation related methods. The pattern detailed structure is depicted in Fig. 4.7. In section 4.5 it is discussed a software tool developed during this work which offers an intuitive interface to generate custom pattern, like the one just now shown, with high flexibility.

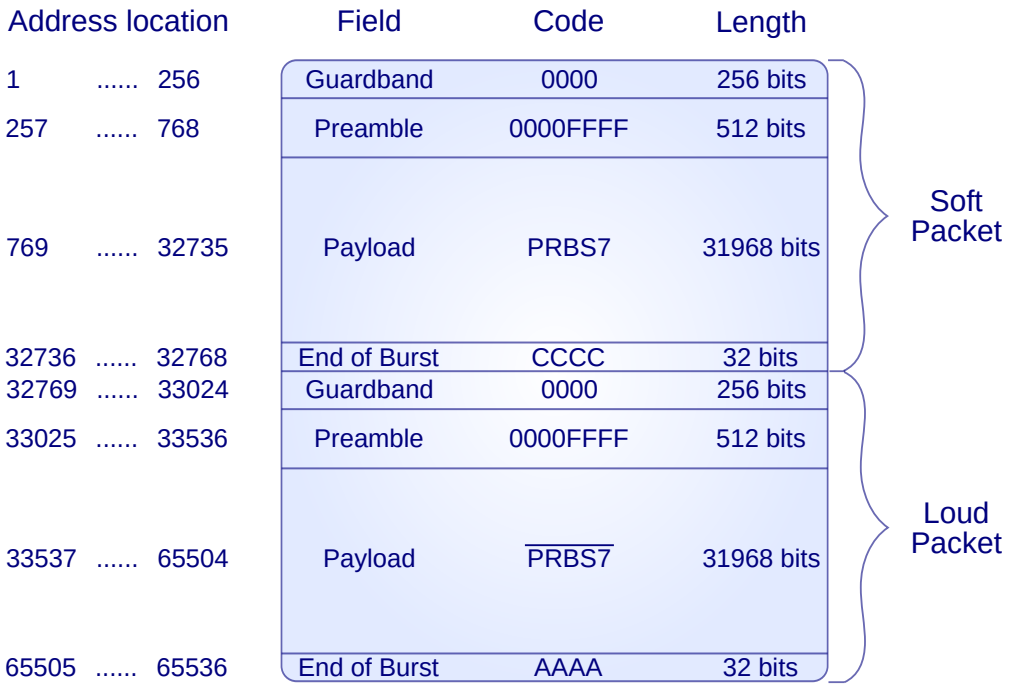

Fig. 4.7: Structure of the pattern loaded in the PG

The waveform generated by the AFG must then be carefully set to match the duration of a single voltage level with the length of a specific packet. In order to keep the system synchronised the AFG was working in burst mode, driven by the PG trigger signal which is sent at every beginning of the pattern transmission. Conveniently adjusting the delay of this trigger to take in account the signals propagation time, the SOA driving function was superimposed with the logical pattern placing the rise/fall time within the guardband field, obtaining the signal time behaviour shown in Fig. 4.8.

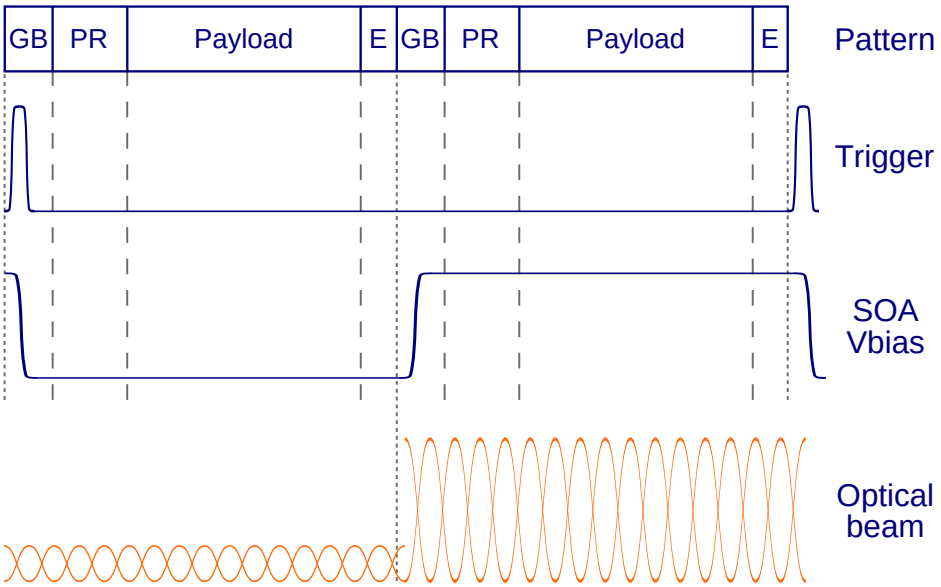

Fig. 4.8: Signals timing scheme of the setup

Examples of the generated signal are shown in Fig. 4.9 where a trace was acquired with a digital communications analyser (DCA) for two values of dynamic range obtained with increasing gap between the driving voltages. The overall performances of the setup will be presented, discussed and compared with the other option in 5.3. We will now continue showing the next burst transmitter scheme.

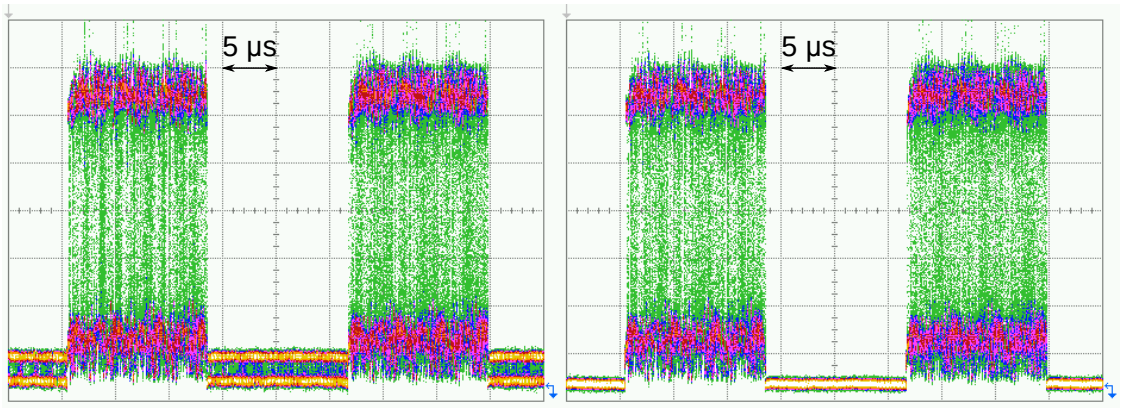

(a) 10 dB dynamic range (b) 20 dB dynamic range

Fig. 4.9: Burst traffic traces acquired with a DCA for two dynamic range

4.3.2 Independent ONU burst transmitter

The second solution developed for burst mode operation focused on obtaining a more realistic scenario to the real operating conditions of a XG-PON system, thus trying to avoid any artificial features added by extraneous devices like the SOA adopted in the previous setup. This new schematic is comprehending two independent ONUs working

separately, emulating different ODN losses and sharing the same OTL.
Two uncooled DFB buried heterostructure MQW DMLs emitting at 1270 nm, similar to the diode used in the previous setup, are used to generate two independent upstream transmissions at 2.5 Gb/s. The relevant parameters of the lasers used in the proposed analysis are reported in Tab. 4.1

Device name	Threshold current (mA)	Wavelength (nm)	Slope efficiency (W/A)	Output power (dBm)
B039	5.9	1269.6	0.078	2.7
B048	5.7	1269.9	0.073	2.3

Tab. 4.1: Laser diodes parameters

The devices are mounted on evaluation boards which provide direct modulation of the lasers from an incoming radio frequency (RF) signal. Two independent PGs supplied with the same 2.5 GHz clock source and working in synchronisation mode are used to drive the two ONUs. The boards have a software interface which offers many configuration settings among which values of bias current and modulation amplitude, acting on the direct modulation process in the way shown in Fig. 4.10. Because lasers with different characteristics can be driven by these boards the mentioned settings can be properly set to provide better performances.

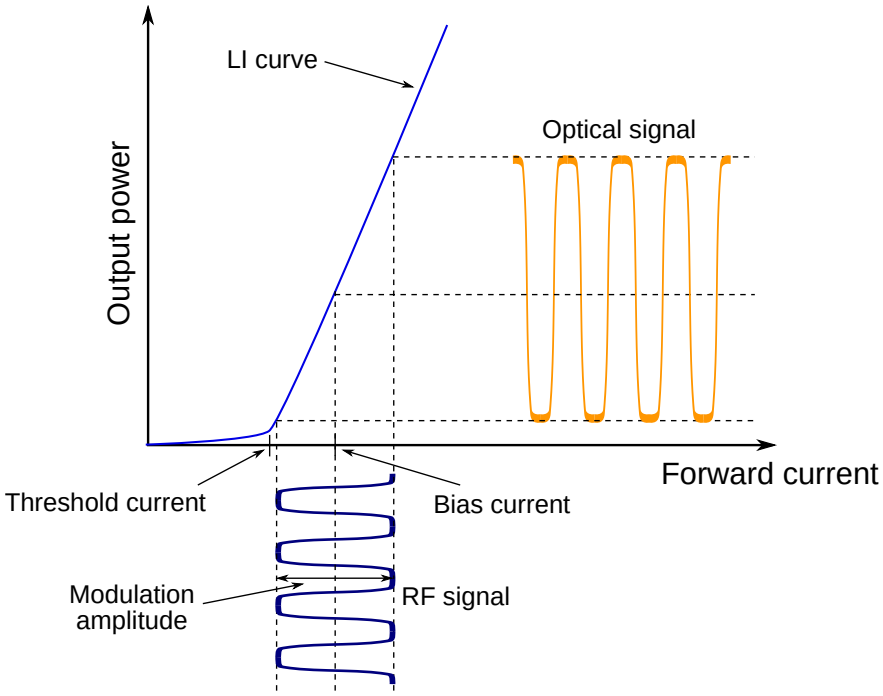

Fig. 4.10: Scheme of laser direct modulation

The two lasers used have slightly different characteristics, hence the transmitters have been tuned to behave similarly adjusting the bias current and modulation amplitude

to control the diodes modulation response. Because of the intrinsic differences and poorly controlled environmental conditions, they are expected to show small differences in performances. That is a realistic situation appearing in XG-PON system, where different ONUs have laser diodes performing differently, with differences in frequency response to the modulation signal, optical power and also emission wavelength. A typical ONU side transmitter, as required in the standard [23], must generate an upstream signal with an ER greater than 8.2 dB and minimum optical power of +2 dBm, which we are able to provide with the mentioned devices. The eye diagrams of the two DMLs for a modulation speed of 2.5 Gb/s are reported in Fig. 4.11, essentially showing no noticeable differences. In a DML the frequency response is not constant but usually showing a peak in correspondence to the relaxation oscillation frequency which can be more or less pronounced depending on the damping factor. By carefully designing this parameters the frequency response of a DML can be optimised for a particular modulation frequency. The laser used in this work are meant for 10 Gb/s modulation speed and the eye diagram obtained at 2.5 Gb/s is showing amplitude overshoot and ripple coming from the peak in the frequency response at the relaxation oscillation frequency.

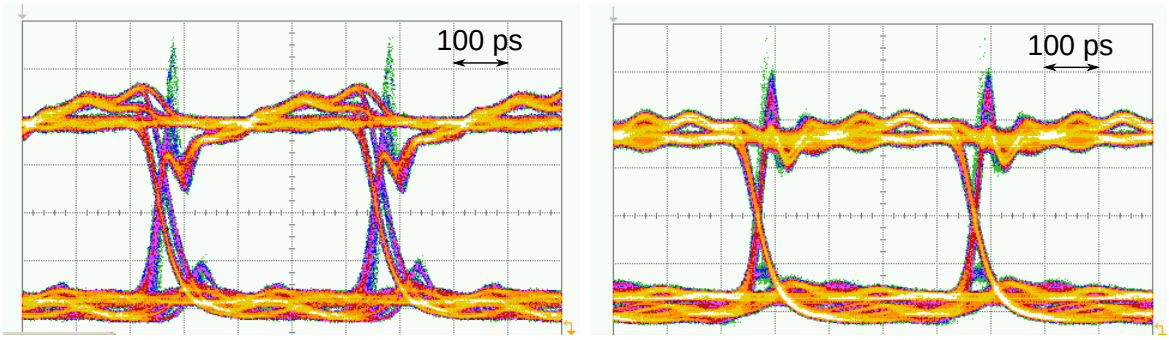

Fig. 4.11: Eye diagrams generated by the two DMLs at 2.5 Gb/s

The evaluation boards adopted also offer a burst mode operation feature which can drive the laser below its current threshold disabling the transmission during the burst off period, whose timing is controlled by a gating signal. This is a necessary condition in a XG-PON system because of multiple ONUs are coexisting and sharing the same network with a TDMA protocol, thus it is not acceptable for every ONU to transmit a high noise power during the burst off period. A power lower than the 0 level one must be granted during the transmission disabled period, otherwise the overlapping of all the quiescent transmissions will cause a relevant amount of noise compromising the active transmission [23] [24]. The burst off feature of the board permits to reach the low power level required by the protocol decreasing the laser bias current as visible in Fig. 4.12 where bias currents are shown during the burst on and off periods. That ensures negligible interference between the ONUs and no impairments arising from

in-band crosstalk are expected for the recommended ONUs number. It is also shown how a single burst transmission from a single transmitter appears (Fig. 4.12).

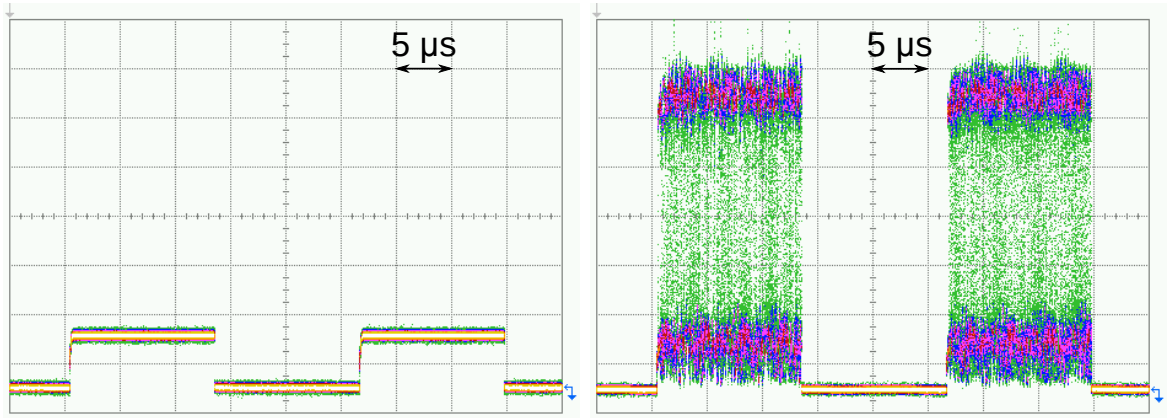

Fig. 4.12: Bias current and modulated signal during burst on and off period

The burst on/off enabling signal of a single ONU is generated by the same PG that provides its modulation data and given that the PGs are synchronised a proper setting of the burst control signals will prevent overlapping in the active periods. During the burst off period no modulation signal is sent to the boards given that no information stream is generated. The burst on/off transients due to the switching of the laser above and below threshold current are shown in Fig. 4.13

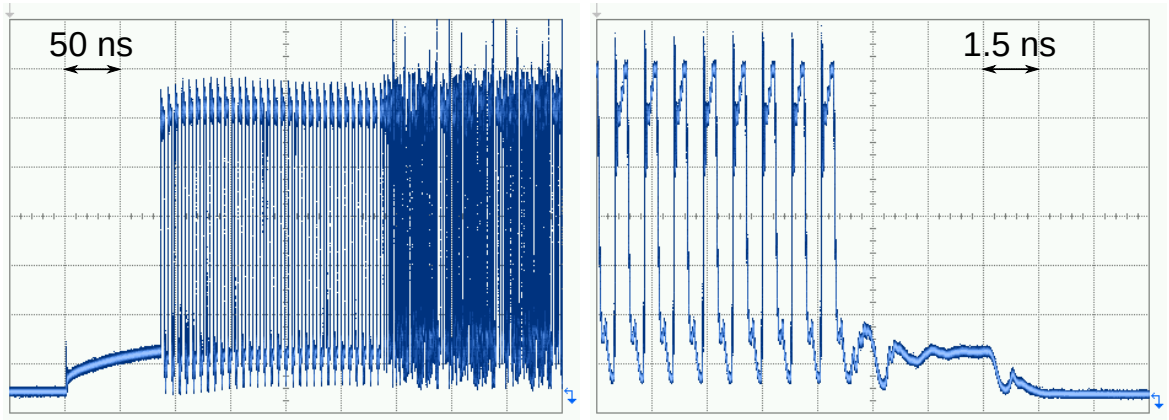

Fig. 4.13: DML burst on and off transients

As apparent the DMLs show a relatively short transient time, suitable to fit the guard times defined by the transmission protocol. The two optical beams coming from the diodes are tuned thus to make the burst on period of one ONU correspondent to the burst off period of the other one; the signals are hence combined together with a 50/50 coupler and transmitted over the 50 km long OTL fibre, as in Fig. 4.14. Adding independently controlled attenuations to the two sources different ODN losses can be emulated obtaining temporally consecutive packets with different powers coexisting in the same network following a TDMA protocol. The attenuation values imposed can be translated to different lengths of the ODN fibre and/or number of splits.

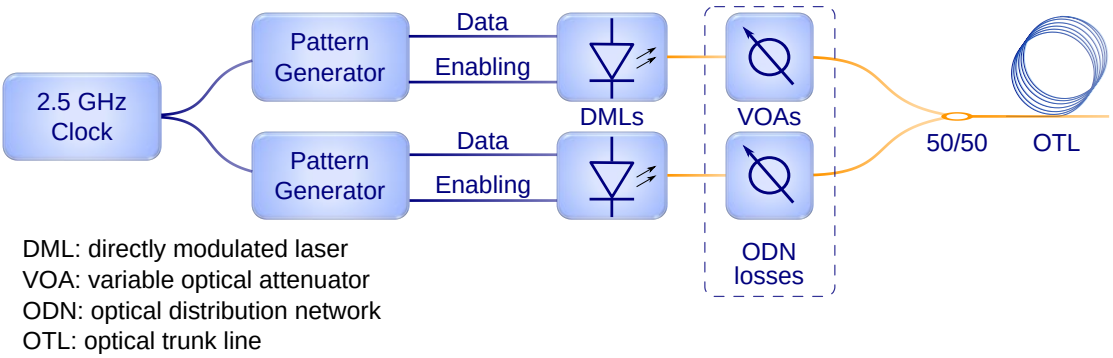

Fig. 4.14: Independent ONUs burst transmitter setup

In order to meet the requirements of a TDMA burst mode operation also in this setup a particular pattern has been used. It is essentially the same of the previous experimental system, with the same field structure but in which this time the two payloads are split to belong to the different PGs. Also here for the two ONUs the payloads was chosen to be PRBS and $\overline{\text{PRBS}}$ in conformity with the previous work. The pattern structure is shown below in Fig. 4.15 along with the correspondent burst enabling signals coming from the PGs in Fig. 4.16. Some examples of DCA traces acquired for multiple dynamic ranges obtained with this transmitter system are shown in Fig. 4.17

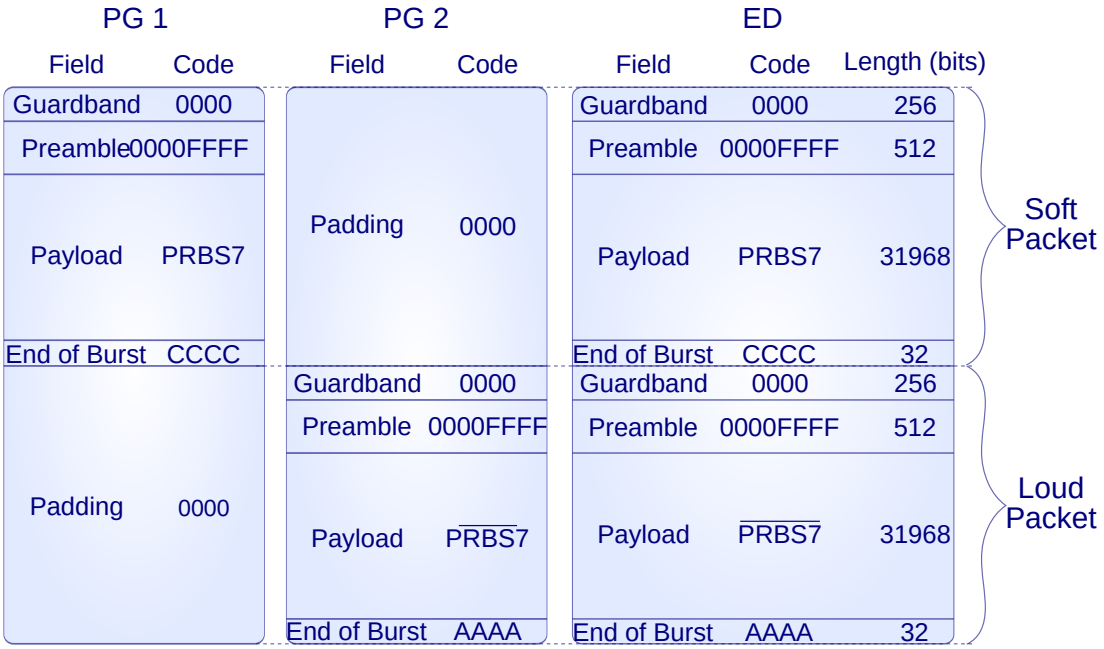

Fig. 4.15: Independent ONUs burst transmitter patterns scheme

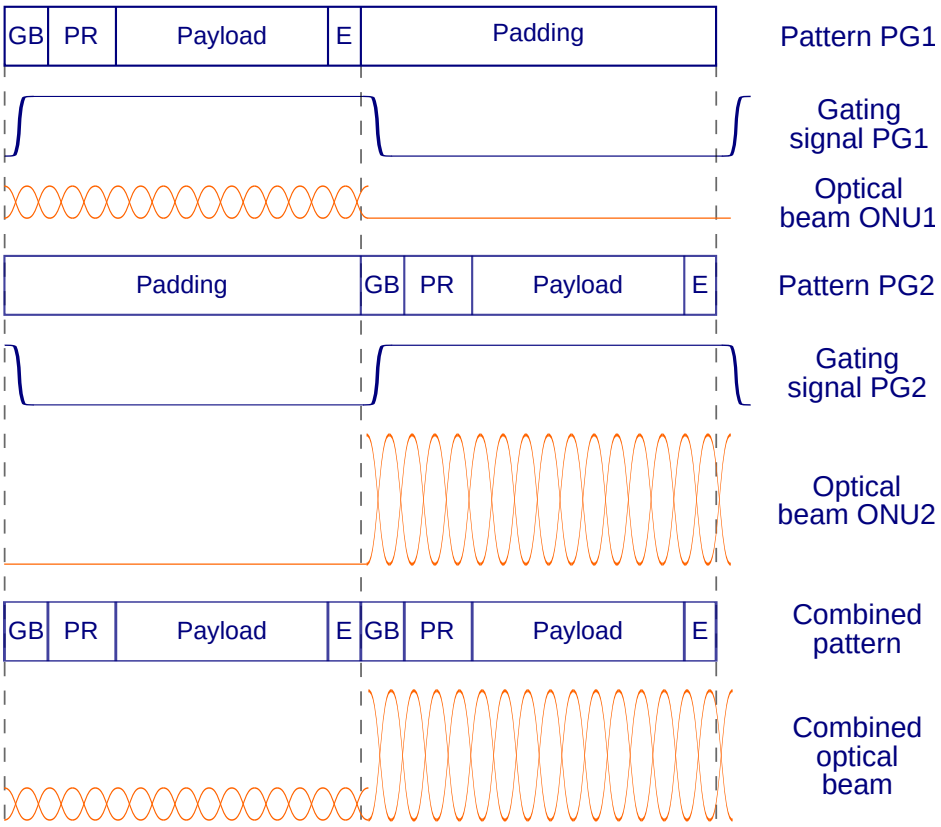

Fig. 4.16: Independent ONUs burst transmitter signals timing

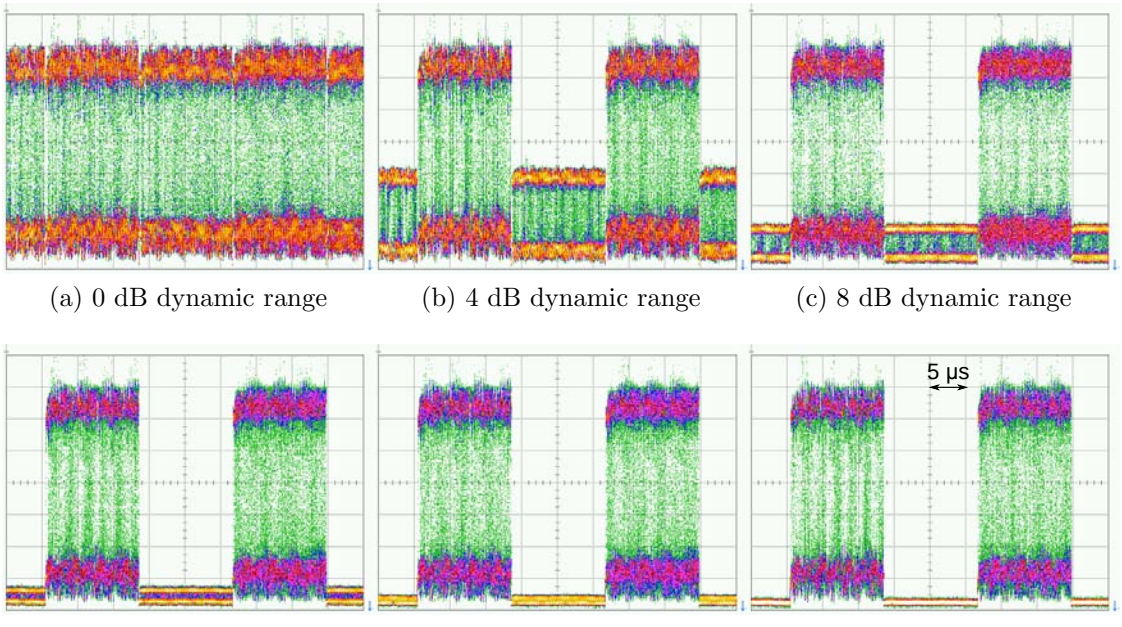

(a) 0 dB dynamic range (b) 4 dB dynamic range (c) 8 dB dynamic range

(d) 12 dB dynamic range (e) 16 dB dynamic range (f) 20 dB dynamic range

Fig. 4.17: Examples of generated TDM packets with increasing dynamic ranges

4.4 Burst mode receiver

Once we reached the capability to generate burst traffic, it has been necessary to develop a receiver capable to deal with that type of transmission. A common receiver with a positive-intrinsic-negative (PIN) or APD photodiode followed by a transimpedance amplifier (TIA) is unable to correctly process incoming burst traffic because of it cannot respond to fast variations in the input optical power, resulting in data loss. Since a burst mode receiver was not available an appropriate system had to be designed, and the basic idea was to operate the equalisation of the incoming powers in the optical domain instead of the electrical (which would require implementing a high specifics TIA with auto-adjusting variable gain [25]). Inverting the operation principle of the SOA based burst transmitter shown earlier in this work, a similar amplifier has been utilised as a packet power equaliser. By driving this SOA with different bias currents it provides a time varying gain, and thus can act as an equaliser if carefully tuned in order to produce a constant output power. The equaliser scheme is presented in Fig. 4.18.

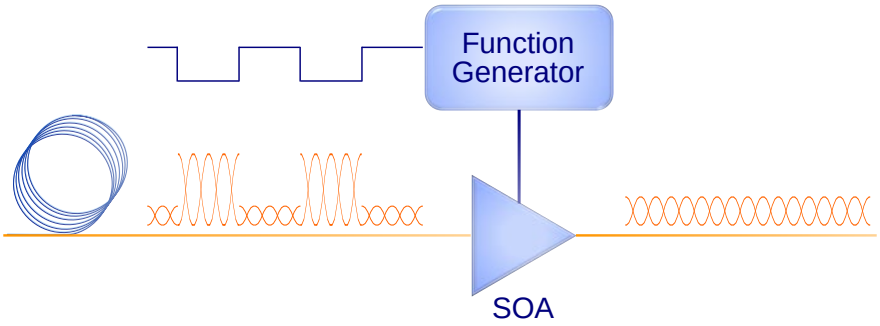

Fig. 4.18: ONU burst setup

In this work we were not focused on the realization of a stand-alone burst mode receiver but to use it to the characterise Raman amplification in XG-PON upstream lin. Thus it has not be implemented an independent control circuitry for the bias current adjustment, it was instead driven by an AFG synchronised with the transmitter. However this does not pose a limitation on the effectiveness of use of the device seen that a properly designed control circuitry would have a response time included in the guardband and preamble fields, without compromising the transmission efficiency. Application of SOAs as upstream packet equaliser in PONs has been reported in works like [26] where the author has shown a low bias current operating SOA being able to equalise packets up to 12 dB dynamic range before transmission over 62 km SMF. In our case given the complete passive structure of the network the SOA will be operating at the OLT side, becoming a pre amplified receiver with equalisation feature, thus without the needing of reaching a high output power. The SOA will hence operate in a regime of higher input saturation power with respect to high forward currents. That

will translate in smaller degradation induced by patterning and thus to the capability of equalising a wider dynamic range without paying important penalties.

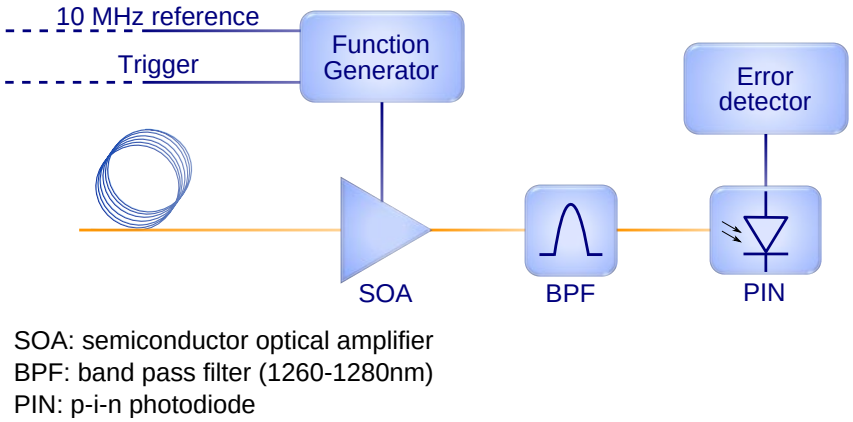

Fig. 4.19: ONU burst setup

The setup diagram of the equaliser is shown in Fig. 4.19. The AFG used in the system have a 10 MHz clock reference input from the transmitter and a trigger signal coming from the PG to be synchronised with the transmission of the pattern. The latter is the same pattern introduced in the previous sections in which two packets are transmitted with different powers; by adjusting the delay of the trigger in order to account for the propagation time of the signal along the fibre, the driving signal of the SOA is properly set to have the transients placed in the guardband period. The actual waveform generated in this case was not a simple square wave but comprehended an adjustable length interval during which no current was provided, thus to switch off the SOA for an arbitrary time in the guardband and avoid amplification of eventual transients coming from the network. The equalised stream was then sent into a PIN photodiode with linear TIA and, after an additional amplification stage as discussed in Appendix A, into an ED. This instrument gives the possibility to specify a logical masking pattern for the BER calculation, thus to choose which portions of the pattern are to be considered. Depending on which packet was being evaluated two different masks were alternated, each of them as long as the data pattern and masking every field but one payload. These logical masks along with the signals occurring in the receiver are shown in Fig. 4.20

Some examples of equalised packets for increasing dynamic ranges are reported in Fig. 4.21 where can be noticed how for lower power of the soft packet its extinction ratio becomes poorer, and also that for higher dynamic ranges the SOA's gain suffers of more pronounced transients. This optical equaliser was capable to adjust the packet powers over a 20 dB dynamic range. The performances of the setup, with a more detailed characterisation and the following system measurements will be presented and discussed in 5.4.

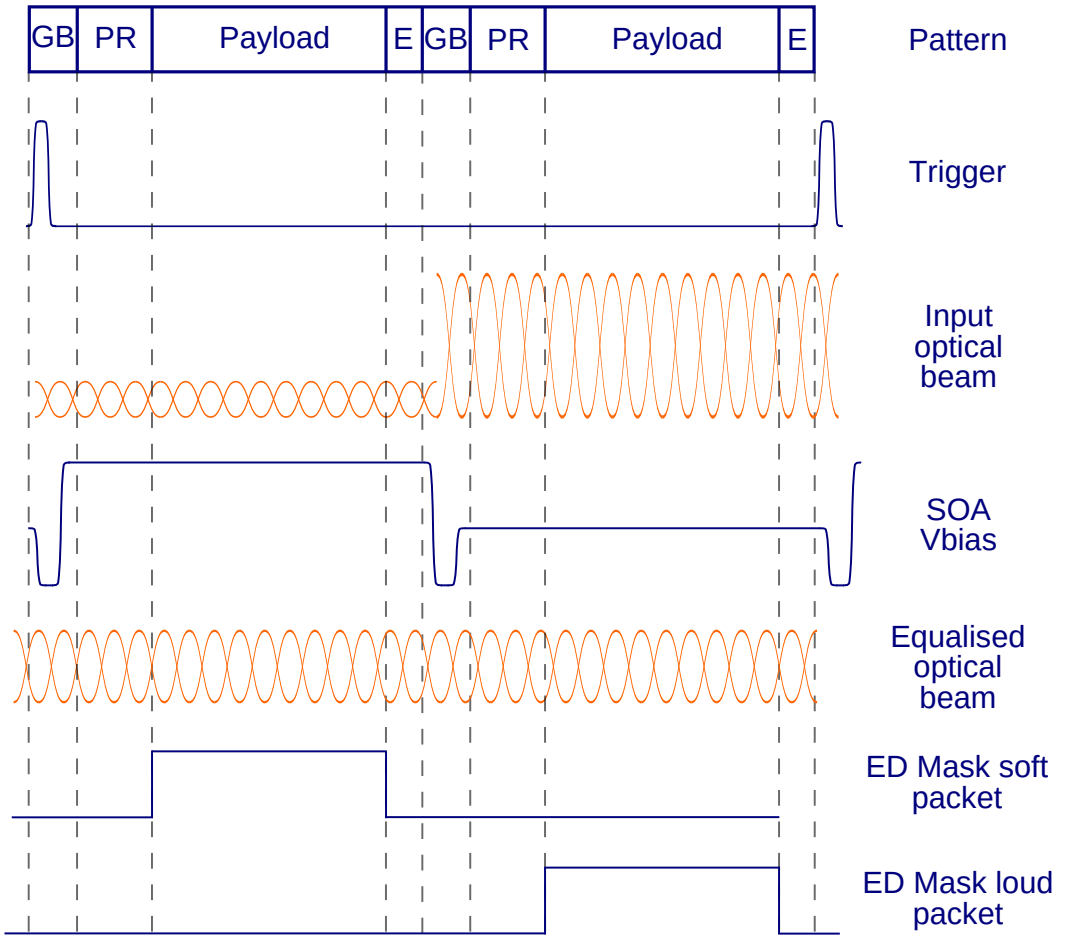

Fig. 4.20: Burst mode equaliser signals timing

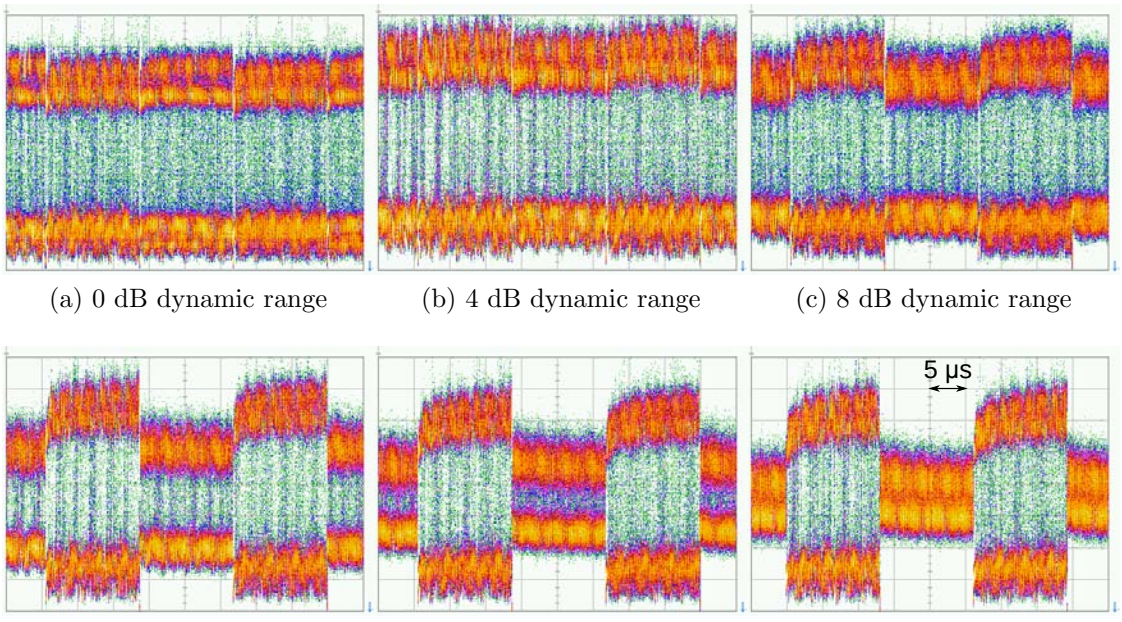

(a) 0 dB dynamic range (b) 4 dB dynamic range (c) 8 dB dynamic range

(d) 12 dB dynamic range (e) 16 dB dynamic range (f) 20 dB dynamic range

Fig. 4.21: Examples of equalised TDM packets with increasing dynamic ranges

4.5 Pattern manager

In this section we will briefly present a software tool developed in LabView during this project which helps in generate arbitrary structured binary pattern to be used in the transmission link, hence loaded in PGs and EDs. In the developing of the test system the capability to shape the data to be transmitted has come out to be a key point to adapt the setup to the needing of every configuration. A tool to easily generate the patterns was thus developed. The graphical user interface (GUI) is shown in Fig. 4.22

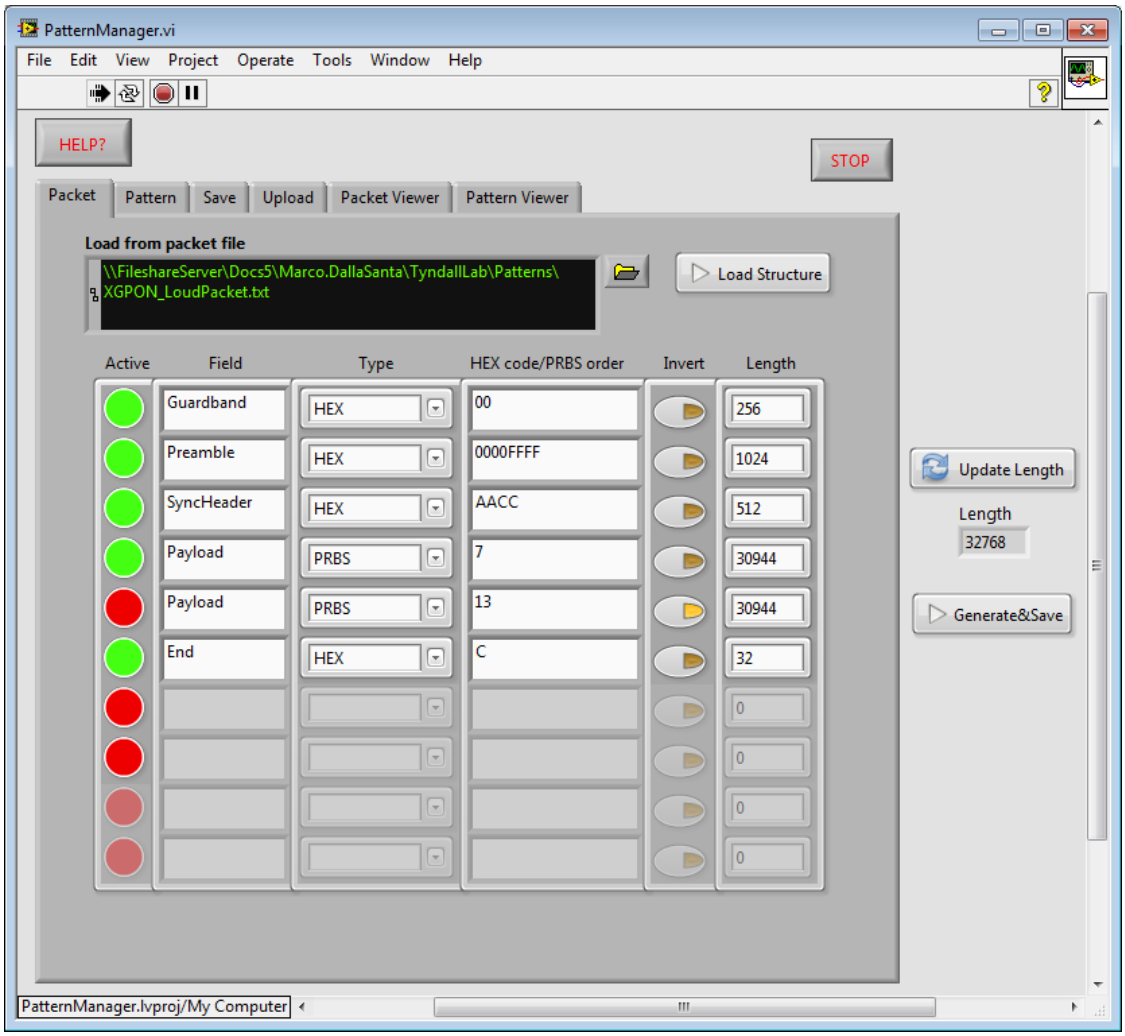

Fig. 4.22: Graphical interface of the software tool

For our purpose the ability to generate any hexadecimal pattern sequence and PRBS of any of the typical orders used in communication analysis entirely covers the necessities. Two inner classes provide this functionality of generate the two types of sequence of any arbitrary length. As can be seen in the screenshot any field of the packet can be associated to a significant name and easily shaped following the user desires. The apposition of these multiple fields form a packet that can be saved in a file and in our case will correspond to the portion of data transmitted by one ONU

in a single burst. Similarly in the following tab of the program multiple packets can be flexibly concatenated to form the desired pattern, the ones presented earlier in this work were obtained using this procedure. Creating an appropriate sequence of zeros and ones also the masking patterns used in the ED for the burst measurements were obtained. To quickly make use of the binary pattern the software offers the possibility to save it in a file format accepted by the various instruments used or directly upload it via a general purpose interface bus (GPIB) interface, distinguishing data and mask patterns. It also has some visualization features to look at the structure of previously saved files.
The software was tested cross checking the transmission performances obtained uploading various of these patterns in a PG and detecting it with the correspondent one generated by the internal tools of the ED, or viceversa. Having performed error free transmission for all the PRBSs generated or arbitrary hexadecimal sequences guarantees the reliability of the tool.

4.6 Conclusions

In this chapter the experimental setups developed in order to perform a comprehensive analysis of the Raman amplifiers characterised in Chapter 3 were presented. We have proposed two different burst transmitter architectures and an optical packet power equaliser suitable to be used, along with a PIN photodiode, as burst mode receiver. A deeper characterisation of the capabilities of these setups and the results that were then obtained in the study of the XG-PON upstream transmission link will be described in the next chapter.

Chapter 5

Raman Based Reach Extender Performances

5.1 Introduction

In Chapter 4 the steps which has brought to the realization of the measurement system were presented. We will now report in this chapter the results obtained with these setups related to the Raman reach extender capabilities, along with interpretations and connections with XG-PON system application.

5.2 Performances in continuous mode

In this initial section we will report the first series of results obtained with the continuous mode evaluation setup described in 4.2. It was logically divided in a ODN with tunable losses and a OTL, the latter with a fixed total loss affecting the probe signal at 1270 nm measured to be 22.6 dB. That was coming from the combined attenuations of the 50 km SMF (the measured loss coefficient at 1270 nm was 0.42 dB/km and the insertion loss of the passive CWDM and BPF components. Hence in order to determine the maximum loss budget supported by the network, which is the sum of the OTL and ODN loss, the last one can progressively be increased.
Considering the worst case scenario stated in the XG-PON protocol, that is a transmitter with minimum launch power of +2 dBm [23], the correspondent ODN loss is calculated as function of the input power into the OTL fibre. Hence for example when that power is equal to -20 dBm, it translates to 22 dB of ODN loss which can accommodate for a 1:64 split ratio, and a total loss budget that would become 44.6 dB summing both the contributions. The total allowed loss budget was obtained monitoring the upstream transmission BER at the OLT side as a function of the ODN attenuation with the fixed OTL loss. This BER is thus measured progressively attenuating the optical power of the upstream signal entering the OTL fibre with a fixed pump power. This is shown in graph 5.1 where on the lower x-axis is written the optical power of the upstream signal entering OTL and on the upper x-axis the correspondent ODN loss calculated as explained previously. Many BER curves were acquired at different pump powers of the Raman reach extender to see how it is affecting the network power budget.

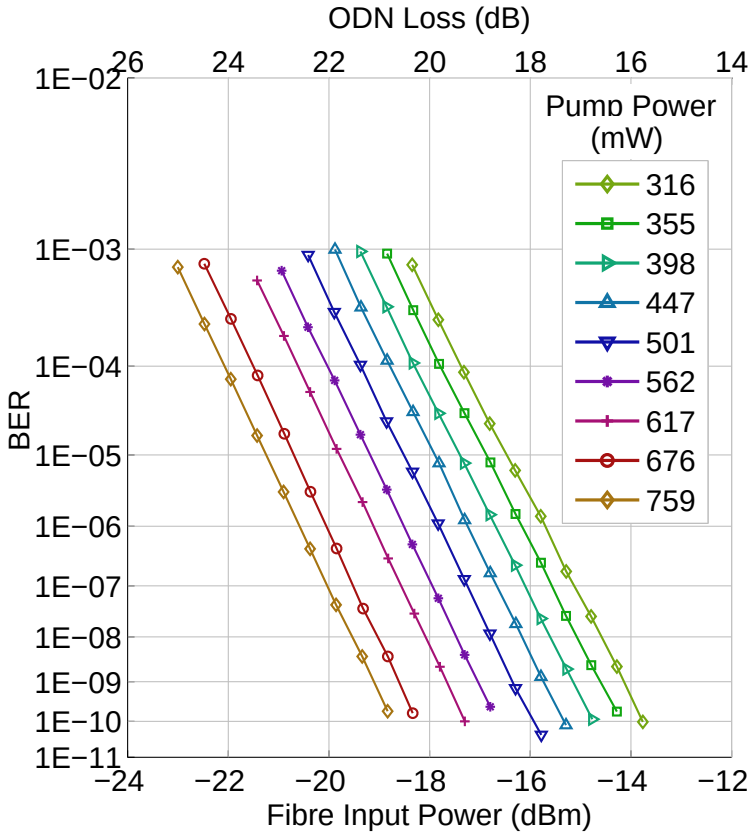

Fig. 5.1: BER in function of OTL input power for multiple pump powers

From the trend it clearly emerges that higher pump powers provide an increasing loss budget; for pump power of 759 mW, considering a BER of 10^{-4} which is the XG-PON pre-forward error correction (FEC) requirement, the higher ODN loss budget measured is equal to 24.1 dB, and thus corresponds to a total supported loss of 46.7 dB. At these conditions the received optical power into the APD was -31 dBm, which is more than 5 dB above its sensitivity measured at BER of 10^{-4}, suggesting the photodiode is working far from the thermal limit. To better characterise the reach extender impact on the transmission link, the experienced gain and resulting OSNR of a probe signal were monitored for increasing ODN loss at pump power of 759 mW. A setup similar to the one previously introduced in Fig. 3.24 was used, obtaining from the OSA also the OSNR measure, at 0.1 nm noise resolution. These two curves are in Fig. 5.2 which shows an appreciable stability in the gain over the 20 dB range of evaluated signal power which means no dependence on the intensity of the upstream signal. The OSNR trend is also clear, linearly increasing with the optical power of the injected probe signal. This can be explained noting that the ASE noise generated by the reach extender is dependent by the Raman pump power, and thus constant for fixed currents driving the pumps. The OSNR is defined as

$$OSNR = \frac{P_1}{P_{noise}} \tag{5.1}$$

where P_1 is the energy of the "1" bit in the optical signal and P_{noise} is the noise power evaluated in a given bandwidth, 0.1 nm in this case. When the pump power is fixed the in-band ASE noise is constant and because it is the major contributes to the optical noise the OSNR trend of Fig. 5.2 is obtained.

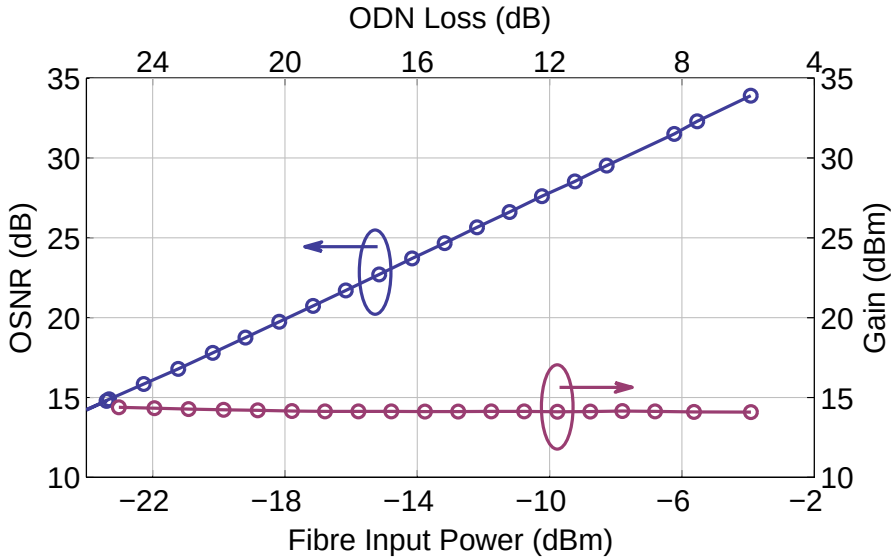

Fig. 5.2: OSNR and Raman on/off gain in function of optical power at the OTL input

To further characterise the system in these conditions, for the same pump power of 759 mW and wide range of input power into the OTL, a series of BER vs APD received optical power were taken, using the same setup of Fig. 4.2 and adding a controlled attenuation before the photodiode. These curves were measured for two different transmitters, the DML already described in one case, and a TLD followed by a Mach-Zehnder modulator (MZM) in the second. This was made to investigate a higher range of input powers and also to see whether high mismatching would have arisen using a different modulation technique. The families of BER vs received power curves are reported in Fig. 5.3 and 5.4.

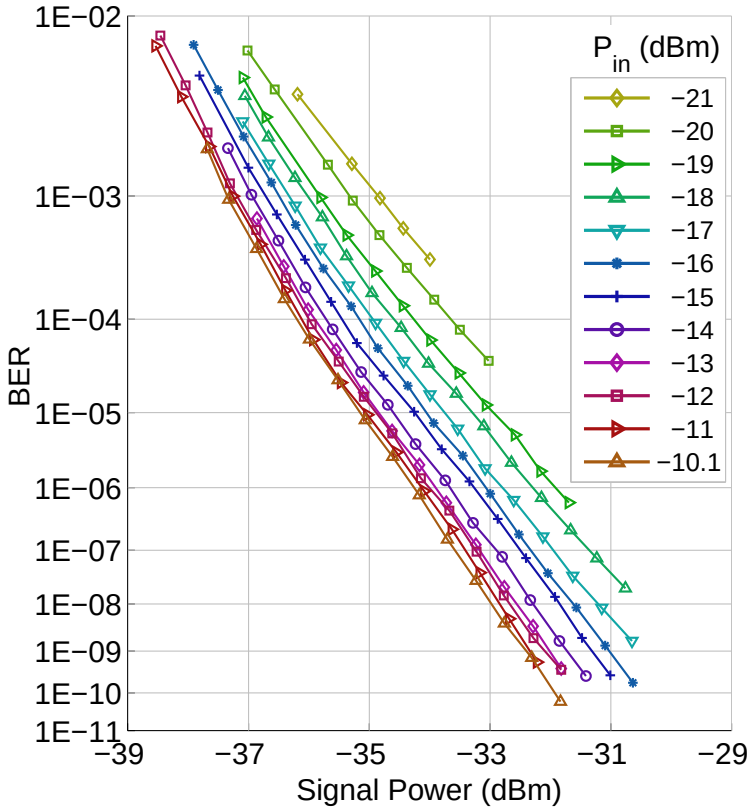

Fig. 5.3: BER curves for multiple fibre input power with DML transmitter

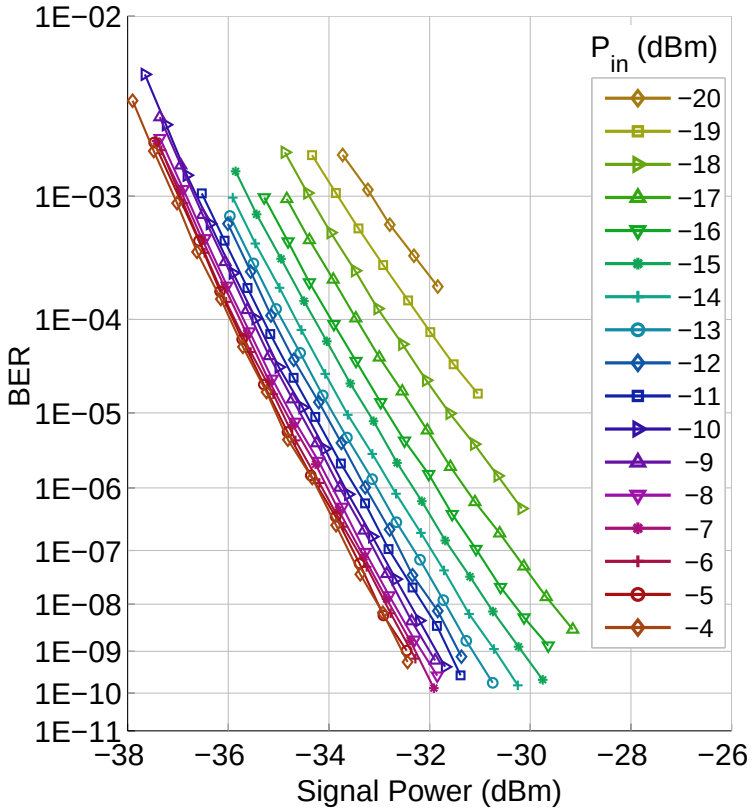

Fig. 5.4: BER curves for multiple fibre input power with SOA + MZM transmitter

The two series of curves behave in a comparable way even though they were obtained with different transmitter, suggesting a common impairment mostly affecting the system. In order to improve the readability of the results a single line has been extracted from the multiple curves by interpolating them and measuring the distances on the x-axis at a chosen BER value, between every splined line and a reference one. In this way a penalty curve is obtained, in term of higher power needed at the receiver to guarantee the same BER. In Fig. 5.5 this penalty trend for the curves in Fig. 5.4 is shown for pump power of 759 mW at the pre-FEC BER of 10^{-4}.

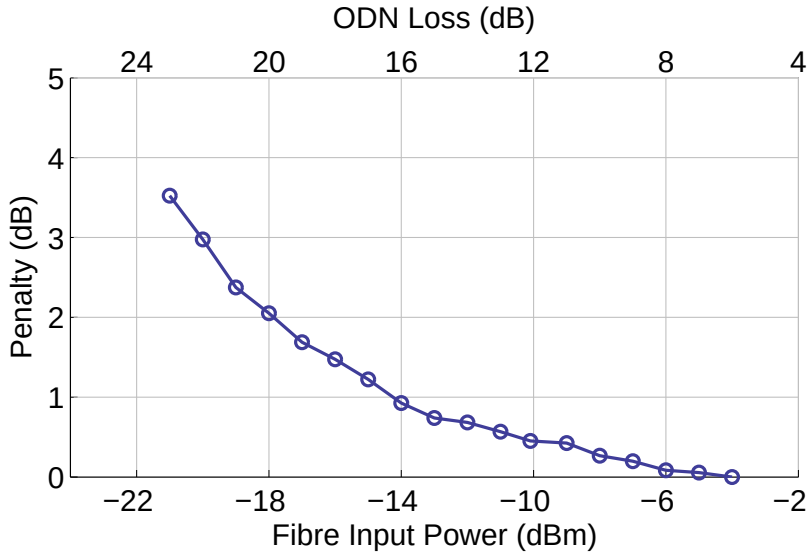

Fig. 5.5: Received power penalty at BER 10^{-4} in function of optical power at the OTL input

A well defined trend is here emerging from the data, showing the signal suffering of increasing impairments as the input power into the OTL decreases. Considering the highest ODN loss of 24.1 dB which was corresponding to a BER of 10^{-4} we already mentioned that the received power was -31 dBm, well above the APD sensitivity. We can also see that in this case the measured OSNR entering the receiver is 16 dB and it gets better as the ODN loss decreases (Fig. 5.2). Under the assumption of equally likely symbols with equal gaussian noise distribution (using the expressions in Eq. 5.7 5.8 5.9) we can estimate a BER lower than 10^{-4} when the OSNR exceeds 9 dB. This means that the OSNR of the received signal was 7 dB better than the required one for BER 10^{-4}. The system thus appears to be not power limited nor OSNR limited. To recognise the dominant contribution degrading the performances, the effect of ASE must be analysed. The ASE noise is responsible for two terms which degrades the electrical signal to noise ratio (SNR) in a receiver: a signal-ASE beat noise, and a ASE-ASE beat noise, whose respective variances are [7]

$$\sigma^2_{sig-ASE|_x} = 4R^2 S_{ASE} P_{sig|_x} B_e \tag{5.2}$$

$$\sigma^2_{ASE-ASE} = 4R^2 S^2_{ASE} B_{opt} B_e \tag{5.3}$$

where R is the photodiode responsivity, B_e is the electrical bandwidth, S_{ASE} is the ASE spectral density, $P_{sig|_x}$ is the optical power of the signal correspondent to symbol x and B_{opt} is the received signal optical band. Usually the first term results to be the dominant one, however in this case, because of the wide band (20 nm) filter used, and the broadband ASE noise of the Raman amplifier, the term B_{opt} becomes very important ($\simeq$ 3.7 THz) and causes the ASE-ASE beat noise to prevail. Simplifying the electrical SNR expression we can thus obtain

$$SNR = \frac{\langle I \rangle^2}{\sigma^2_{ASE-ASE} + \sigma^2_{sig-ASE}} \approx \frac{\langle I \rangle^2}{\sigma^2_{ASE-ASE}} = \frac{(2RP_{sig})^2}{4R^2 S^2_{ASE} B_{opt} B_e} \propto \frac{P^2_{sig}}{S^2_{ASE}} \tag{5.4}$$

obtaining an expression of the SNR proportional to the square of the signal power under the assumption of constant ASE. It would not be true for a situation of dominant signal-ASE beat noise, and that can explain the observed penalty trend. That system design is resulting to be limited by the self-beat noise arising from the 20 nm BPF employed at the receiver side, however this is a necessary design feature to allow the entire XG-PON upstream band to be received at the OLT.
In a carefully designed system, in which all the ONUs's upstream transmissions are guaranteed to be located in a sub-band of the XG-PON upstream one, the use of a narrower filter can be considered as a way to improve the performance; however in that scenario care should be taken to identify possible issues coming from non linearities at high Raman pump power that may be hidden in our analysis by the ASE repercussions.

5.3 Burst mode transmitter characterisation

We have shown in the previous section some significant results obtained on the reach extender impact evaluated in continuous mode. In order to move to a burst mode analysis it is first necessary to characterise the setup capabilities, thus to know which are the limitations imposed by the same, and which are the ranges of investigation admitted. We start here comparing the two transmitters to see which one better suits to such application. A first relevant feature is immediately visible observing the two optical spectrum coming from the considered solutions in Fig. 5.6.
Clearly the solution using a SOA shows a broadband ASE noise due to the BPF which does not provide an efficient noise suppression. The SMSR is much pronounced in the double laser configuration, emulating a more similar scenario to the real XG-PON upstream flow. In that second setup it also visible the wavelength shift between the two ONUs coming from the differences in the transmitter diodes and the uncooled

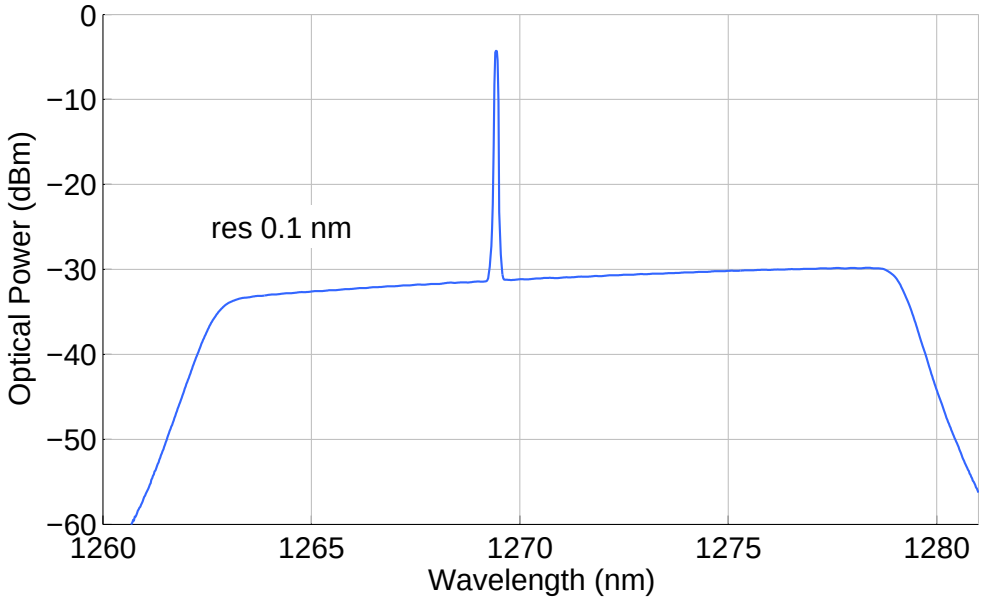

(a) SOA generated burst traffic optical spectrum

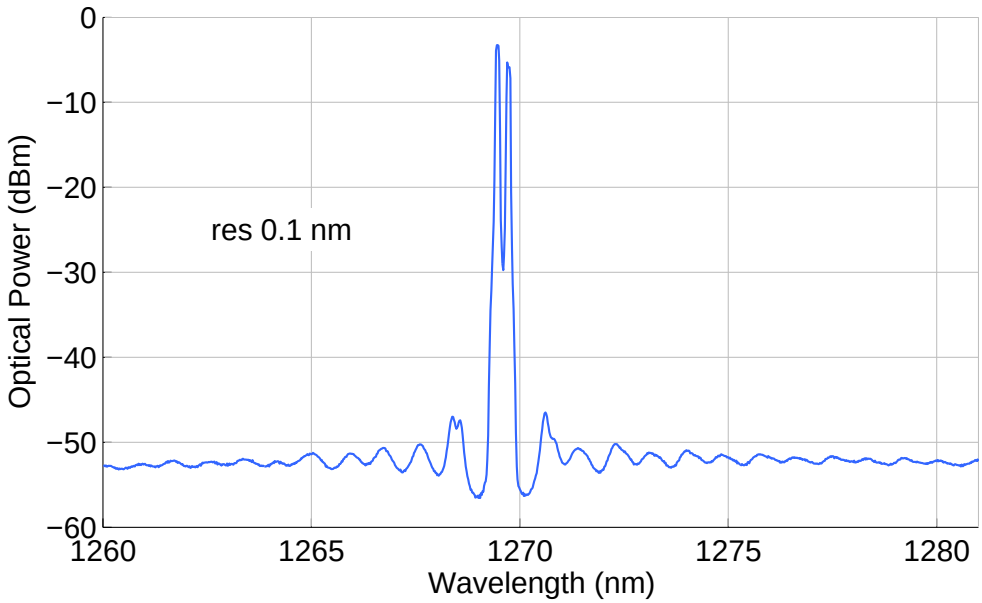

(b) Independent ONUs generated burst traffic optical spectrum

Fig. 5.6: Optical spectrum comparison from the two burst transmitter

operation. To better evaluate how the transmission performances are affected by the transmitter configurations an analysis of the BER trend in function of the received optical power was carried out and reported in the following.

5.3.1 SOA based transmitter

The first solution analysed was the variable gain SOA transmitter. In order to see whether this amplifier could be a suitable device to employ in such a design of the

setup for generation of burst traffic a first evaluation of its performances was carried out in continuous mode regime. The idea was to compare the differences in performances between the signals obtained sweeping the forward current of the SOA while keeping a constant input power. The first type of measures evaluated were the output power and OSNR associated with every forward currents, thus to exploit the reachable dynamic ranges. These measurements were made with the setup in Fig. 5.7 and the results are in Fig. 5.8.

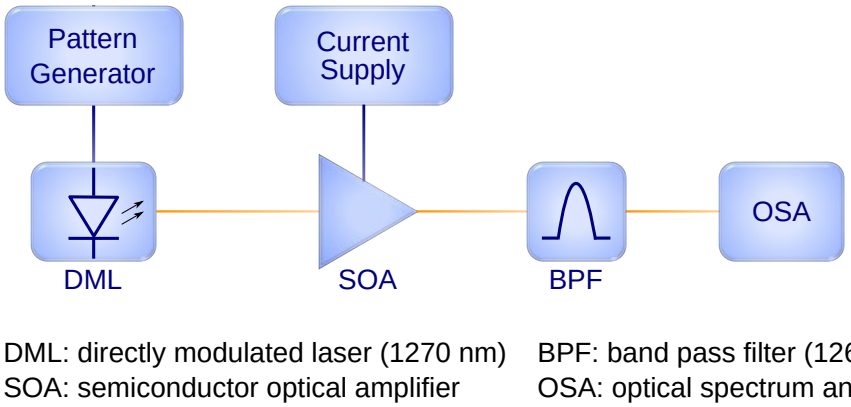

Fig. 5.7: Setup diagram for gain and OSNR characterisation of a SOA with variable gain

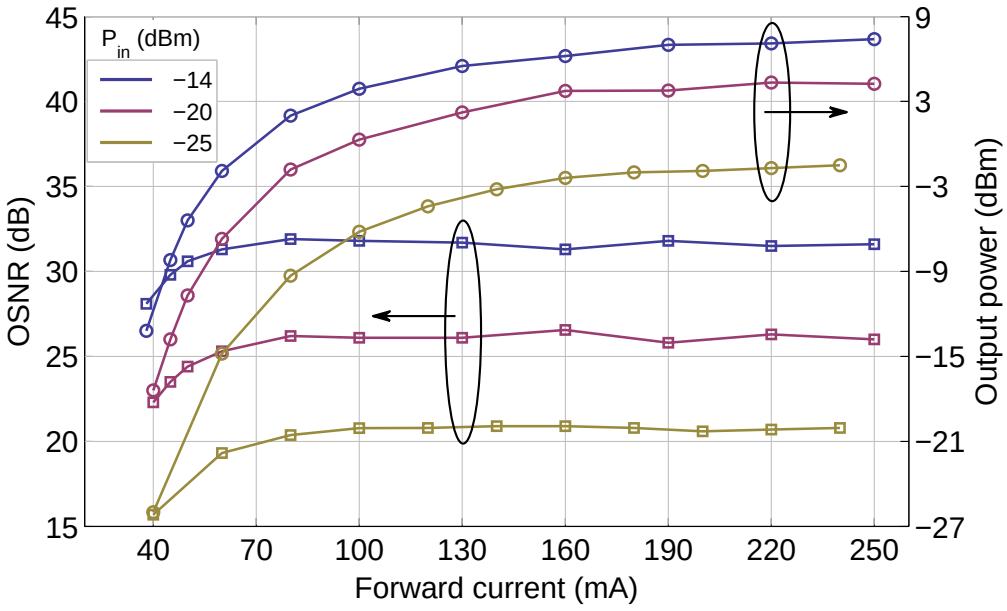

Fig. 5.8: OSNR and optical power of the SOA output signal, for three input powers

Three different input power into the SOA were evaluated, equal to -14 dBm, -20 dBm and -25 dBm. With all these input beams 20 dB of dynamic range can be achieved as clear looking at the gain curves, however for low input power the OSNR appears poor if compared to a DML XG-PON transmitter.

To better observe the signal quality a characterisation was made in term of BER in function of the received power to come across eventual penalties arising from the different operating conditions of the amplifier and the ASE wide band noise. The measurements have been made with the setup in Fig. 5.9 where the OSA was replaced by a VOA to stress the thermal noise, followed by a PIN photodiode and ED. Similarly, keeping the input power into the SOA constant and varying its bias current, different output power streams can be obtained and characterised.

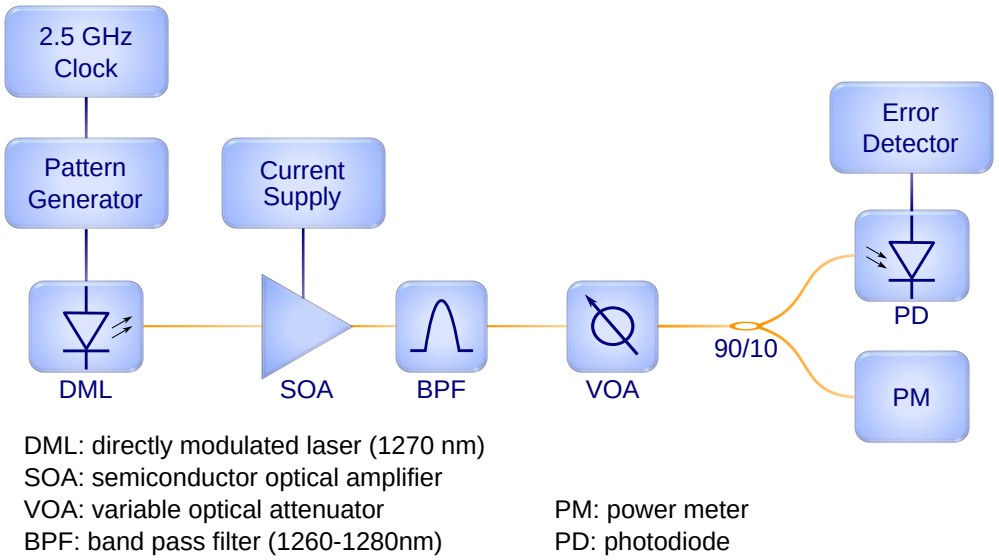

Fig. 5.9: Setup diagram for the continuous mode characterisation of a SOA with variable gain

Once a calibration between the PM and the input beam into the photodiode was made to take in account the power division factor of the coupler, the PM reading permits to monitor the received signal power, adjusted with a VOA, and associate that one with the measured BER. To correctly measure the power of the signal of interest also the ASE power was read for every forward current at which the SOA was driven, and then subtracted to the value of the PM which is integrated all over the optical spectrum covered by its sensitivity.

The results reported in Fig. 5.10 and 5.11 are a series of BER vs optical power curves obtained for two optical beam in input into the SOA with power equal to -20 dBm and -25 dBm, while the bias current was varied over a 200 mA interval to reach a gain range of 20 dB.

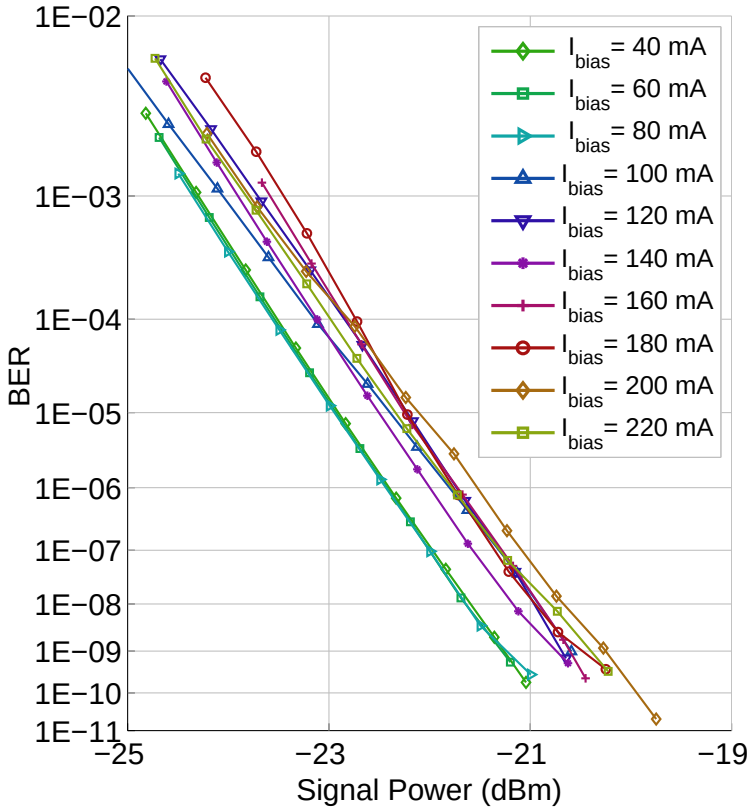

Fig. 5.10: BER curves for multiple bias current at -20 dBm input power

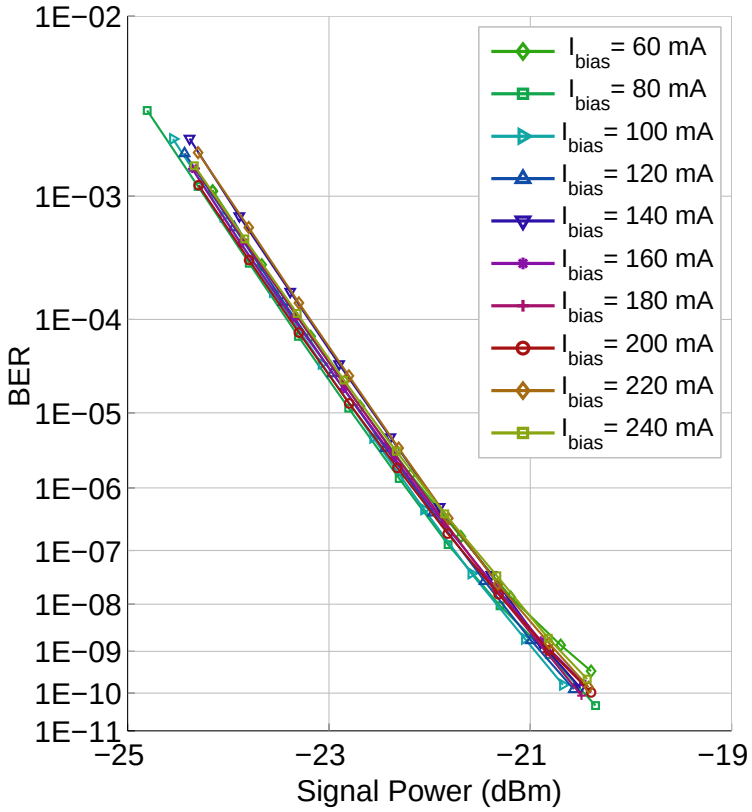

Fig. 5.11: BER curves for multiple bias current at -25 dBm input power

Comparing the two graphs it is evident that for the lower input power into the SOA (-25 dBm) the various BER curves are almost overlapping each other showing no noticeable differences, while for higher input power entering the amplifier the output signal suffers of increasing impairments, caused by the reaching of the SOA saturation operating conditions. In order to extract a useful and clearer trend from this multiple BER curves, for every of them an interpolation of the slope was calculated; then comparing the various resulting lines a penalty curve was obtained. This curve is the distance measured along the x-axis between the various splined lines and a reference one, stating the extra power needed for a particular configuration to reach the same BER of the reference case. In Fig. 5.12 this trend is shown over the 200 mA range of bias current for three different input levels into the SOA equal to -14 dBm, -20 dBm and -25 dBm, obtained at BER value of 10^{-6} and relative to the best performing BER curve.

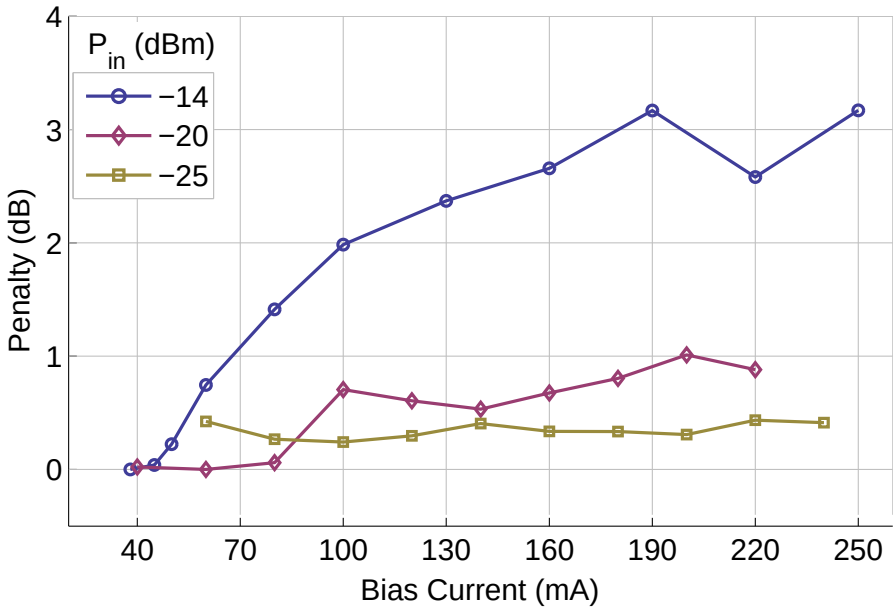

Fig. 5.12: BER penalties measured at BER=10^{-6} over a 20 dB range output power of the SOA, reported for three input powers

It is evident how for the lower SOA input power the transmitter is offering a flat penalty region contained in less than 1 dB in the whole measured range, while increasing that power this penalty becomes an important feature. However to better understand the quality of the amplified signals also the respective OSNR and optical power trends (Fig. 5.8) must be considered. Analysing the combined results we can distinguish two different situations taking place in this burst transmitter when operating at various conditions. On one hand when the SOA input power is high, its output has a suitable power level and an acceptable high OSNR for the whole 20 dB dynamic range. The drawback here is the high impact of patterning which is due to the SOA

reaching the gain saturation regime and hence it is increasing with the bias current; as clearly visible for the input level of -14 dBm it can assume relevant importance causing serious degeneration of the optical signal. On the other side, entering the SOA with a low power causes significant degradation in the signal quality because of the in bans ASE noise added by the amplifier; hence, even though showing appreciable flatness in the BER vs optical power performances, it cannot guarantee comparable values of OSNR and optical power with respect to a typical XG-PON DML transmitter.
Another disadvantage deriving from this setup design is related to the wideness (20 nm) of the bandpass filter employed; that will cause significant out of band ASE power, which will stress the electrical SNR of the optical receiver introducing an important ASE-ASE beat noise. It has then to be remembered that this ASE noise will also experience Raman amplification given its broadband characteristic, causing a reduction in the reach extender efficiency and higher noise at the received which cannot operate a narrow filtering as seen before. This broadband ASE impact will be better discussed and evaluated in 5.4 where the receiver performances are compared for a DML and for this DML and SOA combination.

5.3.2 ONU based transmitter

For what regards the second transmitter setup it is for some aspect easier to characterise because of not employing components adding strong non linearities like the SOA. The possible dynamic ranges achieved are limited only by the maximum emitted power on one side, and the thermal noise on the other given that the mechanism is employing only signal attenuation. To take in account for intrinsic differences of the diodes the performance misalignment between the ONUs was characterised in term of distance of the respective BER curves in function of signal optical power, with the essential setup in Fig. 5.13.

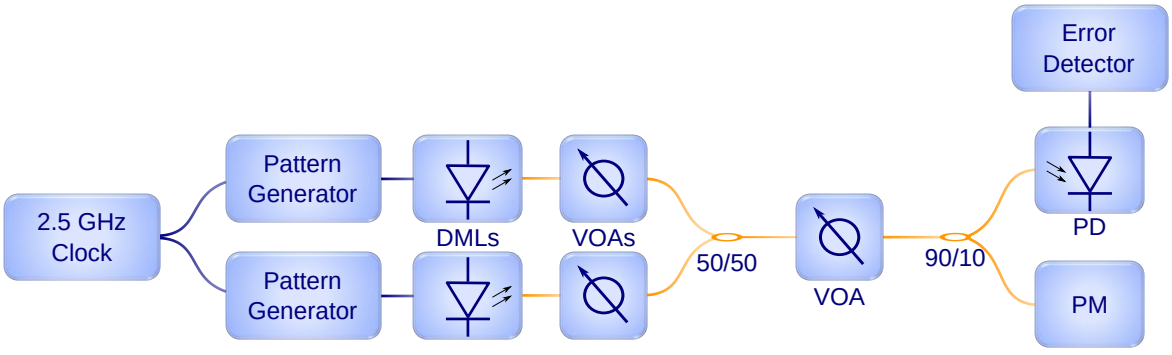

DML: directly modulated laser
VOA: variable optical attenuator
PM: power meter
PD: photodiode

Fig. 5.13: Setup diagram for the continuous mode characterisation of two ONUs

Reference curves were acquired with a 10 GHz PIN photodiode with linear TIA, measured for the two DMLs and for the two different patterns used in the further analysis (PRBS7 and $\overline{\text{PRBS7}}$) in order to come across to eventual mismatches in performances. The resulting lines are also compared with the theoretical limit of the PIN photodiode for increasing thermal noise derived as follow: from the PIN specifics the value of noise equivalent power (NEP) is 12.5 pW$\sqrt{\text{Hz}}$ which is the minimum detectable power for a certain electric bandwidth B_e giving a SNR equal to 1. Assuming $B_e = 2.5$ GHz and the thermal noise to be the main noise source, that can lead to an estimate of the minimum power detectable by the PIN, which we will name P_{floor}, equal to

$$P_{floor} = NEP\sqrt{B_e} \tag{5.5}$$

from that, the OSNR of the incoming optical stream, and hence the electrical SNR in output from the PIN diode can be expressed as

$$OSNR = \frac{P_1}{P_{floor}} = \frac{2P_{in}}{P_{floor}} \tag{5.6}$$

$$\text{with} \qquad SNR = OSNR^2 \tag{5.7}$$

under the assumption of equal gaussian noise distribution for both "1" and "0" symbols ($\sigma_0 = \sigma_1$), negligible "0" associated current ($I_0 = 0$) and thermal noise prevalence in the PIN receiver ($\sigma_T > \sigma_S$), the Q factor can be derived as [27]

$$Q = \frac{\sqrt{SNR}}{2} \tag{5.8}$$

and consequently the BER expressed in function of Q as

$$BER = \frac{1}{2} erfc\left(\frac{Q}{\sqrt{2}}\right) \tag{5.9}$$

The results of the different acquisitions along with the theoretical trend derived as above are shown in Fig. 5.14. Clearly no noticeable differences are evident between the two transmitters and the two testing sequences, and no large discrepancy appears between the approximate expression of the thermal noise limit and the experimental results, suggesting that no major impairments are affecting the measurement system. Some of the considerations made on the elaboration of the electrical signal generated by the photodiode are reported in Appendix A along with results on different configurations and the respective resultant reliability. An additional reference curve was taken with a burst mode measurement, to see whether the driving boards or the lasers are adding some deficiency to the transmission. The setup used was hence the same but with burst traffic, employing the pattern and masking technique described in 4.3.2 and 4.4. The comparison between the two transmitters are shown in Fig. 5.15

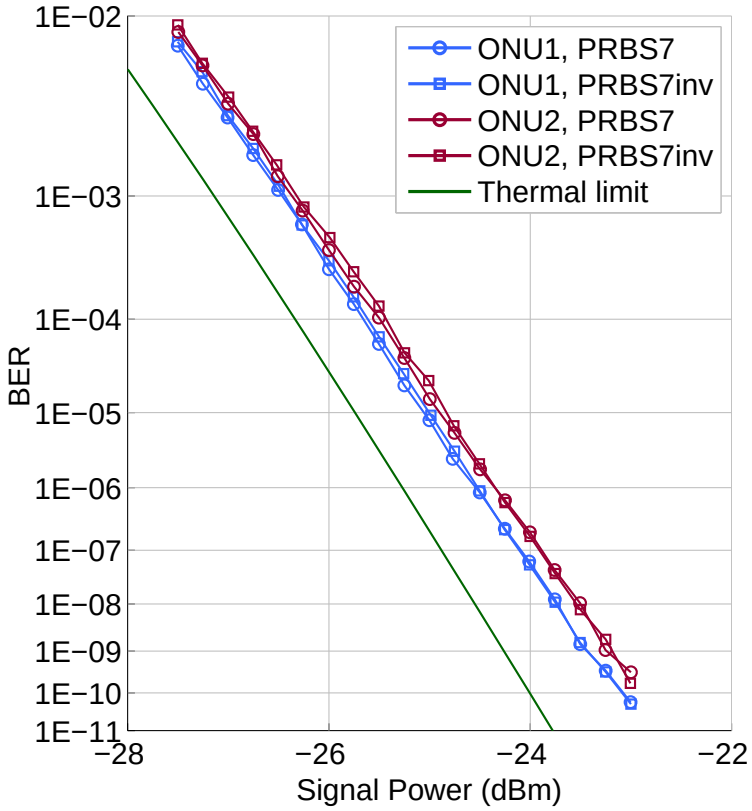

Fig. 5.14: BER performances comparison in continuous mode operation

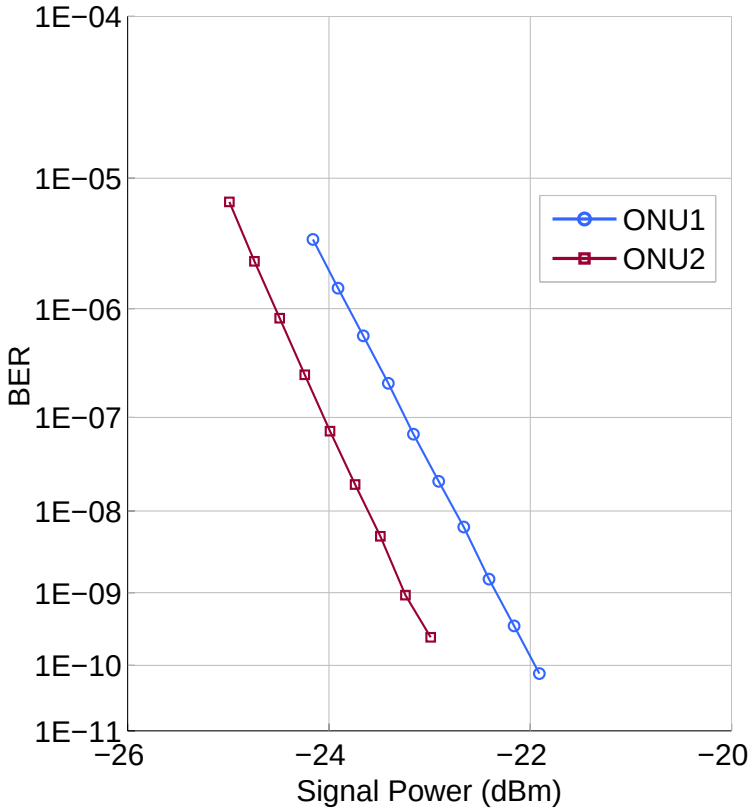

Fig. 5.15: BER performances comparison acquired in burst mode

In this case a significant difference appears between the two, and comparing this curves with the continuous mode it come out that some penalty is paid in the first ONU. However the absence of flooring in the BER and the comparable slope indicates that only higher thermal noise is degrading the transmission, suggesting that a lower ER is guaranteed by that transmitter in burst mode operation. The results arising from the following analysis can thus be related in the same way to the two ONUs, just remembering an initial slight penalty is already there.

5.4 Burst mode equaliser characterisation

With a similar approach the first characterisation of the expected performances of the SOA based equaliser has been done comparing the values of BER in function of the received optical signal power in continuous mode. Different curves of BER have been measured for decreasing input power into the SOA and a consequent increasing in the driving current in order to maintain a constant output power. The setup of the experiment is represented in the figure below.

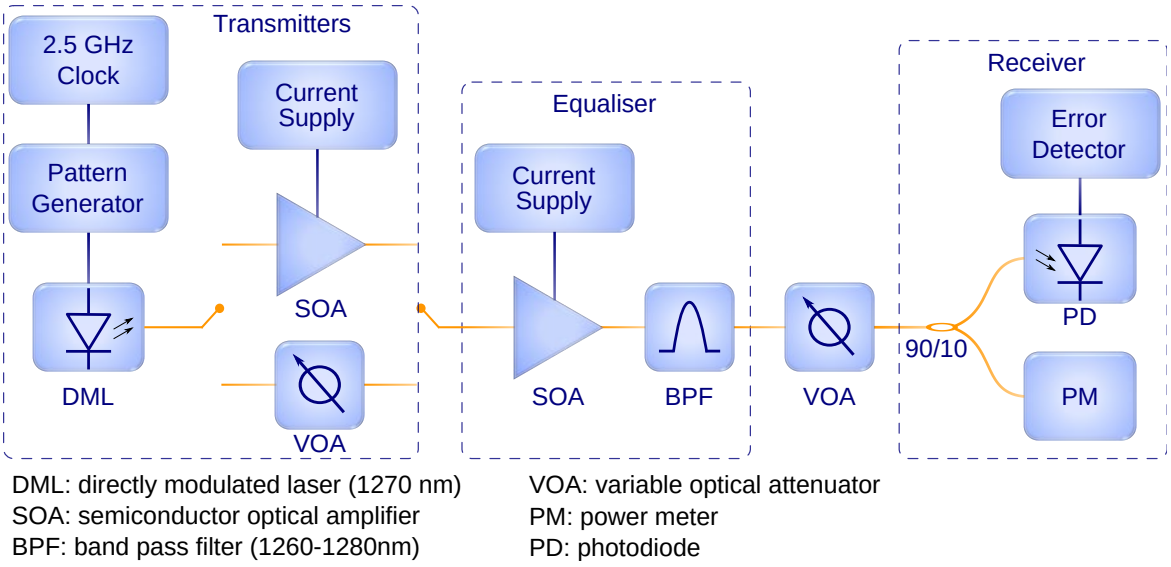

Fig. 5.16: Setup diagram for the characterisation of the SOA based equaliser

Both the transmitters were tested in this analysis, to also compare the performances of the two and to test a wider range of input powers. In the first series of BER curves in Fig. 5.17 the transmitter was a simple DML with variable attenuation and the output power of the equaliser was kept constant to -4 dBm. In the second case of Fig. 5.18 the input was provided by a DML followed by a SOA and the equaliser output target power was -1 dBm.

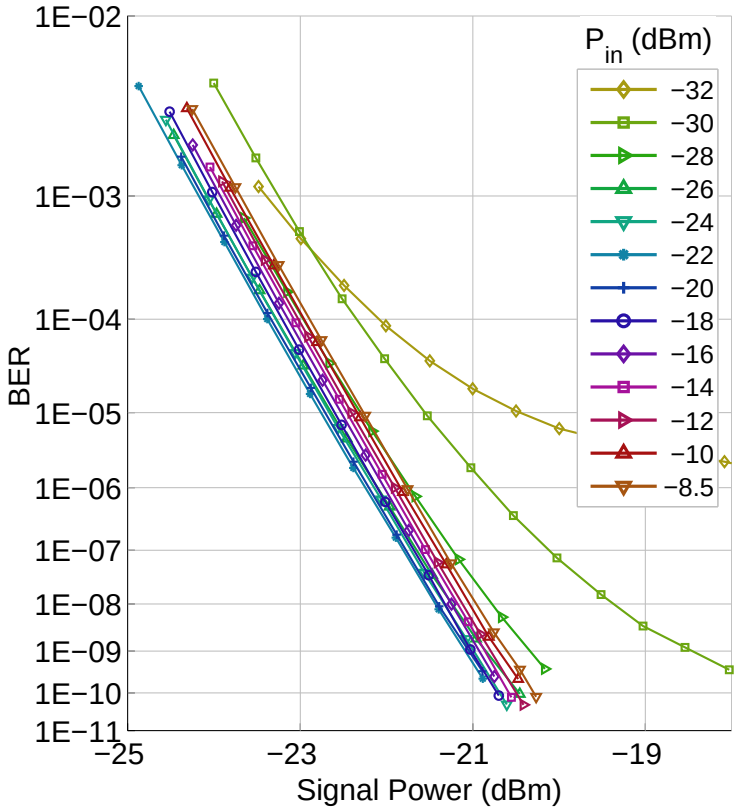

Fig. 5.17: BER curves for multiple bias current with DML input signal, P_{out}=-4 dBm

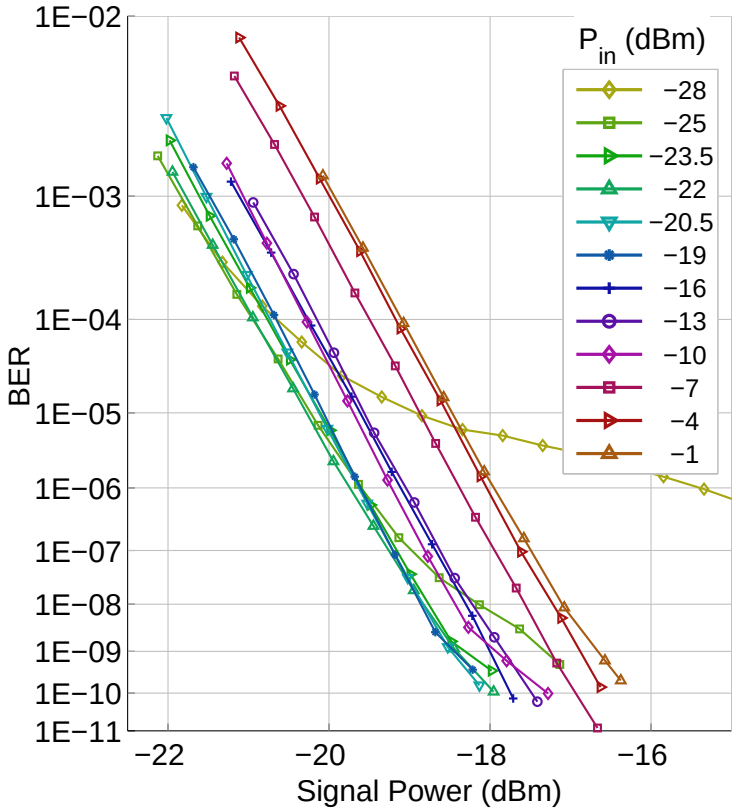

Fig. 5.18: BER curves for multiple I_{bias} with DML+SOA input signal, P_{out}=-1 dBm

The general trend appearing from the graphs shows the better performances for intermediate input power values, with two sources of degradation arising at the extremity; respectively the OSNR degradation for low input power and patterning effect for higher ones. It is also evident a more pronounced degradation in the case of amplified transmitter, due to its wide band ASE which causes a significant ASE-ASE beat noise term, similarly to what seen previously in the continuous mode reach extender analysis.
Also here from the observed series of BER curve the trend can be shown by defining a penalty quantity as the increase needed in the received signal optical power to reach the same BER value of a reference curve. The penalty is here shown for a BER value of 10^{-9}. It is hence more evident the fast OSNR degradation on one side, and the increasing weight of patterning effect for input powers greater than -20 dBm. In the DML case the limit on the measure of high SOA input powers was the low output power of the transmitter. However comparing the two curves we can expect that the penalty will start to rise going beyond -6 dBm, hence to observe a 20 dB range of input power with penalty lower than 1 dB.

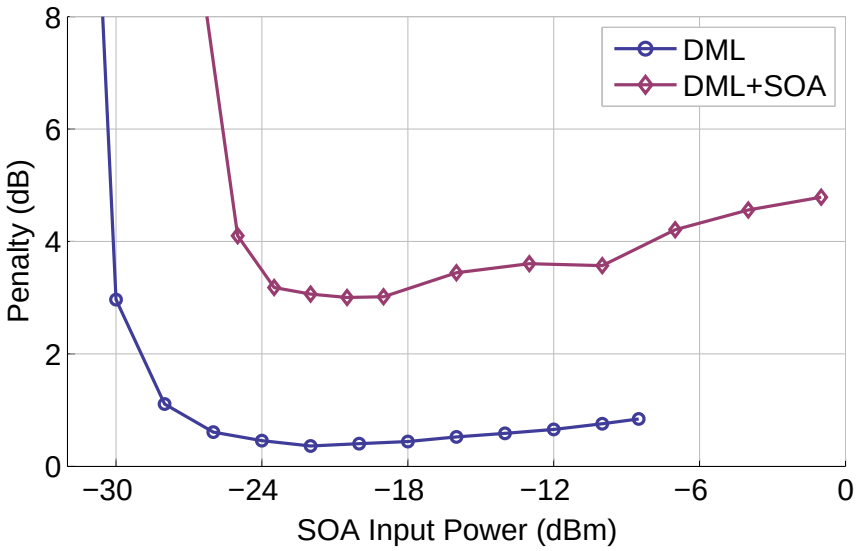

Fig. 5.19: Optical power penalty incoming transmission from DML and DML+SOA transmitter

From the results obtained so far it is possible to operate a choice relative to the better performing transmitter: seen the impairments caused by the ASE noise when a SOA is employed and because of the other solution has shown stable and robust synchronisation between the ONUs without visible consequences on the system, the burst transmitter based on two independent transmitters will be adopted for the burst mode analysis on the Raman reach extender reported in the next section.

5.5 Performances in burst mode analysis

After having evaluated the capabilities of the testing system, in this section we will present some noticeable results of Raman amplification obtained in burst mode operation. Having chosen the second burst transmitter the overall setup looks like in Fig. 5.20

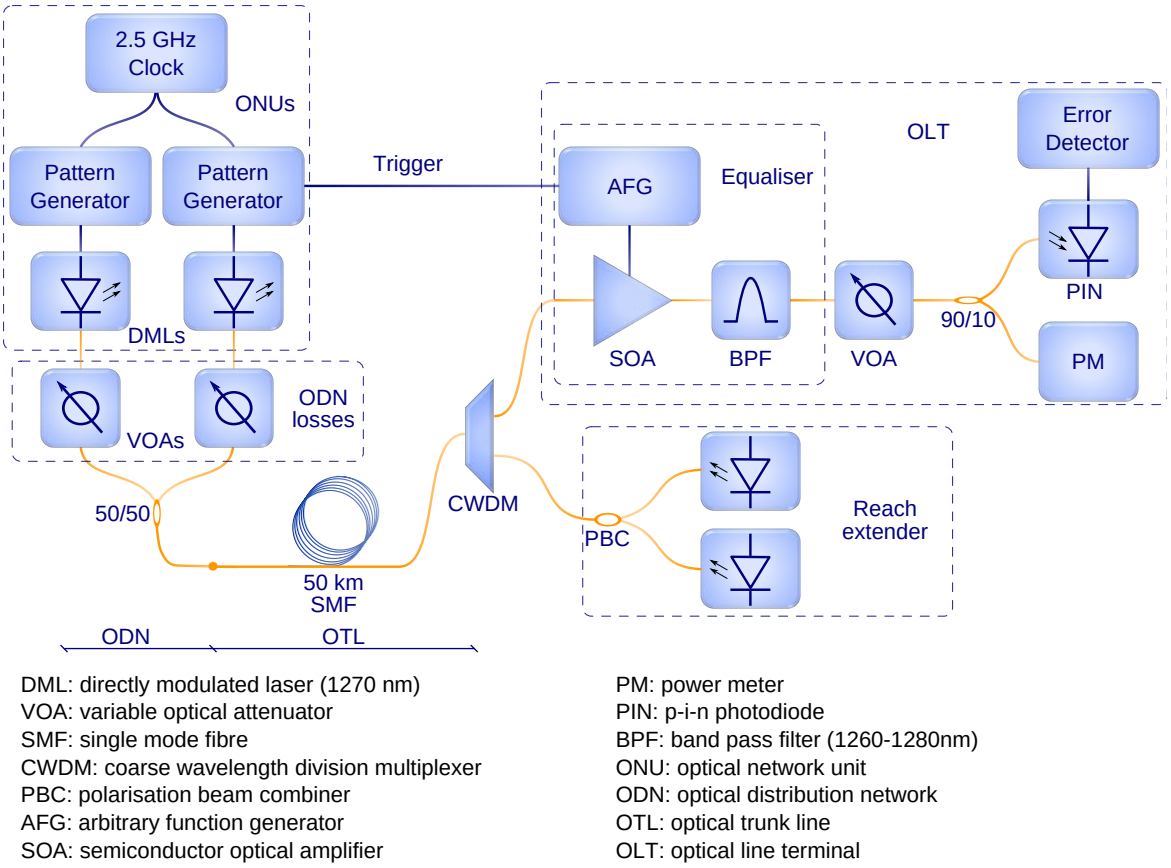

Fig. 5.20: Burst mode reach extender characterisation setup diagram

The various parts of the system are the one already described in the rest of this work. In order to find out eventual differences occurring between the continuous and burst mode scenario, a similar analysis was carried on. Multiple BER vs input power curves were acquired while varying the dynamic range of the OTL input signals, or in other words the optical power of the soft packet, with and without the 50 km fibre and reach extender. The reference back to back measurements were made placing instead of the OTL fibre an attenuator with value equal to the net power loss of the network, that is the difference between fibre and components loss and the Raman gain. In that way the received optical powers entering the receiver were guaranteed to be the same of the second runs of measurements with the Raman pumps on, and also the operation voltages supplied to the SOA were maintained unchanged between the two cases, thus to exclude dissimilarities arising from the different working regime of the

amplifier. The results are shown in Fig. 5.21 and 5.22 in the form of series of BER curves distinguished between the loud and soft packet and compared for the equaliser without fibre and the whole reach extender setup. The employed Raman pump power was the maximum of 759 mW, having measured the best performances in the previous analysis for that case.

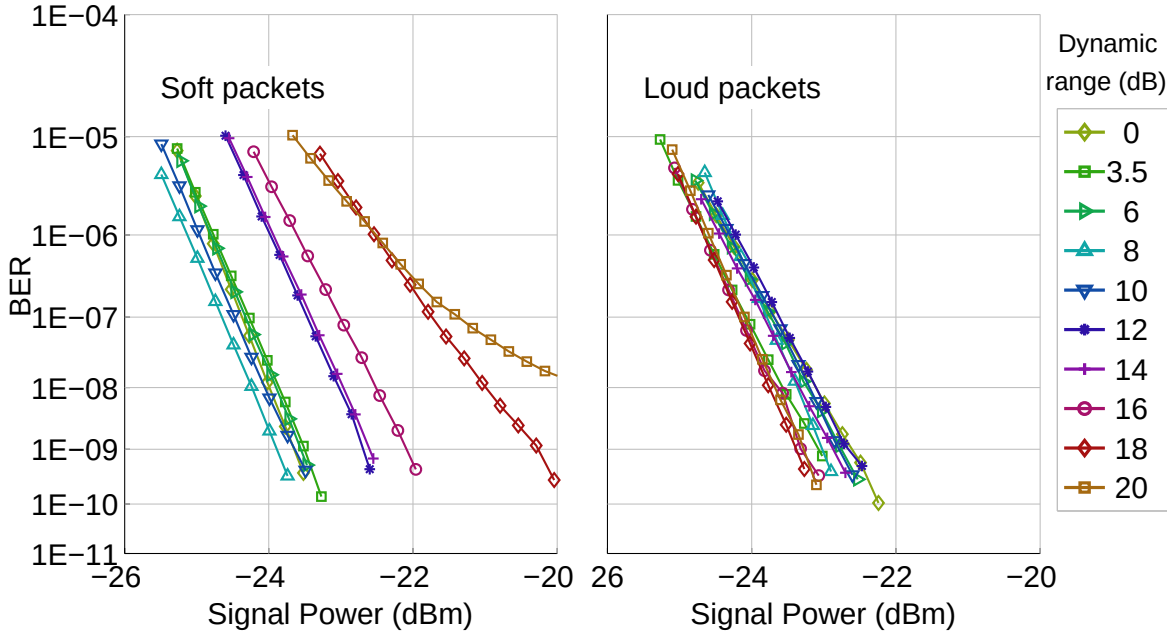

Fig. 5.21: BER multiple curves of the back to back equaliser measurements

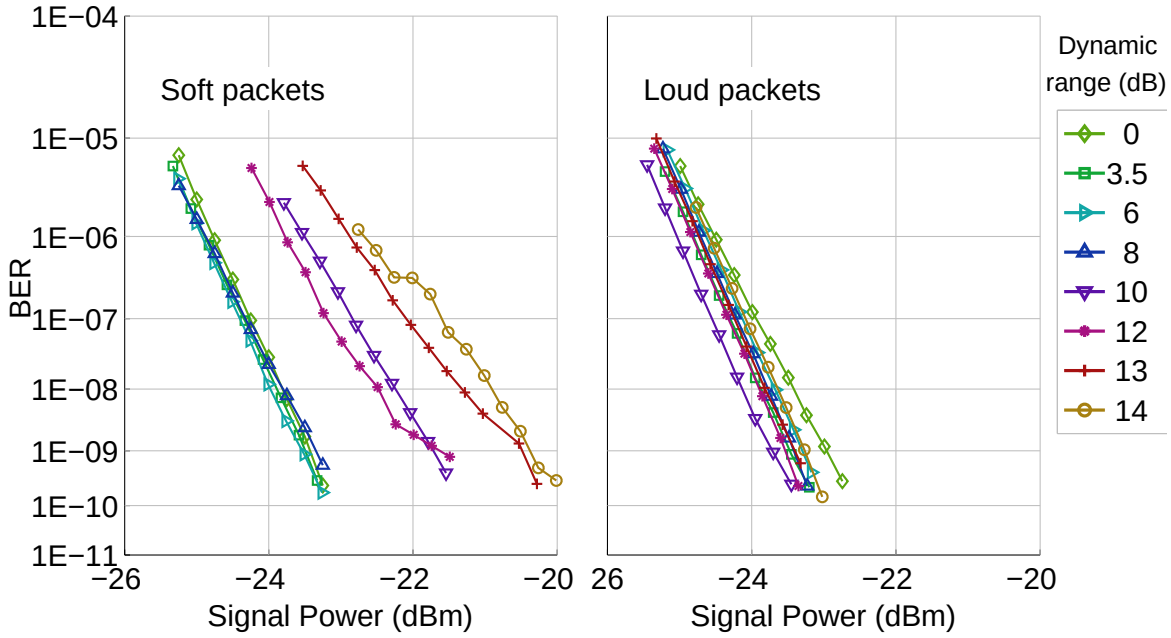

Fig. 5.22: BER multiple curves measured with the XGPON reach extender

The loud packets, which in both cases and for all the curves are reaching the receiver with the same optical power and processed with the same forward current, are not

showing any evident degradation. Moving the analysis on the soft packet the back to back analysis shows a degradation coming from reaching the sensitivity of the pre-amplified receiver made of the SOA and the PIN, being the received signal power to loo to be amplified without heavy OSNR degradation. The highest dynamic range measured corresponds to a received power of -31 dBm which in line with what found in the continuous mode characterisation of the equaliser is showing heavy BER flooring. With the reach extender the degradation is becoming manifest for lower dynamic range meaning that input power into the OLT lower than -17 dBm are not supported with these configuration. The difference with the continuous mode setup comes from the lower sensitivity of the SOA equaliser and PIN receiver with respect to the APD, while the discrepancy with the back to back curve has to be ascribed to the ASE noise generated by SRS which we already saw to be the network limiting factor causing ASE-ASE beat noise. To better prove this statement an optical power penalty curve is traced for the soft packet BER curves in both cases, and compared with the one in continuous mode, all of these three obtained for BER of 10^{-6}. It was not possible to show the penalty curve for the BER pre-FEC value of 10^{-4} because the burst mode setup cannot synchronise the pattern, and hence measure the BER, for rates of about 10^{-5} or higher.

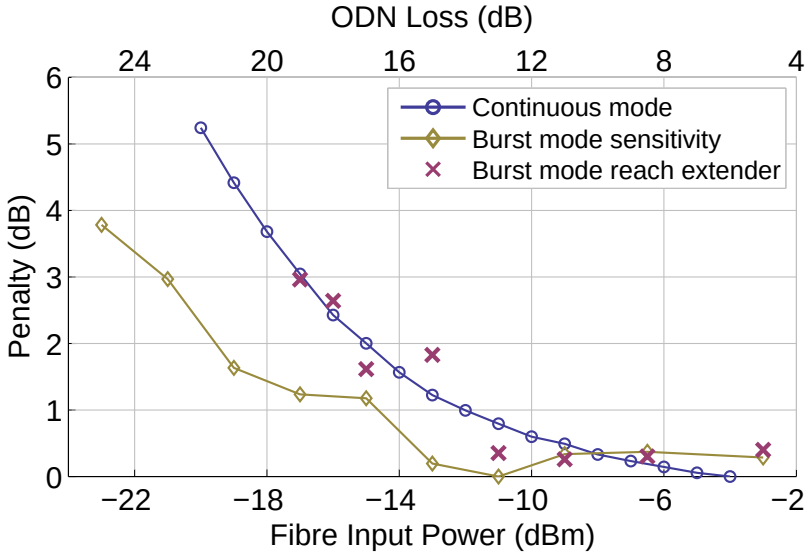

Fig. 5.23: Received power penalty for three cases of interest at BER 10^{-6}

The back to back measurement is well beyond the continuous mode curve, hence is not adding greater impairments to the performances and is not affecting the reach extender burst measurements. These measures are showing appreciable agreement with the continuous mode analysis for the range of input optical powers that was possible to investigate with the resultant sensitivity of the receiver. We can thus infer that the actual burst mode operation is not causing extra impairments to the transmission link.

In order to reveal the presence of eventual short time transient in burst mode due to the SOA equaliser or Raman reach extender, with an offline analysis of the received data the errors location in the pattern was obtained for various situations of faulty transmission. A total of $2 \cdot 10^6$ bits were acquired for every trace shown here and processed with a software tool to get the error location in the pattern, as well as the possibility to measure the BER relative to only some fields of the whole sequence or to separately look at eye diagram of the soft and loud packet. Because of the limited amount of bits recorded, the measurements were made for a BER value in the field of interest of about $5 \cdot 10^{-4}$; the bars of the histograms are representing the number of errors measured for 100 bits intervals of the sequence. In the first figure (5.24) we compare the error distribution for equal power packets in the case of a back to back measurement with only the equaliser, and with the Raman amplifier in 50 km fibre.

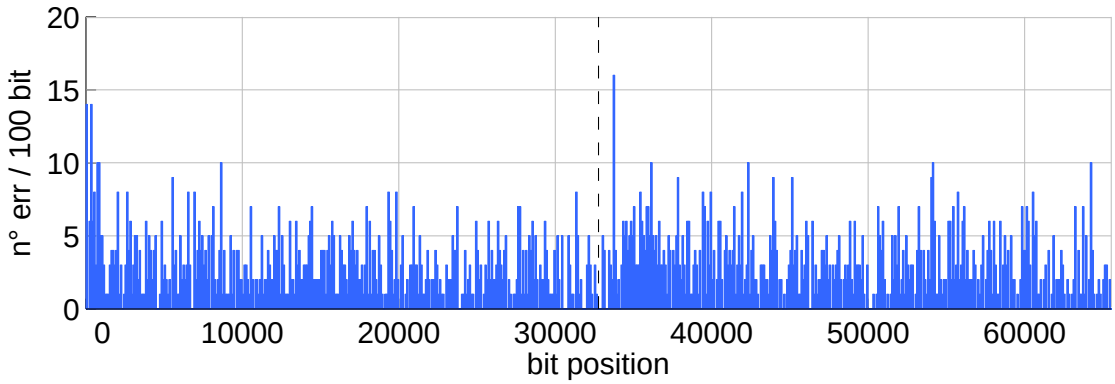

(a) Back to back measurements

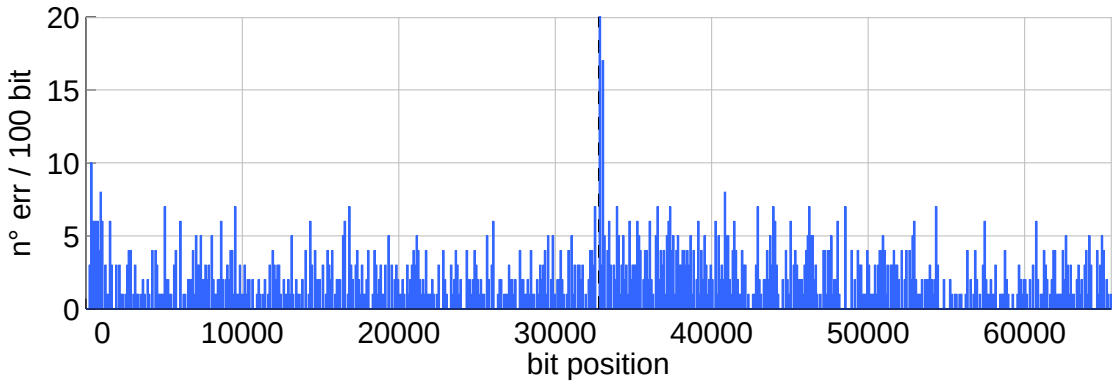

(b) Raman amplified 50 km SMF link

Fig. 5.24: BER location in the whole pattern for 0 dB dynamic range

No appreciable transients coming from the reach extender gain variation are detected, as the two cases behave similar; it is visible the error peak during the SOA switch operation, which however does not have repercussions on the measured performances being well confined in time in the guardband and preamble periods.
In Fig. 5.25 the same analysis is proposed for a 14 dB dynamic range, the maximum reached in the amplified transmission link, even now comparing the measurements

relative to the equaliser only and then to the 50 km link. In this case the stressed packet was the soft one, hence the second portion of the pattern which is the loud one was error free.

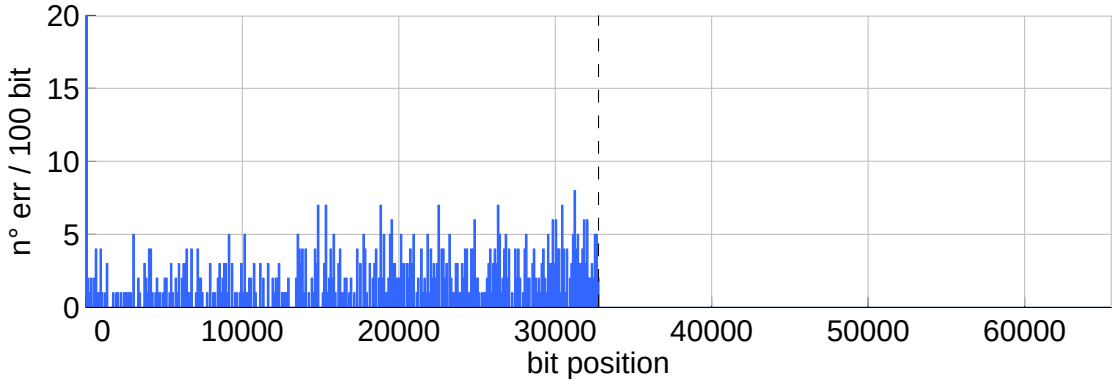

(a) Back to back measurements

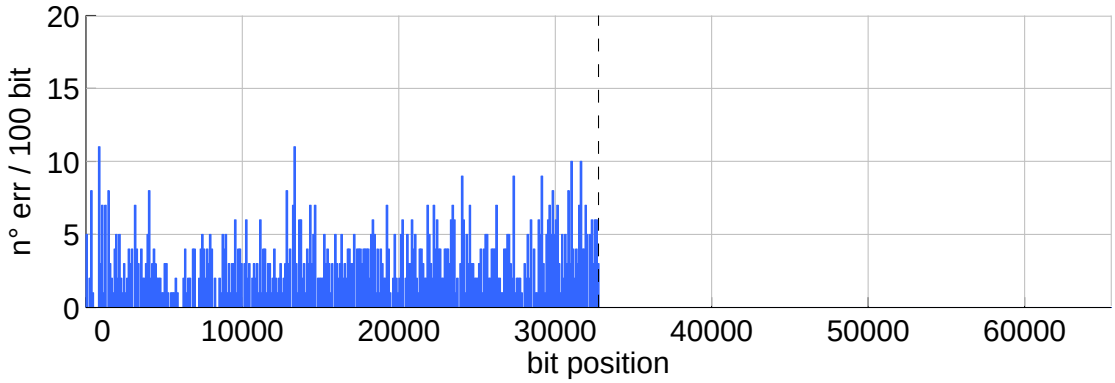

(b) Raman amplified 50 km SMF link

Fig. 5.25: BER location in the soft packet for 14 dB dynamic range

Also the BER location in the loud packet is here reported to see whether it is suffering from time varying amplification gain; when the loud packet is stressed with thermal noise the soft one is evidently compromised.

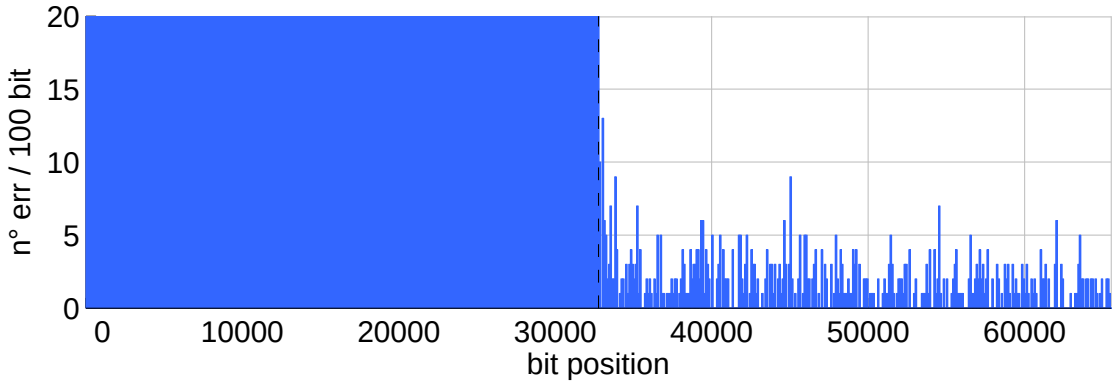

Fig. 5.26: BER location in the loud packet for 14 dB dynamic range, in Raman amplified 50 km SMF link

Even now no important trend are indicating the presence and repercussion of gain transients in the amplified link, for both soft and loud packets; that suggests that Raman fast time response, along with the counter propagating configuration which mitigates the fibre induced transients, make reach extender based on Raman amplification a viable solution for burst traffic amplification.

5.6 Conclusions

In this final chapter the performances of the reach extender were evaluated measuring the link BER as a function of the optical power entering the receiver in various scenarios. A first analysis conducted in continuous mode has shown the Raman amplifier capabilities in terms of provided gain and minimum OSNR, measured for a comprehensive range of input power to cover the XG-PON application. The configuration and devices chosen for the amplifier were not showing issues due to non linearities and the major penalty was coming from the wide band ASE-ASE beat noise, which cannot be avoid in the receiver design unless special precautions are taken in the network design. Afterwards the chosen system for burst mode operation was characterised, showing capability of working with a 20 dB dynamic range, and the continuous mode measurements were confirmed in a link providing full burst mode operation over 50 km SMF with the Raman based reach extender. A maximum dynamic range of 14 dB was reached because of the limitation introduced by the receiver sensitivity, and up to this point the burst mode results were in agreement with the continuous mode one. The results suggest that the Raman amplifier did not introduce any transients in the gain as was also verified using an error location technique which did not evidence any error concentration within the pattern.

Chapter 6

Conclusions and Future Work

In this work for the first time the use of QD lasers as Raman pumps for amplification in the 1270 nm XG-PON upstream bandwidth was reported.
An exhaustive characterisation of the salient aspects of these lasers was carried on in Chapter 3 along with the building of the Raman reach extender and a quantification of the achievable Raman on off gain in the scenario of interest. Suitable spectral features and high output powers of the pumps were revealed, as well as high temperature insensibility. The reach extender module was able to provide a maximun pump power of 759 mW at the wavelength of 1210 nm. A Raman gain of 14 dB was obtained for the wavelength in analysis (1270 nm) in a 50 km SMF, in line with the theoretical analysis. In the XG-PON upstream band the measured gain was between 10 and 16.5 dB but the gain spectrum was showing a 20 nm wide flatness region around 1280 nm with less than 2 dB variation from the maximum value. This suggests that with a 10 nm lower Raman pump amplification in the entire upstream band can be achieved with a single pump laser. The gain also showed polarisation insensitivity thanks to the backward configuration and no efficiency loss when increasing the pump power.
In Chapter 4 we focused the attention in describing how various test setups were realised for a proper characterisation of the XG-PON reach extender. A setup for the analysis of the transmission link in continuous mode was at first presented, emulating transmission over 50 km SMF and a 64 split-ratio. In the following a burst transmitter was proposed for a more detailed analysis, able to generate burst transmission with data flow including guardband and preamble times with a dynamic range higher than 20 dB. A burst receiver was built using a SOA as optical power equaliser able to work for a 20 dB dynamic range.
The most significant results showing the impact of Raman amplification in the optical band 1260-1280 nm were reported in Chapter 5. Firstly the continuous mode analysis was shown thus to give an idea of the reach extender capabilities and the resulting impairments arising in the network. The gain was supporting transmission over 50 km SMF, which corresponds to the OTL length, with an upstream input power to the OTL which translates in a 64 split-ratio in the ODN. Afterwards a characterisation of the burst setup was made showing ability to emulate a transmission with 20 dB dynamic range. The burst mode results of the reach extender were then proposed up to a maximum dynamic range of 14 dB and compared with the previous one. Accordance in the measurements taken in continuous and burst mode suggests no important issues

coming from the burst traffic operation taking place in the network. A further analysis was conducted with an error location technique to show that SRS is not causing gain transients.

After the results demonstrated in this work further works are still of interest in this field. A deeper analysis of the efficiency of the pump operating above cut-off frequency would show the feasibility of employing a higher frequency pump laser (1200 nm) for XG-PON upstream band.
The analysis of hybrid scheme of Raman amplification employing both a co and counter propagating pump signal can be studied and considered to further increase the network capabilities in length and split ratio, at the price of an active node in the outside plan.
A deeper analysis of Raman gain efficiency in special fibres can open to the design of hybrid networks with a few kilometres span of high gain fibre providing Raman amplification instead of the long OTL which may be not long enough in already installed networks.
These and other aspects can be the starting point for following research works on this topic that can lead to a deeper knowledge of the application of Raman scattering in the improvement of FTTH technology.

Bibliography

[1] Cisco, "Cisco VNI: Visual Networking Index," Tech. Rep., 2010.

[2] P. J. Winzer and R. Essiambre, "Advanced optical modulation formats," *Proceedings of the IEEE*, vol. 94, no. 5, pp. 952–985, 2006.

[3] Ministry of Internal Affairs and Communications, Japan, "White Paper, Information and Communications in Japan," Tech. Rep., 2013.

[4] Point Topic, "White Paper, World Broadband Statistics," Tech. Rep., 2013.

[5] F. Effenberger, "The xg-pon system: Cost effective 10 gb/s access," *Lightwave Technology, Journal of*, vol. 29, no. 4, pp. 403–409, Feb 2011.

[6] S. Namiki, S. Koji, N. Tsukiji, and S. Shikii, "Challenges of Raman Amplification," *Proceedings of the IEEE*, vol. 94, no. 5, pp. 1024–1035, 2006.

[7] C. Headley and G. P. Agrawal, *"Raman Amplification in Fiber Optical Communication Systems"*. Elsevier Academic Press, 2005.

[8] F. Effenberger, D. Clearly, O. Haran, G. Kramer, L. Ruo Ding, M. Oron, and T. Pfeiffer, "An introduction to pon technologies [topics in optical communications]," *Communications Magazine, IEEE*, vol. 45, no. 3, pp. S17–S25, 2007.

[9] www.quaternian.org, [Online; accessed August-2014].

[10] D. Nesset, D. Grossman, S. Appathurai, J. Fitzgerald, P. Wright, K. Farrow, and S. Yang, "Field experiment with a hardened GPON reach extender with dual-parenting protection," in *Optical Communication, 2008. ECOC 2008. 34th European Conference on*, 2008, pp. 1–2.

[11] D. Nesset, K. Farrow, and P. Wright, "Bidirectional, Raman extended GPON with 50 km reach and 1:64 split using wavelength stabilised pumps," in *Optical Communication (ECOC), 2011 37th European Conference and Exhibition on*, 2011, pp. 1–3.

[12] D. Nesset and P. Wright, "Raman extended GPON using 1240 nm semiconductor quantum-dot lasers," in *Optical Fiber Communication (OFC), collocated National Fiber Optic Engineers Conference, 2010 Conference on (OFC/NFOEC)*, 2010, pp. 1–3.

[13] Z. Benyuan and D. Nesset, "GPON reach extension to 60 km with entirely passive fibre plant using Raman amplification," in *Optical Communication, 2009. ECOC '09. 35th European Conference on*, 2009, pp. 1–2.

[14] J. Bromage, "Raman amplification for fiber communications systems," *Lightwave Technology, Journal of*, vol. 22, no. 1, pp. 79–93, 2004.

[15] K. Rottwitt and J. H. Povlsen, "Analyzing the fundamental properties of raman amplification in optical fibers," *Lightwave Technology, Journal of*, vol. 23, no. 11, pp. 3597–3605, 2005.

[16] T. Tanaka, K. Torii, M. Yuki, H. Nakamoto, T. Naito, and I. Yokota, "200-nm Bandwidth WDM Transmission around 1.55 μm using Distributed Raman Amplifier," in *Optical Communication, 2002. ECOC 2002. 28th European Conference on*, vol. 5, Conference Proceedings, pp. 1–2.

[17] D. Bimberg, N. Kirstaedter, N. N. Ledentsov, Z. I. Alferov, P. S. Kop'ev, and V. M. Ustinov, "InGaAs-GaAs quantum-dot lasers," *Selected Topics in Quantum Electronics, IEEE Journal of*, vol. 3, no. 2, pp. 196–205, 1997.

[18] J. Thomson, H. Summers, P. Smowton, E. Herrmann, P. Blood, and M. Hopkinson, "Temperature dependence of the wavelength of quantum dot lasers," in *Semiconductor Laser Conference, 2000. Conference Digest. 2000 IEEE 17th International*, pp. 135–136.

[19] L. V. Asryan and S. Luryi, "Temperature-insensitive quantum dot laser," in *Semiconductor Device Research Symposium, 2001 International*, pp. 359–363.

[20] R. Debusmann, T. W. Schlereth, S. Gerhard, W. Kaiser, S. Hofling, and A. Forchel, "Gain Studies on Quantum-Dot Lasers With Temperature-Stable Emission Wavelength," *Quantum Electronics, IEEE Journal of*, vol. 44, no. 2, pp. 175–181, 2008.

[21] www.innolume.com, [Online; accessed August-2014].

[22] A. R. Chraplyvy, "Limitations on lightwave communications imposed by optical-fiber nonlinearities," *Lightwave Technology, Journal of*, vol. 8, no. 10, pp. 1548–1557, 1990.

[23] "Recommendation ITU-T G.987 : 10-Gigabit-capable passive optical network (XG-PON) systems," Tech. Rep., 2012.

[24] C. Antony, G. Talli, P. D. Townsend, J. Bauwelinck, D. W. Smith, and I. Lealman, "High extinction switching of SOAs for in-band crosstalk reduction in PON," *Electronics Letters*, vol. 44, no. 14, pp. 872–873, 2008.

[25] M. Nakamura, Y. Imai, Y. Umeda, J. Endo, and Y. Akatsu, "1.25-Gb/s burst-mode receiver ICs with quick response for PON systems," *Solid-State Circuits, IEEE Journal of*, vol. 40, no. 12, pp. 2680–2688, 2005.

[26] C. Antony, G. Talli, and P. D. Townsend, "SOA based upstream packet equalizer in 10Gb/s extended-reach PONs," in *Optical Fiber Communication - incudes post deadline papers, 2009. OFC 2009. Conference on*, 2009, pp. 1–3.

[27] G. P. Agrawal, *"Fiber-Optic Communication Systems, third edition"*. Wiley, 2002.

Appendix A

In this appendix we will discuss the electrical amplification stage for the RF signal generated by a photodiode before sending it to the ED. Even though this may seem a marginal component when talking about photonics network it has often become a critical aspect, assuming a determinant relevance in the overall performances of the setup. In fact without paying the necessary attention on this element it may easily become the bottleneck of the system and prevent accurate measurements.
In the following sections we propose some analysis and results measured with the setup in Fig. A.1, which is the simplest optical transmission configuration and thus permits the evaluation of the receiver with the less possible amount of external factors adding impairments to the system. The essential design permits to relate any observed changes in performances to the unique modification made on the DUT. Increasing the attenuation introduced by the VOA the thermal noise progressively affects the signal causing increase of the BER, and observing the different trends of BER vs received power the amplifier stages will be compared.

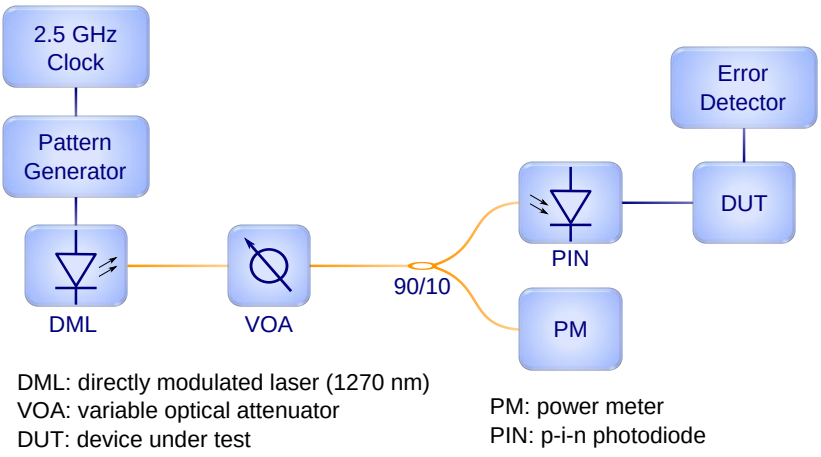

Fig. A.1: Setup for evaluation of the electrical amplification stage

.1 Electrical receiver performances

The first case analysed was making use in the setup of a photodiode with a typical responsivity of 0.8 A/W in the band of interest and a high gain TIA with gain magnitude of 1000 V/A, for a conversion gain of about 800 V/W. The minimum NEP was 24 pW/$\sqrt{\text{Hz}}$ and for operation at 2.5 Gb/s these two aspects were guaranteeing a minimum amplitude of the output electrical signal, when reducing the optical power to stress the thermal noise limit, of $\simeq$ 6-7 mV peak to peak (pp) even for the higher BERs; amplifying this stream with a single amplifier was hence sufficient to obtain a

suitable input signal into the ED whose sensitivity was < 50 mV pp at 10 Gb/s for BER 10^{-12}.

In this scenario some configurations were compared for the single stage amplifier, considering different low-pass filtering solutions and two types of amplifier. The first was a broadband linear amplifier with typical 15 dB gain; the second a limiting amplifier generating an output signal with constant amplitude in the order of 400 mV pp, working without issues for low input signals till 6 mV pp. The relevant configurations considered are sketched in Fig. A.2

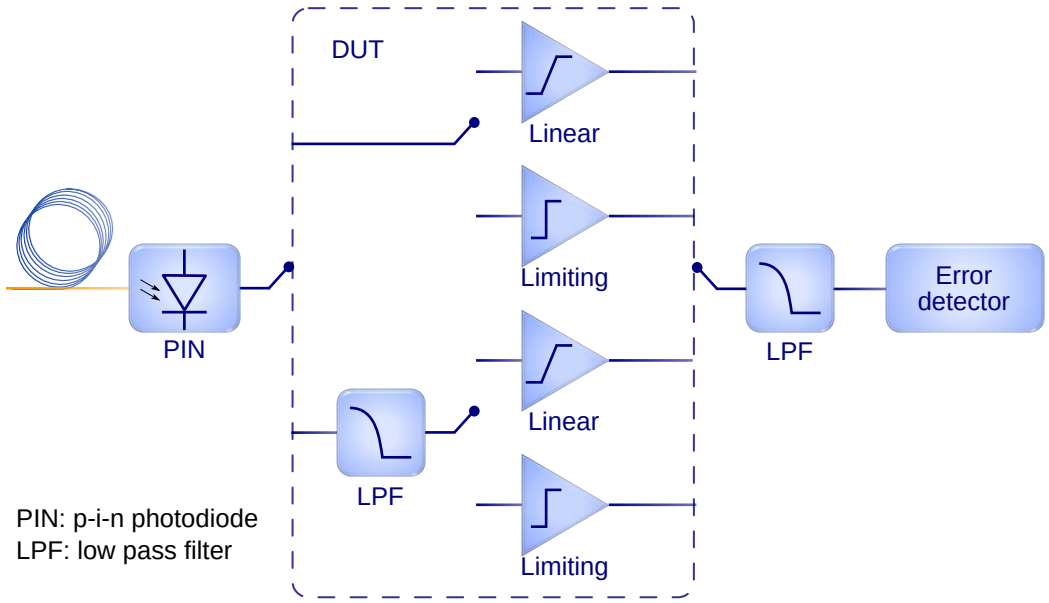

Fig. A.2: Setup for evaluation of the electrical amplification stage impact

Repeated runs of measurements were acquired for every one of the proposed combinations in order to evaluate the accuracy of the obtained results. In general a double low pass filtering of the electrical signal resulted in better performances removing the high frequency components of the noise affecting the signal. A statistical analysis is shown in Fig. A.3 for the linear and limiting electrical amplifier employing two 2.5 GHz Bessel function low pass filters. The BER vs optical power curves shown are the average values obtained from fifty repeated measurements under the same conditions. Also shown are the errorbars which are expressing the standard deviations of the set of measures acquired for every point. The reference confidence interval plotted in the side is the theoretical standard deviations that should be obtained in a reliable scenario, calculated from the number of bits transmitted and the measured BER in every case, assuming gaussian noise distribution.

The linear amplifier is showing much higher variance in the results, coming from the ED optimization routine for the voltage threshold and sampling point which gives less reliable results when the input eye is more closed and noisy. Indeed the limiting amplifier which is generating a high voltage amplitude signal, results to be much

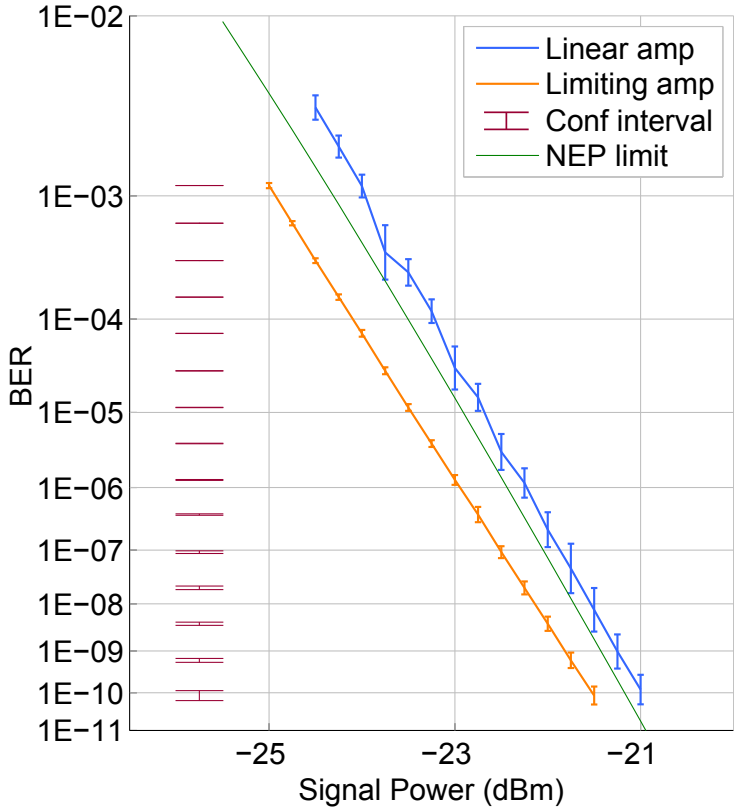

Fig. A.3: Average BER curves and standard deviations obtained from 50 acquisitions for two electrical amplifier configurations

easier to be interpreted by the receiver. It is important to notice that this pronounced amplification is not introducing any form of degradation in the signal, which is actually performing better in both stability and mean value of necessary optical power. Because of the optimization algorithm of the ED is based on the identification of BER isolines in the eye diagram, like shown in Fig. A.4, it is also evident how in an eye diagram with higher noise and lower aperture the mean average is not a straight line but depends on the BER value. In fact in the linear amplifier curve are visible slight differences in the alignment performance depending on the lower BER threshold that was reached in the contour identification. Seen these results all the measurements reported in this work, when a PIN photodiode with the above mentioned characteristics was employed, were acquired with the limiting electrical amplifier stage and double filtering after the optical-electrical converter.

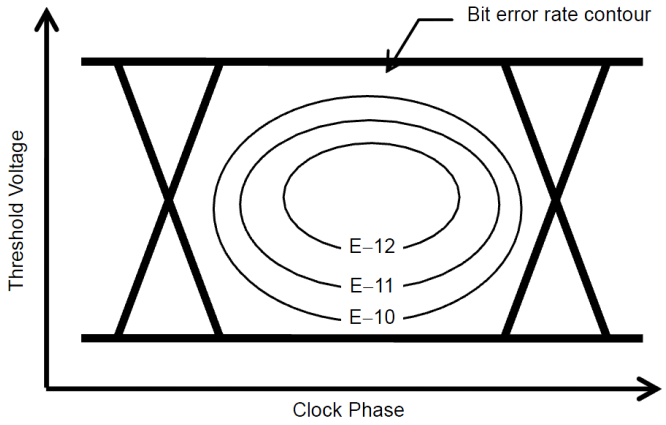

Fig. A.4: BER isolines contour in eye diagram

.2 Electrical receiver in TIA low output power scenario

Another scenario was encountered when using a different PIN photodiode whose typical conversion gain was about 400 V/W and NEP 12.5 pW/$\sqrt{\text{Hz}}$. This lower optical power detectable coming from the better sensitivity and less conversion gain brings to a voltage output level of about 1-2 mV pp for the higher BERs. Starting from the previous results the two better configuration were replied, and a third one was added as visible in Fig. A.5. Because of the very low amplitude in output from the photodiode none of the single stage amplifiers were able to guarantee appreciable performances, not being able to provide a sufficient gain the linear amplifier to permit the ED to work away from its sensitivity, and working below the minimum required input amplitude (6 mV pp) the limiting one. Hence a double amplification stage was made and compared to the others as visible in Fig. A.6.
Comparing the results obtained it is evident that only the new options permits to operate in a regime in which the optical thermal noise is the main impairment source, and thus obtain sensed BER vs optical power characterisations. In fact the other curves are not showing a linear constant slope in the log(erfc) scale used for the BER, following the trend of the thermal noise. Hence all the acquisition results reported in this work with the use of a photodiode with low RF output power were employing this double stage electrical amplifier.

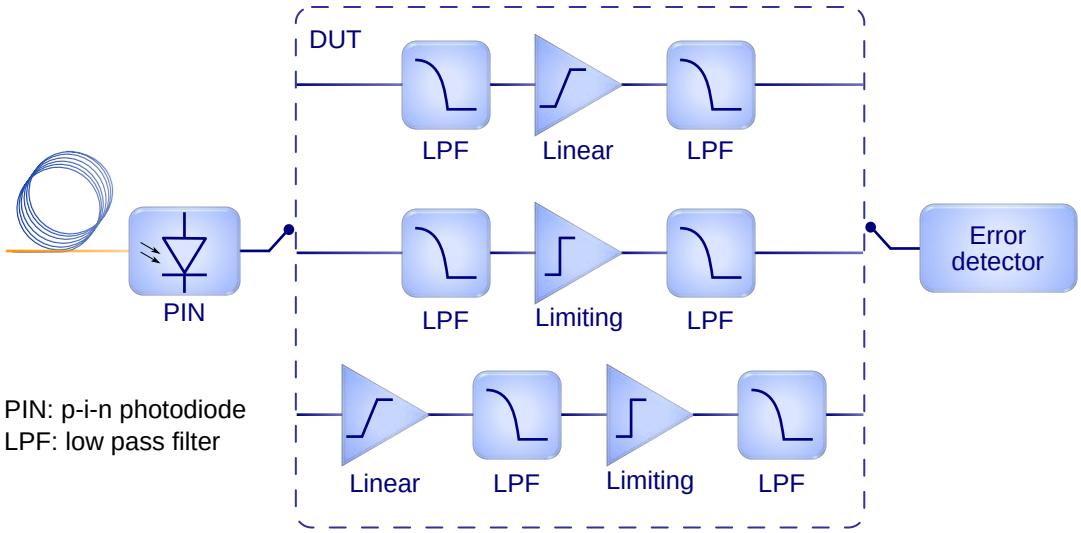

Fig. A.5: Setup for evaluation of the electrical amplification stage impact with low electrical output power

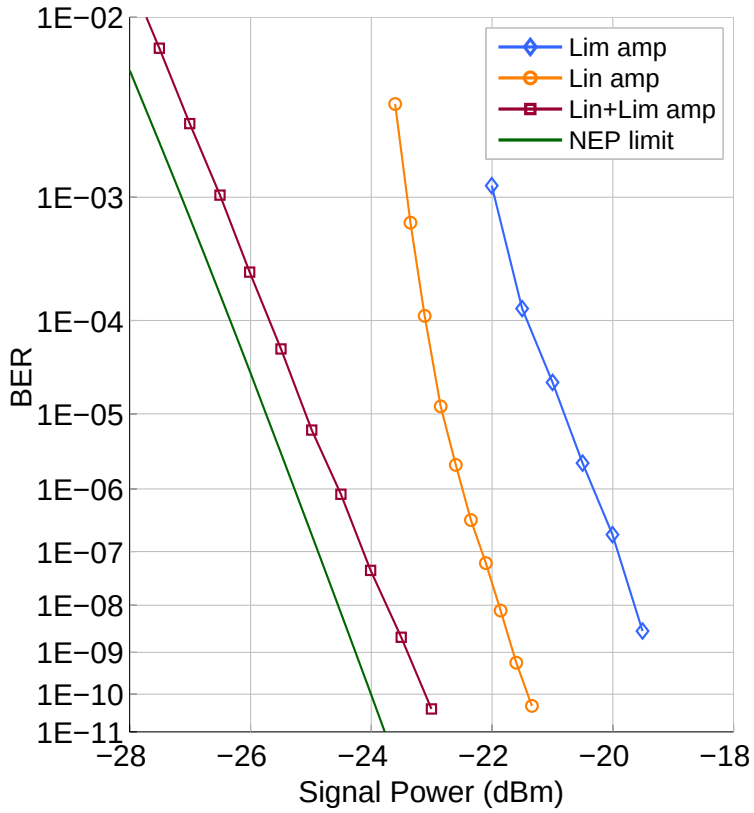

Fig. A.6: BER vs optical power curves for three electrical amplifier configurations